CHAPTER 4

Synthetic seismograms and data analysis for a spherical Earth

4.1 Excitation of modes . Until now, we have been considering solutions to the homogeneous equations. We now consider the case when we have $\mathbf{f}$, an equivalent body force distribution, acting as a forcing function. Our basic equations can be written as (3.39):

$$\rho_0 \frac{\partial^2 \mathbf{s}}{\partial t^2} = \mathbf{L}(\mathbf{s}) + \mathbf{f} \tag{4.1}$$

The k'th free oscillation where $\mathbf{s} = \mathbf{s}_k e^{i\omega_k t}$ satisfies

$$\mathbf{L}(\mathbf{s}_k) + \rho_0 \omega_k^2 \mathbf{s}_k = 0 \tag{4.2}$$

These solutions are orthogonal and normalized such that

$$\int_V \rho_0 \mathbf{s}_{k'}^\star \mathbf{s}_k \, dV = \delta_{kk'} \tag{4.3}$$

Because of the completeness of the eigenfunctions of a self-adjoint operator, we can look for solutions to 4.1 of the form

$$\mathbf{s} = \sum_k a_k(t) \mathbf{s}_k(\mathbf{r}) \tag{4.4}$$

Substitution in 4.1 gives

$$\rho_0 \sum_k \frac{\partial^2 a_k}{\partial t^2} \mathbf{s}_k = \sum_k a_k(t) \mathbf{L}(\mathbf{s}_k) + \mathbf{f} \tag{4.5}$$

Using 4.2 gives

$$\sum_k \left[\rho_0 \omega_k^2 a_k(t) \mathbf{s}_k + \rho_0 \frac{\partial^2 a_k}{\partial t^2} \mathbf{s}_k \right] = \mathbf{f} \tag{4.6}$$

To isolate a single $a_k(t)$, we multiply through by $\mathbf{s}_k^\star$ and integrate over the volume of the Earth. Using 4.3 then gives

$$\omega_k^2 a_k(t) + \frac{\partial^2 a_k}{\partial t^2} = \int_V \mathbf{s}_k^\star \cdot \mathbf{f}(t) \, dV = F_k(t) \quad \text{say} \tag{4.7}$$

We anticipate that $\mathbf{f}$ will be confined to a small volume around the source so $F_k(t)$ is really the result of a localized integral over the source region. The solution to 4.7 is

$$a_k(t) = \frac{1}{\omega_k} \int_{-\infty}^{t} \sin\left[\omega_k (t - t')\right] F_k(t') \, dt' \tag{4.8}$$

Equation 4.8 is not in its most useful form because an earthquake source has a body force density which is not localized in time – in fact the behavior must be nearly step-like:

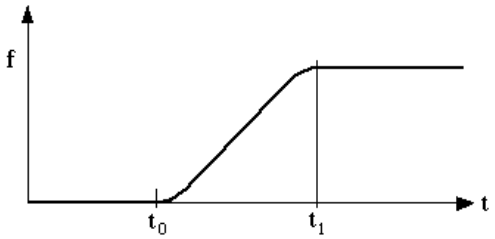

t_0 is the origin time of the event and $t_1 - t_0$ gives the event duration. Note that $\partial \mathbf{f}/\partial t$ is localized in time which leads us to integrate 4.8 by parts. Re-write 4.8 as

$$a_k(t) = -\frac{1}{\omega_k^2} \int_{-\infty}^{t} \frac{d}{dt'}[1 - \cos(\omega_k(t-t'))]F_k(t')\,dt'$$

$$= \frac{1}{\omega_k^2} \int_{-\infty}^{\infty} [1 - \cos(\omega_k(t-t'))]\frac{\partial}{\partial t}F_k(t')\,dt' \tag{4.9}$$

We now assume that the motion is zero before t=0 and define

$$C_k(t) = [1 - \cos(\omega_k t)]H(t) \tag{4.10}$$

(where $H(t)$ is the Heaviside step function) then

$$a_k(t) = \frac{1}{\omega_k^2} \int_{-\infty}^{\infty} C_k(t-t')\frac{\partial}{\partial t}F_k(t')\,dt'$$

$$= \frac{1}{\omega_k^2} C_k(t) * \frac{\partial}{\partial t}F_k(t) \tag{4.11}$$

Our formal solution to 4.1 can now be written

$$\mathbf{s}(\mathbf{r}, \mathbf{r}_0, t) = \sum_k \frac{1}{\omega_k^2}\mathbf{s}_k(\mathbf{r})\frac{\partial}{\partial t}F_k(\mathbf{r}_0, t) * C_k(t) \tag{4.12}$$

where $\mathbf{r}$ is the receiver location and $\mathbf{r}_0$ is the source location. That is,

$$\frac{\partial F_k}{\partial t} = \int_{V_S} \mathbf{s}_k^\star \cdot \frac{\partial \mathbf{f}}{\partial t}\,dV \tag{4.13}$$

where V_S is defined by the region in which $\mathbf{f}$ is non-zero. The sum in 4.12 is taken over all modes but, because we are interested only in a finite frequency band, we need include only those modes with frequencies (ω_k) within that band.

Our remaining task is to evaluate 4.13 for a particular model of the seismic source. We begin with a rather general discussion of phenomenological descriptions of seismic sources. By this we mean that we shall not try to model all the complicated processes which occur during the earthquake rupture but we shall try and find an equivalent representation which accurately models the low-frequency radiation of the source.

4.2 Moment tensors . The exact equations of motion in the presence of a gravitational field are:

$$\left.\begin{aligned} \rho\frac{D^2\mathbf{s}}{Dt^2} &= \nabla\cdot\mathbf{S} - \rho\nabla\phi \\ \text{and}\quad \nabla^2\phi &= 4\pi G\rho \end{aligned}\right\} \tag{4.14}$$

where $\mathbf{S}$ is the true physical stress tensor. Equations 4.14 are physical laws and are true everywhere. Up to this point, we have been considering approximate solutions to 4.14, *i.e.*, we have assumed that we have small oscillations and a linear (elastic) constitutive relationship. We anticipate that these approximations will not be valid everywhere and identify the *source region* as the place where our approximations fail. We then define the difference between our model tensor, $\mathbf{T}$, and the true physical stress, $\mathbf{S}$, as Γ – the *stress glut*:

$$\mathbf{S} = \mathbf{T} - \Gamma \tag{4.15}$$

Comparison with 2.33 gives an expression for the equivalent body force in terms of Γ:

$$\mathbf{f} = -\nabla \cdot \Gamma \tag{4.16}$$

Thus $\mathbf{f}$ is the negative of the divergence of a second order symmetric tensor (because both $\mathbf{S}$ and $\mathbf{T}$ are symmetric). For simplicity, we shall assume that no discontinuity intersects the source region. We can then use Gauss' theorem in its simple form and show

$$\int_{V_S} \mathbf{f}\, dV = -\int_{V_S} \nabla \cdot \Gamma\, dV = -\int_{S} \Gamma \cdot \hat{\mathbf{n}}\, dS = 0 \tag{4.17}$$

(because Γ is zero on the boundary of the source region). This result shows that no net force is applied to the Earth. Because of the symmetry of Γ, we can also show that the source exerts no net torque *i.e.*,

$$\int_{V_S} \mathbf{x} \times \mathbf{f}\, dV = 0$$

We now define the *seismic moment tensor*, M_{ij} as

$$M_{ij}(t) = \int_{V_S} \Gamma_{ij}\, dV \tag{4.18}$$

so that, for a point source, $M_{ij} = \Gamma_{ij}$.

To make the algebra a little simpler, we define a local Cartesian coordinate system with $x_1 \equiv r$ (up), $x_2 \equiv \theta$ (south) and $x_3 \equiv \phi$ (east). In index notation, equation 4.16 becomes $f_j = -\partial \Gamma_{ij}/\partial x_i$. Now consider

$$\frac{\partial}{\partial x_k}(x_i \Gamma_{kj}) = \frac{\partial x_i}{\partial x_k}\Gamma_{kj} + x_i \frac{\partial}{\partial x_k}\Gamma_{kj}$$

Using the fact that $\partial x_i/\partial x_k = \delta_{ik}$, integrating over the source volume gives

$$\int_{V_s} \frac{\partial}{\partial x_k}(x_i \Gamma_{ij})\, dV = \int_{V_s} \Gamma_{ij}\, dV - \int_{V_s} x_i f_j\, dV \tag{4.19}$$

By Gauss' theorem, the integral on the left hand side is zero so we end up with

$$M_{ij} = \int_{V_S} x_i f_j\, dV = \int_{V_S} \Gamma_{ij}\, dV \tag{4.20}$$

This equation makes clear why M_{ij} is called the "seismic momemt tensor" with each element of M_{ij} related to a force couple with forces in the i direction and moment arm in the j direction (or vice-versa).

We now return to the evaluation of 4.13. We have to perform an integral over the source region and we suppose that the wavelengths of the modes being excited are much larger than the source dimension. If we also restrict attention to the case where there are no discontinuities intersecting the source region, we can expand $\mathbf{s}_k^\star$ in a Taylor series centered about a fiducial point, $\mathbf{x}_0$, within the source region. Thus (dropping the mode index, k)

$$s_j^\star = s_j^\star(\mathbf{x}_0) + (x_i - x_{0_i})\frac{\partial s_j^\star}{\partial x_i}(\mathbf{x}_0) + \frac{(x_i - x_{0_i})(x_l - x_{0_l})}{2!}\frac{\partial^2 s_j^\star}{\partial x_i \partial x_l}(\mathbf{x}_0) + \cdots \tag{4.21}$$

Substitution into 4.13 and using 4.17 gives

$$\begin{aligned}\frac{\partial F_k}{\partial t} =& \frac{\partial s_i^\star}{\partial x_j}(\mathbf{x}_0)\int\limits_{V_s} x_j \frac{\partial f_i}{\partial t}\, dV \\ &+ \tfrac{1}{2}\,\frac{\partial^2 s_i^\star}{\partial x_k \partial x_l}(\mathbf{x}_0)\left[\int\limits_{V_s} x_k x_l \frac{\partial f_i}{\partial t}\, dV - x_{0k}\int\limits_{V_s} x_l \frac{\partial f_i}{\partial t}\, dV - x_{0l}\int\limits_{V_s} x_k \frac{\partial f_i}{\partial t}\, dV\right] + \cdots\end{aligned} \tag{4.22}$$

Now let

$$\frac{\partial M_{ikl}}{\partial t} = \int\limits_{V_s} x_k x_l \frac{\partial f_i}{\partial t}\, dV = \frac{\partial M_{ilk}}{\partial t} \tag{4.23}$$

then with 4.20 we have

$$\frac{\partial F_k}{\partial t} = \frac{\partial s_i^\star}{\partial x_j}(\mathbf{x}_0)\frac{\partial M_{ij}}{\partial t} + \tfrac{1}{2}\,\frac{\partial^2 s_i^\star}{\partial x_k \partial x_l}(\mathbf{x}_0)\left[\frac{\partial M_{ikl}}{\partial t} - x_{0k}\frac{\partial M_{il}}{\partial t} - x_{0l}\frac{\partial M_{ik}}{\partial t}\right] + \cdots \tag{4.24}$$

Often, we need only retain the first term in 4.24. Remember that the origin of our coordinate system can be taken to be within the source region and we could easily let $\mathbf{x}_0$ be the origin. It is then easy to see that the second term in 4.24 will vanish as the source volume tends to zero. Then (using a dot for time derivative)

$$\begin{aligned}\frac{\partial F_k}{\partial t} \simeq& \frac{\partial s_i^\star}{\partial x_j}\frac{\partial M_{ij}}{\partial t} \qquad \text{(point source)} \\ =& \frac{\partial s_1^\star}{\partial x_1}\dot{M}_{11} + \frac{\partial s_2^\star}{\partial x_2}\dot{M}_{22} + \frac{\partial s_3^\star}{\partial x_3}\dot{M}_{33} + \left(\frac{\partial s_1^\star}{\partial x_2} + \frac{\partial s_2^\star}{\partial x_1}\right)\dot{M}_{12} \\ &+ \left(\frac{\partial s_1^\star}{\partial x_3} + \frac{\partial s_3^\star}{\partial x_1}\right)\dot{M}_{13} + \left(\frac{\partial s_2^\star}{\partial x_3} + \frac{\partial s_3^\star}{\partial x_2}\right)\dot{M}_{23} \\ =& \epsilon_{11}^\star \dot{M}_{11} + \epsilon_{22}^\star \dot{M}_{22} + \epsilon_{33}^\star \dot{M}_{33} + 2\epsilon_{12}^\star \dot{M}_{12} + 2\epsilon_{13}^\star \dot{M}_{13} + 2\epsilon_{23}^\star \dot{M}_{23}\end{aligned}$$

Thus

$$\dot{F}_k = \epsilon_k^\star : \dot{M} \tag{4.25}$$

where ϵ_k is the strain tensor of the kth mode evaluated at the source location. Equation 4.25 is easier to manipulate if we write out the double dot.
Let

$$\left.\begin{aligned}\psi_1 &= \dot{M}_{11} = \dot{M}_{rr} & e_1 &= \epsilon_{11} \\ \psi_2 &= \dot{M}_{22} = \dot{M}_{\theta\theta} & e_2 &= \epsilon_{22} \\ \psi_3 &= \dot{M}_{33} = \dot{M}_{\phi\phi} & e_3 &= \epsilon_{33} \\ \psi_4 &= \dot{M}_{12} = \dot{M}_{r\theta} & e_4 &= 2\epsilon_{12} \\ \psi_5 &= \dot{M}_{13} = \dot{M}_{r\phi} & e_5 &= 2\epsilon_{13} \\ \psi_6 &= \dot{M}_{23} = \dot{M}_{\theta\phi} & e_6 &= 2\epsilon_{23}\end{aligned}\right\} \tag{4.26}$$

then

$$\dot{F}_k = \sum_{i=1}^{6} e^{\star}_{ki}\psi_i \tag{4.27}$$

Thus, for a point source, 4.12 becomes

$$\mathbf{s}(\mathbf{r},\mathbf{r}_0,t) = \sum_k \frac{1}{\omega_k^2} s_k(\mathbf{r}) \left[\sum_{i=1}^{6} e^{\star}_{ki}(\mathbf{r}_0)\psi_i\right] \star C_k(t) \tag{4.28}$$

and our source is represented by the six numbers, ψ_i, which in general are functions of time. Note that, if the duration of the event is small, the moment tensor will have a step function behavior so the $\psi_i(t)$ will be δ-functions. The convolution in 4.28 can then be replaced by a product.

Equation 4.28 is our basic result and allows us to model seismic data at long periods (for even quite large events). For the largest events, we need more terms in the Taylor series expansion for $s^{\star}_k$. Indeed, if our fiducial point, x_0, is not the true location of the source, we can also generate an apparently complicated radiation pattern and equation 4.21 may not converge quickly. It is sometimes useful to vary the source location so that higher order terms are minimized. For example, if we write

$$\dot{F}_k = \frac{\partial s^{\star}_i}{\partial x_j}\dot{M}_{ij} + \tfrac{1}{2}\frac{\partial^2 s^{\star}_i}{\partial x_k \partial x_l}\dot{\tilde{M}}_{ikl} \tag{4.29}$$

where

$$\dot{\tilde{M}}_{ikl} = \frac{\partial M_{ilk}}{\partial t} - x_{0k}\frac{\partial M_{il}}{\partial t} - x_{0l}\frac{\partial M_{ik}}{\partial t}$$

then we might vary x_0 until the two-norm of $\dot{\tilde{M}}_{ikl}$ is minimized. The resulting value of x_0 which minimizes $||\dot{\tilde{M}}_{ijk}\dot{\tilde{M}}_{ijk}||$ is sometimes called the centroid location, [cf Dziewonski *et al.*, (1981) JGR, v86, p.2825].

Problem 4.1 Suppose you have estimated $\dot{M}_{ikl}$ and $\dot{M}_{il}$ from some seismic recordings for a particular value of x_0. Make an estimate of the centroid location which minimizes the two norm of $\dot{\tilde{M}}_{ijk}$. Compare your answer with the result given in the appendix of the Dziewonski *et al.*, ,1981 paper.

The procedure for finding a "centroid" location often moves an earthquake from the known location (e.g., as determined by surface faulting). Part of this may be due to the fact that low-frequency data "see" an average location of the whole rupture while a body-wave location (such as in the P.D.E.) is determined by the location of the onset of rupture. Another problem is that 3-D structure will map into the relocation and can also be confused with finite rupture propagation effects.

The moment tensor expansion technique of representing $\dot{F}_k$ becomes inefficient if we need many terms in the expansion. M_{ij} has 6 independent elements but M_{ijk} has 18 and M_{ijkl} has 30. The total number of unknowns specifying the mode excitation goes from 6 to 24 to 54. An alternative procedure is to specify a particular kind of rupture (e.g., a propagating line rupture) and calculate the moment tensors in terms of a few parameters specifying the rupture (e.g., rupture orientation and velocity). Backus 1977a,b [GJRAS, v51, p. 1–46] gives a thorough discussion of this.

4.3 Moment tensors and double couples . We work with a local cartesian coordinate system centered about a point in the source volume. We use $x_1 \equiv r$ (up), $x_2 \equiv \theta$ (South), and $x_3 \equiv \phi$ (East). Suppose we have a double-couple oriented in the 1-2 plane:

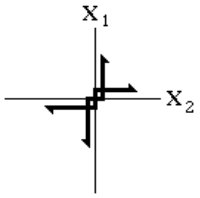

The moment tensor for this source looks like

$$M_{ij} = \begin{bmatrix} 0 & M_{12} & 0 \\ M_{21} & 0 & 0 \\ 0 & 0 & 0 \end{bmatrix}$$

where $M_{12} = M_{21} = M_0$ say. The eigenvalues of M_{ij} are $\pm M_0$ and 0. Generally, the double-couple will not be aligned with our coordinate system but if we rotate the source with a rotation matrix, we will not change the eigenvalues of the moment tensor. The orientation of a double-couple is specified by the orientation of the fault plane and the motion of one wall of the fault with respect to the other (the "slip" direction). The fault orientation is traditionally specified by the fault strike (σ), dip (δ) and slip (γ) angles. We can also specify it by the normal to the fault plane ($\hat{\mathbf{n}}$) and a unit vector in the direction of slip ($\hat{\mathbf{s}}$). If there is no gapping or interpenetration then

$$\hat{\mathbf{n}} \cdot \hat{\mathbf{s}} = 0$$

Consider the diagram below.

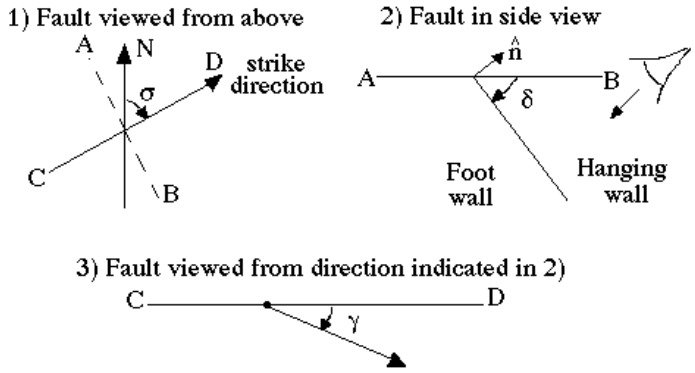

The angle between North and the trace of the fault on a horizontal surface is called the strike. The usual convention is that strike is measured positively clockwise from North with the fault dipping to the right. The dip of the fault is the angle the fault plane makes with a horizontal plane. This is measured positively down from the horizontal. A vertical fault plane has a dip of 90°. The slip of the fault has various conventions. It represents the motion of the hanging wall (the one on top) with respect to the foot wall (the one on the bottom) and is measured in the fault plane. The usual convention is to measure the slip direction anticlockwise from the horizontal strike direction. A normal fault then has a slip of 270°, a thrust fault has a slip of 90° and strike slip faults have slips of 0° or 180°.

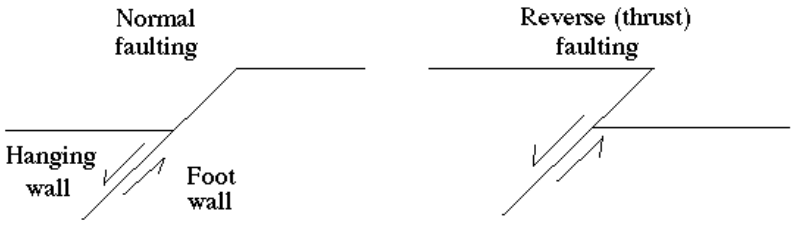

A little geometry gives

$$\begin{aligned} \hat{n}_1 &= \cos\delta \\ \hat{n}_2 &= \sin\delta\sin\sigma \\ \hat{n}_3 &= \sin\delta\cos\sigma \end{aligned}$$

We can also write $\hat{\mathbf{s}}$ in terms of the strike, dip and slip:

$$\begin{aligned}\hat{s}_1 &= -\sin\gamma\sin\delta \\ \hat{s}_2 &= -\cos\gamma\cos\sigma - \sin\gamma\cos\delta\sin\sigma \\ \hat{s}_3 &= \cos\gamma\sin\sigma - \sin\gamma\cos\delta\cos\sigma\end{aligned}$$

The equivalent force system for a double-couple is such that one force couple is oriented in the $\hat{\mathbf{n}}$ direction with the "moment arm" perpendicular to this in the $\hat{\mathbf{s}}$ direction. The other couple is oriented in the $\hat{\mathbf{s}}$ direction with its moment arm in the $\hat{\mathbf{n}}$ direction. As far as the radiation pattern is concerned, we can interchange $\hat{\mathbf{n}}$ and $\hat{\mathbf{s}}$ (or equivalently, the fault plane and auxilliary plane) with no change in the observed waveforms). Thus

$$M_{ij} = M_0(n_i s_j + s_i n_j)$$

gives the moment tensor elements equivalent to a double-couple.

Note that a double-couple requires four numbers $(M_0, \sigma, \delta, \gamma)$ to describe it whereas a general moment tensor has six independent numbers (remember that it is symmetric). We can therefore specify a more complicated source than a double-couple with the moment tensor. If the moment tensor is trace-free $(M_{11} + M_{22} + M_{33} = 0)$ as it is for a double-couple, it means that the radiation pattern has no isotropic component as would be generated by an explosive or implosive source. Natural sources do not seem to have a significant isotropic component so the condition that the moment tensor is trace-free is often imposed "a priori". This reduces the number of independent moment tensor elements to five (which is still more than that needed for a double-couple).

As we shall see, it is more convenient to solve for the five elements of $\mathbf{M}$ in a linear problem than to solve the non-linear problem for M_0, σ, δ and γ which specify the double-couple. The resulting moment tensor can be decomposed in a variety of ways. A convenient way of visualising the moment tensor solution is to decompose it into a 'major double-couple" and a "minor double-couple". If the moment tensor is already a double-couple, it has eigenvalues $(\lambda, 0, -\lambda)$. Generally this will not be true and we work with the trace-free (deviatoric) part of $\mathbf{M}$:

$$M_{ij} = \frac{1}{3}M_{kk}\delta_{ij} + D_{ij}$$

where, by construction, $\mathbf{D}$ is trace-free. We now decompose $\mathbf{D}$ into its eigenvalues and eigenvectors:

$$\mathbf{D} = \mathbf{U}\boldsymbol{\Lambda}\mathbf{U}^T$$

where $\boldsymbol{\Lambda}$ is a diagonal matrix of eigenvalues with

$$\boldsymbol{\Lambda} = (\lambda_1, \lambda_2, \lambda_3)$$

$$\text{and} \quad |\lambda_1| > |\lambda_2| > |\lambda_3|$$

$$\text{and} \quad \lambda_1 + \lambda_2 + \lambda_3 = 0$$

This last relationship follows because the trace of $\mathbf{D}$ is equal to the trace of $\boldsymbol{\Lambda}$. Now let

$$\boldsymbol{\Lambda}_1 = (\lambda_1, -\lambda_1, 0) \quad \text{and} \quad \boldsymbol{\Lambda}_3 = (0, -\lambda_3, \lambda_3)$$

so that $\boldsymbol{\Lambda} = \boldsymbol{\Lambda}_1 + \boldsymbol{\Lambda}_3$ and both $\boldsymbol{\Lambda}_1$ and $\boldsymbol{\Lambda}_3$ have the forms of double-couples. $\mathbf{D}$ can now be written

$$\mathbf{D} = \mathbf{U}\boldsymbol{\Lambda}_1\mathbf{U}^T + \mathbf{U}\boldsymbol{\Lambda}_3\mathbf{U}^T$$

where the first term on the right is the major double-couple and the second term is the minor double-couple. In nearly all cases, the major double-couple is a factor of ten or more greater than the minor double-couple.

If they are of similar magnitude, it is usually because the event is a multiple event (not a point source) or some blunder in the data handling has occurred.

The final step is to go from the eigenvalue/eigenvector decomposition of a double-couple to a description in terms of strike, dip and slip. We write out the explicit form of the moment tensor, $\mathbf{U\Lambda U}^T$, for either double-couple and compare with the expression in terms M_0, $\hat{\mathbf{n}}$ and $\hat{\mathbf{s}}$. Now $\lambda_2 = -\lambda_1 = -M_0$ and $\lambda_3 = 0$ and let $\mathbf{u}^1$ be the eigenvector associated with λ_1 and $\mathbf{u}^2$ be the eigenvector associated with λ_2. We then obtain

$$\hat{\mathbf{n}} = \frac{1}{\sqrt{2}}(\mathbf{u}^1 + \mathbf{u}^2)$$

$$\hat{\mathbf{s}} = \frac{1}{\sqrt{2}}(\mathbf{u}^1 - \mathbf{u}^2)$$

The right hand sides of these equation can be interchanged and the signs of both $\hat{\mathbf{n}}$ and $\hat{\mathbf{s}}$ can be flipped. We fix the sign by using the convention that dip (δ) lies between 0° and 90°. The relation $\hat{n}_1 = \cos\delta$ therefore means that $\hat{n}_1$ must be taken as positive. From the definitions of $\hat{\mathbf{n}}$ and $\hat{\mathbf{s}}$, we obtain

$$\tan\delta = \frac{\sqrt{1-\hat{n}_1^2}}{\hat{n}_1}$$

$$\tan\sigma = \frac{\hat{n}_2}{\hat{n}_3}$$

$$\tan\gamma = \frac{-\hat{s}_1}{\hat{s}_3\hat{n}_2 - \hat{s}_2\hat{n}_3}$$

Interchanging the expressions for $\hat{\mathbf{n}}$ and $\hat{\mathbf{s}}$ gives us first the strike, dip and slip of the fault plane and then the strike, dip and slip of the auxilliary plane. Of course, we can't distinguish between the fault and auxilliary planes unless we have additional information.

Sometimes we will have some information about the orientation of one of the planes of the double-couple. This information would typically be the strike and dip of the fault plane deduced from the local tectonics, or the strike and dip of one plane constrained by a fault plane solution. Given this information, we can compute $\hat{\mathbf{n}}$ and then write

$$\boldsymbol{\psi} = \begin{bmatrix} 2\hat{n}_1 & 0 & 0 \\ 0 & 2\hat{n}_2 & 0 \\ 0 & 0 & 2\hat{n}_3 \\ \hat{n}_2 & \hat{n}_1 & 0 \\ \hat{n}_3 & 0 & \hat{n}_1 \\ 0 & \hat{n}_3 & \hat{n}_2 \end{bmatrix} \begin{bmatrix} -\sin\delta & 0 \\ \cos\delta\sin\sigma & -\cos\sigma \\ \cos\delta\cos\sigma & \sin\sigma \end{bmatrix} \begin{bmatrix} M_0\sin\gamma \\ M_0\cos\gamma \end{bmatrix}$$

or

$$\boldsymbol{\psi} = \mathbf{N}\cdot\mathbf{x}$$

where $\mathbf{x} = (M_0\sin\gamma, M_0\cos\gamma)$ and $\boldsymbol{\psi}$ is the vector of the six elements of the moment tensor (see equation 4.26 below). $\mathbf{N}$ can be computed so $\boldsymbol{\psi}$ is now linearly related to $\mathbf{x}$ which can therefore be found by linear inversion of seismic data in the same way we solve for $\boldsymbol{\psi}$ below. From $\mathbf{x}$, we obtain M_0 and γ:

$$M_0 = |\mathbf{x}| \quad \text{and} \quad \tan\gamma = \frac{x_1}{x_2}$$

which completes the double-couple solution since we are given the strike and dip.

4.4 Greens function in epicentral coordinates . The evaluation of 4.28 is laborious and can be made much faster if we can assume the Earth is spherically symmetric. If this is valid, all $2l+1$ oscillations with the same n, l have the same frequency (i.e., $-l \leq m \leq l$) and we can perform the sum over m analytically. This is most efficiently done if we adopt an epicentral coordinate system with the epicenter at the pole. The advantage of this scheme is that e_k is zero in epicentral coordinates unless $m \leq 2$.

To make the angles we are using completely clear we consider the following spherical triangle:

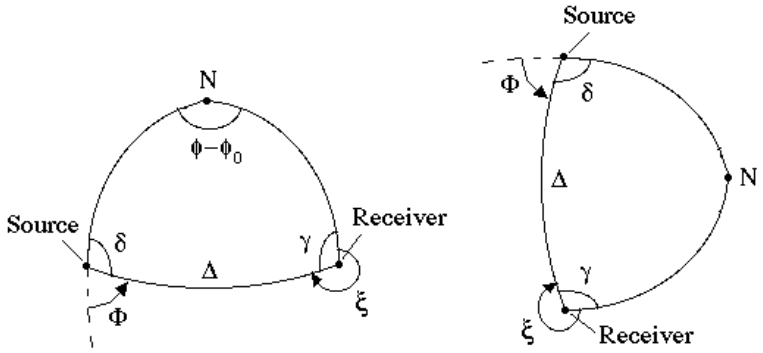

Δ is epicentral distance (colatitude), Φ is epicentral longitude, $\xi = 2\pi - \gamma$.

$$\begin{aligned}
\cos\Delta &= \cos\theta\cos\theta_0 + \sin\theta\sin\theta_0\cos(\phi-\phi_0)\\
\sin\Delta &= (1-\cos^2\Delta)^{\frac{1}{2}}\\
\sin\delta &= \sin\Phi = \sin(\phi-\phi_0)\sin\theta/\sin\Delta\\
\cos\delta &= -\cos\Phi = (\cos\theta - \cos\theta_0\cos\Delta)/(\sin\theta_0\sin\Delta)\\
\sin\xi &= -\sin(\phi-\phi_0)\sin\theta_0/\sin\Delta\\
\cos\xi &= (\cos\theta_0 - \cos\theta\cos\Delta)/(\sin\theta\sin\Delta)
\end{aligned}$$

(The source is at θ_0, ϕ_0 and the receiver is at θ, ϕ). We have given formulae for ξ (which is the azimuth of the source from the receiver measured clockwise from north) because we need it to rotate horizontal components. Consider the receiver

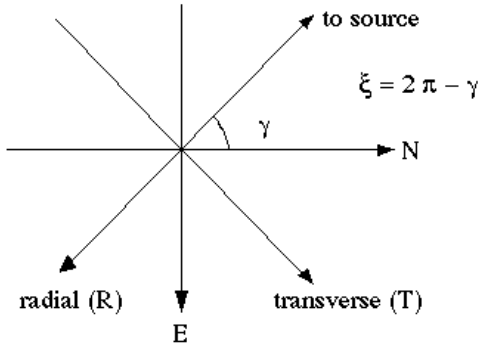

In epicentral coordinates, we shall be using radial and transverse coordinates (i.e., $\hat{\boldsymbol{\theta}}$ and $\hat{\boldsymbol{\phi}}$) but we measure North/South and East/West. A little algebra shows that

$$\begin{aligned}
A_{N-S} &= -\cos\xi\, A_{\hat{\boldsymbol{\theta}}} - \sin\xi\, A_{\hat{\boldsymbol{\phi}}}\\
A_{E-W} &= -\sin\xi\, A_{\hat{\boldsymbol{\theta}}} + \cos\xi\, A_{\hat{\boldsymbol{\phi}}}
\end{aligned}$$

where $A_{\hat{\boldsymbol{\theta}}}$ and $A_{\hat{\boldsymbol{\phi}}}$ are the components of displacement in the radial and transverse direction and A_{N-S},

A_{E-W} are the measured components.

[You sould remenber that θ in the above formulae is geocentric colatitude. Station locations, source locations, etc. are nearly always given in geographic colatitudes. The main difference arises because of the elliptical flattening of the Earth. An exaggerated sketch of the situation is given below.

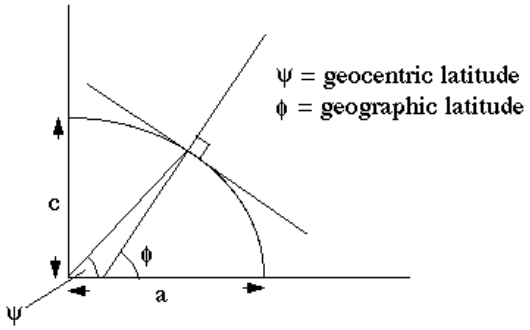

$$\tan\psi = (1-f)^2 \tan\phi$$

where f is the flattening of the Earth, i.e., $f = \frac{a-c}{a} = \frac{1}{298.256}$.]

We now rewrite equation 4.28 to make the sum over m explicit:

$$\mathbf{s}(\mathbf{r}, \mathbf{r}_0, t) = \sum_{n,l} \sum_{i=1}^{6} \left[\sum_{m=-l}^{l} {}_n\mathbf{s}_l^m(\mathbf{r})_n e_{li}^{m^\star} \right] \cdot \psi_i(t) \star \frac{1}{{}_n\omega_l^2}\, {}_nC_l(t) \tag{4.30}$$

where ${}_nC_l(t) = [1 - \cos {}_n\omega_l t]H(t)$.
Note that, for spheroidal modes

$${}_n\mathbf{s}_l^m(\mathbf{r}) = \hat{\mathbf{r}}\, {}_nU_r(r) Y_l^m(\Delta, \Phi) + {}_nV_l(r) \nabla_1 Y_l^m(\Delta, \Phi) \tag{4.31}$$

and, for toroidal modes

$${}_n\mathbf{s}_l^m(\mathbf{r}) = -\hat{\mathbf{r}} \times {}_nW_l(r) \nabla_1 Y_l^m(\Delta, \Phi) \tag{4.32}$$

The strain tensor in spherical polar coordinates is given by equation A22. It is a little tricky to find the limiting values of ϵ at the pole since there are several apparent singularities in equation A22. When ϵ is expressed in terms of generalized spherical harmonics, the value at the pole can be written down by inspection because of the property

$$Y_l^{N,m}(0,0) = \delta_{Nm}.$$

The result of taking this limit is given in Table A1. We now evaluate the sum in 4.30 for the vertical component of a spheroidal mode (the other components follow in a similar fashion). We consider each value of i separately (see equation 4.26).
$i = 1$ (rr component). Note that only $m = 0$ contributes.

$$\begin{aligned}\sum_{m=-l}^{l} {}_n\mathbf{s}_l^m(\mathbf{r})_n e_{l1}^{m^\star}(\mathbf{r}_0) =& \hat{\mathbf{r}}\, {}_nU_l(r_a) Y_l^0(\Delta) \frac{dU}{dr}(r_0) d_l^0 \\ =& \hat{\mathbf{r}}\, {}_nU_l(r_a) \frac{d_nU_l}{dr}(r_0) d_l^0 X_l^0\end{aligned}$$

(Note $Y_l^m = X_l^m e^{im\phi}$, $Y_l^{-m} = (-1)^m Y_l^{m^\star}$, r_a is the receiver radius, r_0 is the source radius, and $X_l^m = X_l^m(\Delta)$)

$i = 2$ ($\theta\theta$ component)

$$\begin{aligned}\sum_{m=-l}^{l} {}_n\mathbf{s}_l^m(\mathbf{r})_n e_{l2}^{m^\star}(\mathbf{r}_0) =&\hat{\mathbf{r}}_n U_l(r_a)\left[\frac{F}{2}d_l^0 X_l^0 + \frac{V}{r_0}d_l^2 X_l^{-2}e^{-2i\Phi} + \frac{V}{r_0}d_l^2 X_l^2 e^{2i\Phi}\right]\\ =&\hat{\mathbf{r}}_n U_l(r_a)\left[\frac{F}{2}d_l^0 X_l^0 + \frac{2V}{r_0}d_l^2 X_l^2\cos 2\Phi\right]\end{aligned}$$

$i = 3$ ($\phi\phi$ component)

$$\begin{aligned}\sum_{m=-l}^{l} {}_n\mathbf{s}_l^m(\mathbf{r})_n e_{l3}^{m^\star}(\mathbf{r}_0) =&\hat{\mathbf{r}}_n U_l(r_a)\left[\frac{F}{2}d_l^0 X_l^0 - \frac{V}{r_0}d_l^2 X_l^{-2}e^{-2i\Phi} - \frac{V}{r_0}d_l^2 X_l^2 e^{2i\Phi}\right]\\ =&\hat{\mathbf{r}}_n U_l(r_a)\left[\frac{F}{2}d_l^0 X_l^0 - \frac{2V}{r_0}d_l^2 X_l^2\cos 2\Phi\right]\end{aligned}$$

$i = 4$ ($r\theta$ component)

$$\begin{aligned}\sum_{m=-l}^{l} {}_n\mathbf{s}_l^m(\mathbf{r})_n e_{l4}^{m^\star}(\mathbf{r}_0) =&\hat{\mathbf{r}}_n U_l(r_a)[\mathrm{X}d_l^1 X_l^{-1}e^{-i\Phi} - \mathrm{X}d_l^1 X_l^1 e^{i\Phi}]\\ =&-\hat{\mathbf{r}}_n U_l(r_a)2\mathrm{X}d_l^1 X_l^1\cos\Phi\end{aligned}$$

where $\mathrm{X} = \frac{dV}{dr} + \frac{U-V}{r}$

$i = 5$ ($r\phi$ component)

$$\begin{aligned}\sum_{m=-l}^{l} {}_n\mathbf{s}_l^m(\mathbf{r})_n e_{l5}^{m^\star}(\mathbf{r}_0) =&\hat{\mathbf{r}}_n U_l(r_a)[i\mathrm{X}d_l^1 X_l^{-1}e^{-i\Phi} + i\mathrm{X}d_l^1 X_l^1 e^{i\Phi}]\\ =&\hat{\mathbf{r}}_n U_l(r_a)\mathrm{X}d_l^1 X_l^1[-ie^{-i\Phi} + ie^{i\Phi}]\\ =&-\hat{\mathbf{r}}_n U_l(r_a)2\mathrm{X}d_l^1 X_l^1\sin\Phi\end{aligned}$$

$i = 6$ ($\theta\phi$ component)

$$\begin{aligned}\sum_{m=-l}^{l} {}_n\mathbf{s}_l^m(\mathbf{r})_n e_{l6}^{m^\star}(\mathbf{r}_0) =&\hat{\mathbf{r}}_n U_l(r_a)\left[\frac{2iV}{r_0}d_l^2 X_l^{-2}e^{-2i\Phi} - \frac{2iV}{r_0}d_l^2 X_l^2 e^{2i\Phi}\right]\\ =&\hat{\mathbf{r}}_n U_l(r_a)d_l^2 X_l^2\frac{4V}{r_0}\sin 2\Phi\end{aligned}$$

In these formulae, $F[= (2U - l(l+1)V)/r]$, X and V should all be evaluated at the source depth, r_0. Summarizing results for all components gives

$$ {}_n\mathbf{G}_l^i = \sum_{m=-l}^{l} {}_n\mathbf{s}_l^m(\mathbf{r})_n e_{li}^{m^\star}(\mathbf{r}_0) = \hat{\mathbf{r}}_n U_l(r_a)g_i + {}_nV_l(r_a)\nabla_1 g_i - \hat{\mathbf{r}}\times {}_nW_l(r_a)\nabla_1 h_i \tag{4.33}$$

with

$$\left.\begin{array}{cc} g_1 = \frac{dU}{dr} d_l^0 X_l^0 & h_1 = 0 \\ g_2 = \frac{F}{2} d_l^0 X_l^0 + \frac{2V}{r_0} d_l^2 X_l^2 \cos 2\Phi & h_2 = \frac{2W}{r_0} d_l^2 X_l^2 \sin 2\Phi \\ g_3 = \frac{F}{2} d_l^0 X_l^0 - \frac{2V}{r_0} d_l^2 X_l^2 \cos 2\Phi & h_3 = -\frac{2W}{r_0} d_l^2 X_l^2 \sin 2\Phi \\ g_4 = -2\mathrm{X} d_l^1 X_l^1 \cos\Phi & h_4 = -2Z d_l^1 X_l^1 \sin\Phi \\ g_5 = -2\mathrm{X} d_l^1 X_l^1 \sin\Phi & h_5 = 2Z d_l^1 X_l^1 \cos\Phi \\ g_6 = \frac{4V}{r_0} d_l^2 X_l^2 \sin 2\Phi & h_6 = -\frac{4W}{r_0} d_l^2 X_l^2 \cos 2\Phi \end{array}\right\} \tag{4.34}$$

and

$$\mathbf{s}(\mathbf{r}, \mathbf{r}_0, t) = \sum_{n,l} \sum_{i=1}^{6} {}_n\mathbf{G}_l^i(\mathbf{r}, \mathbf{r}_0) \psi_i(t) \star \frac{1}{{}_n\omega_l^2} {}_nC_l(t) \tag{4.35}$$

Note that, given a model of the Earth, we can compute everything in this formula except for ψ. ψ is determined by the moment tensor so we can compute synthetic seismograms given a source mechanism.

[Note that

$$d_l^k X_l^k = \frac{1}{2^k} \left(\frac{2l+1}{4\pi} \right) P_l^k(\cos\theta)$$

and can easily be computed using the recursion over l for the P_l^k's (see Appendix B). This is efficient since we usually need all l values up to some maximum l and only a few low values of k ($k \leq 2$ for a point source). In the literature, you will also find the excitations expressed in terms of b_l^k instead of d_l^k and these are related by $d_l^k = (-1)^k k! \mathrm{b}_l^k$ – see equation B21 in appendix B for the definition of b_l^k.]

Equation 4.35 gives us the displacement field at some measurement location, $\mathbf{r}$, but this is not what we actually measure with a seismometer. We now consider the response of a seismometer in more detail.

4.5 Response of a seismometer . Most seismographs are accelerometers and one might expect that all we would have to do is to multiply 4.35 by $-\omega_k^2$ and we would have the acceleration for an oscillation of the form $\mathbf{s}_k e^{i\omega_k t}$. This is not strictly true. When there is vertical motion, the seismometer is moving in a gravity field and tilt occurs. Furthermore, the mode of oscillation itself perturbs the gravitational field and so modifies the acceleration at the recording site (this latter effect is only important at very low frequencies).

We sketch the situation as follows

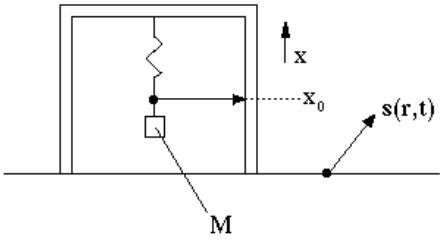

The local Earth displacement is $\mathbf{s}(\mathbf{r}, t)$. The rest position of the seismometer is x_0 and the mass moves an amount x relative to the housing the the instrument. We measure x or, in a fed-back system, the force that must be applied to M to keep M motionless with respect to the housing. We consider the seismometer as a damped oscillator with damping constant γ and natural frequency ω_0. Let $\hat{\mathbf{p}}$ be the polarization vector of the seismometers (e.g., $\hat{\mathbf{p}} = \hat{\mathbf{r}}$ for a vertical component instrument). The total force per unit mass acting on M is given by

$$\hat{\mathbf{p}} \cdot \ddot{\mathbf{s}} + \ddot{x} + \gamma\dot{x} + \omega_0^2(x - x_0) \equiv \hat{\mathbf{p}} \cdot \mathbf{a} \tag{4.36}$$

$\mathbf{a}$ is the "acceleration due to gravity", *i.e.*,

$$\mathbf{a} = -\nabla\phi$$

$$\phi = \phi_0 + \phi_1 + \phi_E \cdots$$

ϕ_E is an external tidal potential but we shall neglect this (since the tides are usually removed from the seismic recordings before processing) and consider ϕ as a sum of the unperturbed gravitational potential, ϕ_0, and the perturbation in ϕ_0 due to the motion, ϕ_1.

Remember that $\nabla\phi_0 = \hat{\mathbf{r}} g_0(r)$, so that in the rest position when $\mathbf{s}$ and ϕ_1 are zero we have

$$-\omega_0^2 x_0 = -\hat{\mathbf{p}}_0 \cdot \hat{\mathbf{r}} g_0(r_a) \tag{4.37}$$

and $\hat{\mathbf{p}}_0$ is the undisturbed polarization vector (remember, we shall have to worry about tilt). r_a is the (undisturbed) radius of the instrument. Equation 4.36 becomes

$$\hat{\mathbf{p}} \cdot \ddot{\mathbf{s}} + \ddot{x} + \gamma\dot{x} + \omega_0^2 x = -\hat{\mathbf{p}} \cdot \hat{\mathbf{r}} g_0(r) + \hat{\mathbf{p}}_0 \cdot \hat{\mathbf{r}} g_0(r_a) - \hat{\mathbf{p}} \cdot \nabla\phi_1$$

r is the instantaneous position of the housing, *i.e.*,

$$r = r_a + \hat{\mathbf{r}} \cdot \mathbf{s}$$

Now we let

$$g_0(r) \simeq g_0(r_a) + \frac{\partial g_0}{\partial r}(r_a)(\hat{\mathbf{r}} \cdot \mathbf{s})$$

so that

$$\ddot{x} + \gamma\dot{x} + \omega_0^2 x = -\hat{\mathbf{p}} \cdot \ddot{\mathbf{s}} - (\hat{\mathbf{p}} - \hat{\mathbf{p}}_0) \cdot \hat{\mathbf{r}} g_0(r_a) - \hat{\mathbf{p}} \cdot \hat{\mathbf{r}} \frac{\partial g_0}{\partial r}(r_a)(\hat{\mathbf{r}} \cdot \mathbf{s}) - \hat{\mathbf{p}} \cdot \nabla\phi_1 \tag{4.38}$$

$\hat{\mathbf{r}} \cdot \mathbf{s}$ varies laterally so there is tilting of the instrument (in general) and this then is given by $\hat{\mathbf{p}} - \hat{\mathbf{p}}_0$.

Consider equation 4.38 for a vertically polarized seismometer, *i.e.*, $\hat{\mathbf{p}} = \hat{\mathbf{r}}$ so (using equation 2.20)

$$\hat{\mathbf{p}} - \hat{\mathbf{p}}_0 = -\frac{1}{r_a}\nabla_1(\hat{\mathbf{r}} \cdot \mathbf{s})$$

and thus

$$\ddot{x} + \gamma\dot{x} + \omega_0^2 x = -\ddot{s}_r - \frac{\partial g_0}{\partial r}(r_a) s_r - \frac{\partial \phi_1}{\partial r}(r_a) \tag{4.39}$$

(Note ∇_1 is perpendicular to $\hat{\mathbf{r}}$ so that the tilt term goes away.) For a horizontally polarized seismometer, we let s_t denote the displacement in the $\hat{\mathbf{t}}$ direction. Then from 4.38 and 2.21

$$\ddot{x} + \gamma\dot{x} + \omega_0^2 x = -\ddot{s}_t - \frac{1}{r_a}(\hat{\mathbf{t}} \cdot \nabla_1 s_r) g_0(r_a) - \frac{\hat{\mathbf{t}}}{r_a} \cdot \nabla_1 \phi_1 \tag{4.40}$$

The right hand side of 4.39 and 4.40 is a direct measure of the force (per unit mass) on the seismometer and so is proportional to what is actually measured in a fed-back system. For a vertical component, we have (in addition to the acceleration of the Earth's surface) the effect of movement in a gravity gradient and an effect due to the redistribution of mass due to the motion. For a horizontal component we have an effect due to tilt and also an effect due to redistribution of mass.

We now consider the right hand side of 4.39 and 4.40 for a particular mode of oscillation of the Earth. Since we are on the surface of the Earth, ϕ_1 satisfies Lapaces equation, so

$$\phi_1(r) = \phi_1(r_a)\left(\frac{r_a}{r}\right)^{l+1}$$

and also

$$\frac{dg_0}{dr}(r_a) = -\frac{2g_0}{r_a}.$$

Equation 4.39 now reads

$$-\ddot{s}_r - \frac{\partial g_0}{\partial r}(r_a)s_r - \frac{\partial \phi_1}{\partial r}(r_a) = \omega_k^2 s_r + \frac{2g_0}{r_a}s_r + \frac{l+1}{r_a}\phi_1(r_a) \tag{4.41}$$

This is valid at the surface. A buried seismometer where $\rho_0(r_a) \neq 0$ has a response like

$$\omega_k^2 s_r + \frac{2g_0(r_a)}{r_a}s_r - \left[\frac{d\phi_1}{dr} + 4\pi G\rho_0(r_a)s_r\right]$$

Inspection of 4.41 shows that, if the radial component of displacement is given by $\hat{\mathbf{r}}_n U_l(r_a)Y_l^m$ times an excitation factor, an accelerometer will measure $\hat{\mathbf{r}}_n AU_l Y_l^m$ times an excitation factor, where

$${}_nAU_l = {}_n\omega_l^2\,{}_nU_l(r_a) + \frac{2g_0(r_a)}{r_a}{}_nU_l(r_a) + \frac{l+1}{r_a}{}_n\Phi_{1l}(r_a) \tag{4.42}$$

or

$$AU = AU_1 + AU_2 + AU_3 \quad \text{say}$$

Here is a table of values:

mode	AU_1/AU	AU_2/AU	AU_3/AU	ω mHz
${}_0S_2$	.815	.667	-.482	.309
${}_0S_{10}$	.983	.025	-.008	1.726
${}_8S_1$	.991	.009	–	2.871

It is only at very low frequencies that we make a significant error if we neglect AU_2 and AU_3.

For the horizontal component of a spheroidal mode, the displacement is proportional to ${}_nV_l(r_a)\hat{\mathbf{t}}\cdot\nabla_1 Y_l^m$ and the right hand side of 4.40 can be written

$$\hat{\mathbf{t}}\cdot[\omega_k^2\mathbf{s} - \frac{1}{r_a}\nabla_1 s_r g_0(r_a) - \frac{1}{r_a}\nabla_1\phi_1]$$

$$= \hat{\mathbf{t}}\cdot[\omega_k^2\,{}_nV_l - \frac{{}_nU_l}{r_a}g_0 - \frac{1}{r_a}{}_n\Phi_{1l}]\nabla_1 Y_l^m$$

so that we measure on acceleration times an excitation vector where the acceleration scalar, ${}_nAV_l$, is given by

$${}_nAV_l = \omega_k^2\,{}_nV_l - \frac{{}_nU_l}{r_a}g_0 - \frac{1}{r_a}{}_n\Phi_{1l} \tag{4.43}$$

or

$$AV = AV_1 + AV_2 + AV_3$$

A table of values:

mode	AV_1/AV	AV_2/AV	AV_3/AV	ω mHz
${}_0S_2$	-.118	2.133	-1.015	.309
${}_0S_{10}$	.868	.140	-.008	1.726
${}_8S_1$	1.045	-.045	–	2.871

Note the relatively drastic effect of tilt on the measured acceleration of ${}_0S_2$ – this is largely because the frequency is so low that the AV_2 and AV_3 become relatively more important.

Finally we note that a toroidal mode has no vertical motion and no tilting and does not disturb the gravitational field. The acceleration scalar for a toroidal mode is therefore

$$AW =_n \omega_l^2 {}_nW_l(r_a)$$

4.6 Source retrieval . When we measure acceleration, 4.35 becomes

$$\mathbf{a}(\mathbf{r}, \mathbf{r}_0, t) = \sum_{n,l} \sum_{i=1}^{6} {}_n\mathbf{G}_l^i(\mathbf{r}, \mathbf{r}_0)\psi_i(t) \star \frac{1}{{}_n\omega_l^2} {}_nC_l(t) \tag{4.44}$$

where (4.32) now becomes modified to read

$${}_n\mathbf{G}_l^i = \hat{\mathbf{r}}\, {}_nAU_l(r_a)g_i + {}_nAV_l(r_a)\nabla_1 g_i - \hat{\mathbf{r}} \times {}_nAW_l(r_a)\nabla_1 h_i$$

Before we can use 4.44 to model real data, we must include the effect of attenuation. We calculate this effect using perturbation theory. From chapter 2, we found that a linear viscoelastic medium with weak, nearly frequency independent attenuation has "elastic" moduli which can be written, e.g.,

$$\mu(\omega) = \mu_0(\omega_r)\left[1 + \frac{2}{\pi Q_\mu} \ln\left(\frac{\omega}{\omega_r}\right) + \frac{i}{Q_\mu}\right]$$

where ω_r is a reference frequency. We are currently interested in the small imaginary perturbation, ***i.e.***,

$$\mu \to \mu + \delta\mu \quad \text{where} \quad \delta\mu = \frac{i\mu_0}{Q_\mu} \tag{4.45}$$

As we shall show in later sections, this results in a perturbation to the squared frequency of the mode, ***i.e.***,

$$\omega_k^2 \to \omega_k^2 + \delta(\omega_k^2)$$

In this case, $\delta(\omega_k^2)$ is purely imaginary, so by analogy with 4.45, we write

$$\frac{\delta(\omega_k^2)}{\omega_k^2} = \frac{i}{Q_k}$$

where Q_k is the Q of the kth mode. We rearrange this to give

$$\delta\omega_k = \frac{i\omega_k}{2Q_k} = i\alpha_k$$

so

$$\omega_k \to \omega_k + i\alpha_k \quad \text{with} \quad \alpha_k = \frac{\omega_k}{2Q_k} \tag{4.46}$$

Later on, we shall see how to compute Q_k given Q_μ as a function of depth (and frequency) inside the Earth. For now, we assume this has been done so that any oscillatory motion, $e^{i\omega_k t}$, now acquires an exponetial decay factor, $e^{-\alpha_k t}$. Equation 4.44 can now be modified to include this by modifying ${}_nC_l(t)$ so that

$${}_nC_l(t) = [1 - \cos({}_n\omega_l t)e^{-{}_n\alpha_l t}]H(t) \tag{4.47}$$

Suppose we are given a model of the Earth. Inspection of 4.44 shows that we can calculate everything but $\psi_i(t)$ – the source mechanism.
Define

$$\mathbf{B}_i(\mathbf{r}, \mathbf{r}_0, t) = \sum_{n,l} \frac{1}{{}_n\omega_l^2} {}_n\mathbf{G}_l^i(\mathbf{r}, \mathbf{r}_0)_n C_l(t) \tag{4.48}$$

so equation 4.44 reads

$$\mathbf{a}(\mathbf{r}, \mathbf{r}_0, t) = \sum_{i=1}^{6} \mathbf{B}_i(\mathbf{r}, \mathbf{r}_0, t) \star \psi_i(t) \tag{4.49}$$

If we now denote a single component of recording for the $(\mathbf{r}, \mathbf{r}_0)$ source-receiver pair by the index j and Fourier transform 4.49, we obtain

$$a_j(\omega) = \sum_{i=1}^{6} B_{ij}(\omega)\psi_i(\omega) \tag{4.50}$$

which is a parameter-estimation problem for the unknown vector ψ_i. Note that if $\psi_i(t)$ is δ-like in time then ψ_i will be nearly independent of frequency. In practice, we often assume that all elements of ψ_i have the same time dependence, *i.e.*,

$$\psi_i(t) = \psi_i s(t) \tag{4.51}$$

Furthermore, the exact shape of $s(t)$ has only a weak effect on the shape of the long-period spectrum. We usually use a triangle function

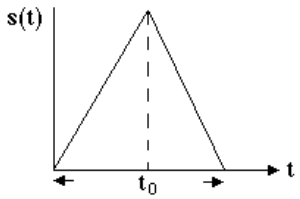

The triangle is the convolution of a boxcar of length $t_0/2$ with itself and the spectrum of a boxcar is just

$$\begin{aligned}
\int_0^{t_0/2} e^{-i\omega t}\, dt &= \left[-\frac{1}{i\omega} e^{-i\omega t}\right]_0^{t_0/2} = \frac{1}{i\omega} - \frac{1}{i\omega} e^{-i\omega t_0/2} \\
&= \frac{2e^{-i\omega t_0/4}}{2i\omega}[e^{i\omega t_0/4} - e^{-i\omega t_0/4}] \\
&= \frac{2e^{-i\omega t_0/4}}{\omega} \sin\frac{\omega t_0}{4} = \frac{t_0}{2} e^{-i\omega t_0/4} \operatorname{sinc}(\frac{\omega t_0}{4})
\end{aligned}$$

The spectrum of a triangle function is just the square of this, *i.e.*,

$$s(\omega) = \frac{t_0^2}{4} e^{-i\omega t_0/2} \operatorname{sinc}^2(\frac{\omega t_0}{4}) \tag{4.52}$$

The important factor in 4.52 is the apparent origin shift of $e^{-i\omega t_0/2}$ (the sinc^2 term is very slowly varying at low frequencies for all but the largest events). This effect can sometimes be seen in the data for big events if a body-wave determined origin time is used in the calculations. The low frequency energy "sees" a later time than the body waves as the relevant periods are longer than the rupture time and so see an average of the whole rupture. In contrast, the P-wave origin time corresponds to the onset of rupture.

One way to proceed is to make a guess of t_0, compute $s(\omega)$ then include this effect in $B_{ij}(\omega)$. We may then solve 4.50 for 6 frequency-independent numbers. t_0 may be varied until the best fit to the data is achieved.

A reasonable question is: How much information do we need to be able to solve 4.50 for ψ_i? If ψ_i is frequency independent then it might be thought that we only need six extimates of $a(\omega)$ at a single recording for six different frequencies to get a solution. This is not quite true. Inspection of 4.34 shows that, for a particular station, g_i is made up of a linear combination of four functions: $(\frac{dU}{dr}d_l^0 X_l^0,\ \frac{F}{2}d_l^0 X_l^0,\ \frac{V}{r_0}d_l^2 X_l^2,$ $\mathrm{X}d_l^1 X_l^1)$ so that B_{ij} will be rank deficient if we have only one recording. This deficiency will be formally removed if we have two vertical component recordings at different epicentral longitudes or two out of three components of recording at a single station. In practice we need 5 or 6 well-distributed stations to get well-constrained solutions and, even then, ambiguities will arise for certain kinds of events. A particular problem arises with "shallow" events ("shallow" being a relative term which is related to the vertical wavelength of a mode). The fourth and fifth components of g_i and h_i are proportional to the $\epsilon_{r\theta}$ and $\epsilon_{r\phi}$ strains (cf. 4.34). These strains are related through the shear modulus to the horizontal tractions which are required to be zero at the free surface. We therefore anticipate that the fourth and fifth columns of B_{ij} will be much smaller than the others for shallow events. This means that ψ_4 and ψ_5 do not contribute to the observed seismic energy for such events and so cannot be recovered. This is an important problem if we are interested in the source (e.g., its total moment) but is less important if we are only concerned with modeling the seismic data.

Problem 4.2

Assume that the source is a double-couple and is a shallow thrust event (slip angle = 270°). Your procedure for estimation of ψ gives you the solution with $||\psi||$ minimized. Explain why your answer has a dip angle of 45° and the smallest possible moment. If you know that the dip angle is about 20° , by how much should your estimate of moment be increased?

Usually when we fit for the moment tensor elements, we assume that the source is deviatoric and so apply the constraint that $M_{rr} + M_{\theta\theta} + M_{\phi\phi} = 0$. We can also apply a "plane constraint" if the source is a double-couple and the strike and dip of one plane is known (e.g., from a fault-plane solution).

We conclude this discussion of source retrieval by considering some of the reasons why solution of 4.50 may not allow us to fit the data as well as we would like. One obvious cause of misfit is noise. At low frequencies, small earthquakes are incapable of exciting large amplitudes and there will be little visible signal. We usually work in the 2–6 mHz band and find that we can successfully retrieve source mechanisms for events with moments greater than about 10^{26} dyne cm ($M_S \geq 6.5$). We find that the percentage variance reduction is independent of source size for events above $2 - 3 \times 10^{26}$ dyne cm so that the true noise is not the cause of misfit. The "noise" is actually scaling with the size of the event and so is "signal generated noise" – a euphemism for unmodeled signal. This unmodeled signal is mainly due to 3-D structure. You already know that apparent center frequencies of modes vary from great-circle to great-circle and will only occasionally agree with the frequency predicted by the model. Inspection of 4.50 shows that both $\mathbf{B}$ and $\mathbf{a}$ are "spikey." Schematically, we have

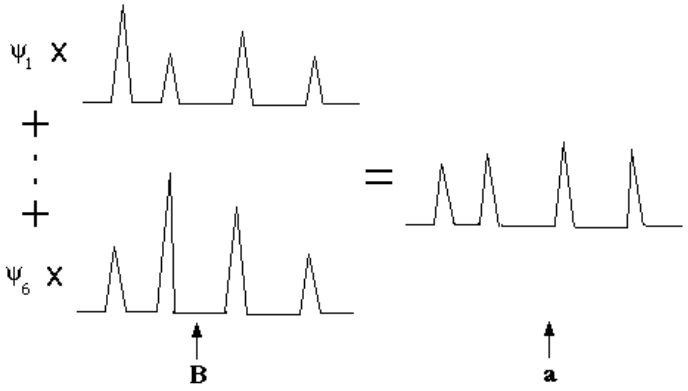

Given the fact that the spikes are not going to be perfectly aligned, we should expect that our solution will be biased to small moment (*i.e.*, we always end up fitting to the flanks of peaks). This is indeed the case

and adjusting the solution to match the power in the data usually results in about a 10% increase in moment (source orientation seems to be relatively unaffected).

There are other sources of error. For the largest events, we expect that the effects of finite rupture and source mislocation will be important. These effects are very similar to the effects of 3-D structure and consequently it is difficult to see details of the rupture process. Better Greens functions computed for good 3-D models will be required before details of the earthquake source can be divined from long-period data.

Even with spherical Earth Greens functions, we can often achieve a 70% variance reduction and produce precise synthetic seismograms (see Fig. 1, chapter 1). It appears to be true that all deep events (≥ 400 km) are extremely well fit while only about half the shallow events show good variance reductions. The reason for this remains obscure.

4.7 Perturbation theory – spherical Earth . In this section we consider what happens when we perturb our Earth model. Eventually we shall consider the effect of a general perturbation but, for now, we shall restrict attention to perturbations which are spherically symmetric. In particular, the theory will allow us to compute the attenuation rate of a mode but it will also allow us to iteratively improve spherical Earth models to fit observations of mode frequencies.

We consider the effect of a perturbation in elastic properties and density. Our operator $\mathbf{L}$ becomes perturbed as does the displacement field and frequency, *i.e.*,

$$\begin{aligned}
\mathbf{L} &\to \mathbf{L} + \delta\mathbf{L} \\
\rho_0 &\to \rho_0 + \delta\rho_0 \\
\phi_0 &\to \phi_0 + \delta\phi_0 \\
\mathbf{s}_k &\to \mathbf{s}_k + \delta\mathbf{s}_k \\
\phi_{1k} &\to \phi_{1k} + \delta\phi_{1k} \\
\omega_k^2 &\to \omega_k^2 + \delta\omega_k^2
\end{aligned}$$

and our unperturbed solution satisfies equation 4.2:

$$\mathbf{L}(\mathbf{s}_k) + \rho_0\omega_k^2\mathbf{s}_k = 0$$

For now, we consider only perturbations such that the perturbed field satisfies all the boundary condition. Since $\mathbf{s}_k$ satisfies the boundary conditions, it follows that $\delta\mathbf{s}_k$ satisfies the boundary conditions and we use the result from section 3.9

$$-\omega_k^2 \int_V \rho_0 \mathbf{s}_k^\star \cdot \mathbf{s}_k \, dV = \int_V \mathbf{s}_k^\star \mathbf{L}(\mathbf{s}_k) \, dV \tag{4.53}$$

To first-order in the small perturbation we have

$$\begin{aligned}
-\omega_k^2 \int_V \rho_0 \mathbf{s}_k^\star \cdot \mathbf{s}_k \, dV - \delta\omega_k^2 \int_V \rho_0 \mathbf{s}_k^\star \cdot \mathbf{s}_k \, dV - \omega_k^2 \int_V \delta\rho_0 \mathbf{s}_k^\star \cdot \mathbf{s}_k \, dV \\
- \omega_k^2 \int_V \rho_0 \delta\mathbf{s}_k^\star \cdot \mathbf{s}_k \, dV - \omega_k^2 \int_V \rho_0 \mathbf{s}_k^\star \cdot \delta\mathbf{s}_k \, dV \\
= \int_V \mathbf{s}_k^\star \mathbf{L}(\mathbf{s}_k) \, dV + \int_V \mathbf{s}_k^\star \delta\mathbf{L}(\mathbf{s}_k) \, dV + \int_V \mathbf{s}_k^\star \mathbf{L}(\delta\mathbf{s}_k) \, dV + \int_V \delta\mathbf{s}_k^\star \mathbf{L}(\mathbf{s}_k) \, dV
\end{aligned} \tag{4.54}$$

Using 4.2, 4.53 and the self-adjointness of the operator $\mathbf{L}$, *i.e.*,

$$\int_V \mathbf{s}_k^\star \mathbf{L}(\delta\mathbf{s}_k) \, dV = \int_V \delta\mathbf{s}_k \mathbf{L}(\mathbf{s}_k^\star) \, dV$$

we end up with

$$\delta\omega_k^2 \int_V \rho_0 \mathbf{s}_k^\star \cdot \mathbf{s}_k \, dV = \int_V \mathbf{s}_k^\star \delta\mathbf{L}(\mathbf{s}_k) \, dV + \omega_k^2 \int_V \delta\rho_0 \mathbf{s}_k^\star \cdot \mathbf{s}_k \, dV \tag{4.55}$$

Equation 4.55 is our basic result. Note that it does not depend upon $\delta\mathbf{s}_k$ so, given $\delta\rho_0$, $\delta\mu$ and $\delta\kappa$ (so that $\delta\mathbf{L}$ may be computed) we can find $\delta\omega_k^2$. Equation 4.55 is not yet in a computationally useful form. We proceed by using the vector spherical harmonic representation of the displacement field of a toroidal or spheroidal mode:

$$\mathbf{s}_{k_{Toroidal}} = -\hat{\mathbf{r}} \times W \nabla_1 Y_l^m$$

$$\mathbf{s}_{k_{Spheroidal}} = \hat{\mathbf{r}} U Y_l^m + V \nabla_1 Y_l^m$$

where U, V and W are functions of radius for each mode. We can substitute these forms into equation 4.55 and perform the integrals over θ and ϕ analytically. Not surprisingly, we find that (for a spherical perturbation) the result is independent of the azimuthal order number, m. We are left with integrals over radius:

$$\delta\omega_k^2 \int_0^a \rho_0 N r^2 \, dr = \int_0^a \left[K' \delta\kappa + M' \delta\mu + R\delta\rho_0 \right] r^2 \, dr \tag{4.56}$$

where, for spheroidal modes:

$$N = U^2 + l(l+1)V^2$$

$$K' = \left(\frac{dU}{dr} + F \right)^2$$

$$M' = \tfrac{1}{3} \left(2\frac{dU}{dr} - F \right)^2 + \frac{l(l+1)}{r^2} \left(r\frac{dV}{dr} - V + U \right)^2 + \frac{1}{r^2}(l+2)(l-1)l(l+1)V^2$$

$$R = 2U \left(\frac{d\phi_1}{dr} + 4\pi G U \rho_0 - F\frac{d\phi_0}{dr} \right) + \frac{2}{r} V \phi_1 l(l+1) - \int_r^a 8\pi G \rho_0 U F \, dr - \omega_k^2 N$$

and, for toroidal modes:

$$N = l(l+1)W^2$$

$$K' = 0$$

$$M' = \frac{l(l+1)}{r^2} \left(r\frac{dW}{dr} - W \right)^2 + \frac{1}{r^2}(l+2)(l-1)l(l+1)W^2$$

$$R = -\omega_k^2 N$$

(Note that $d\phi_0/dr = g_0$). Equation 4.56 is our result but before we go on to use it, let us reconsider perturbation theory for the simple Sturm-Liouville problem that we set in section 3.7. This is already in terms of the radial eigenfunctions so we can derive the toroidal part of equation 4.56 very simply. We have

$$L(y) = (py')' - qy = -\lambda\tilde{\rho}y$$

where $y = W/r$, $p = \mu r^4$, $q = \mu r^2(l+2)(l-1)$, $\tilde{\rho} = \rho_0 r^4$, and $\lambda = \omega_k^2$. L is self-adjoint, *i.e.*,

$$\int y_i L(y_j) \, dr = \int y_j L(y_i) \, dr$$

Now

$$\int_A^B yL(y)\,dr = \int_A^B y(py')'\,dr - \int_A^B qy^2\,dr = [ypy']_B^A - \int_A^B \left[p(y')^2 + qy^2\right]\,dr \tag{4.57}$$

Now py' is proportional to the horizontal traction which must be zero at both boundaries for a mode solution. Thus 4.57 becomes

$$\int_A^B yL(y)\,dr = -\int_A^B \left[p(y')^2 + qy^2\right]\,dr = -\lambda \int_A^B \tilde{\rho} y^2\,dr \tag{4.58}$$

This we obtain on substitution of the original variables:

$$\omega_k^2 \int \rho_0 W^2 r^2\,dr = \int \left[\mu r^2 \left(\frac{dW}{dr} - \frac{W}{r}\right)^2 + \mu(l+2)(l-1)W^2\right]\,dr \tag{4.59}$$

Now from 4.55 we can write

$$-\delta\omega_k^2 \int \tilde{\rho} y_k^2\,dr = \int y_k \delta L(y_k)\,dr + \omega_k^2 \int \delta\tilde{\rho} y_k^2\,dr$$

$$\text{where} \quad \delta L(y_k) = (\delta p y_k')' - \delta q y_k$$

Hence

$$\int y_k \delta L(y_k)\,dr \equiv -\int [\delta p (y_k')^2 + \delta q y^2]\,dr$$

(we have assumed that the perturbed field matches the boundary conditions) and we get

$$\delta\omega_k^2 \int \tilde{\rho} y_k^2\,dr = \int [\delta p (y_k')^2 + \delta q y_k^2]\,dr - \omega_k^2 \int \delta\tilde{\rho} y_k^2\,dr \tag{4.60}$$

Equation 4.60 can now be converted to the usual form using the substitutions on the previous page, *i.e.*,

$$\delta\omega_k^2 \int \rho_0 r^2 W^2\,dr = \int \delta\mu \left[r^2 \left(\frac{dW}{dr} - \frac{W}{r}\right)^2 + (l+2)(l-1)W^2\right]\,dr - \omega_k^2 \int \delta\rho_0 r^2 W^2\,dr \tag{4.61}$$

If we multiply 4.61 through by $l(l+1)$ we get

$$\delta\omega_k^2 \int \rho_0 N r^2\,dr = \int [M'\delta\mu + R\delta\rho_0] r^2\,dr \tag{4.62}$$

where N, M' and R are defined as in 4.56.

4.8 Attenuation . We now return to the problem of computing the attenuation rate of a mode. From section 4.6 we have perturbations of the form

$$\delta\mu = \frac{i\mu}{Q_\mu} \quad \text{and} \quad \delta\kappa = \frac{i\kappa}{Q_\kappa} \tag{4.63}$$

leading to a perturbation in ω_k^2 given by

$$\frac{\delta\omega_k^2}{\omega_k^2} = \frac{i}{Q_k} \tag{4.64}$$

(this gives the attenuation rate of the mode $\alpha_k = \omega_k/2Q_k$). Q_μ and Q_κ are functions of both depth and frequency and are a phenomenological description of dissipation processes. Q_μ gives the attenuation in

shearing processes while Q_κ gives the attenuation in compressional and dilatational processes. We assume that there is no imaginary part to the density ("imperfect inertia"?). Substitution of 4.63 and 4.64 into 4.56 gives

$$Q_k^{-1}\omega_k^2 \int_0^a \rho_0 N r^2 \, dr = \int_0^a \left[\kappa K' Q_\kappa^{-1} + \mu M' Q_\mu^{-1}\right] r^2 \, dr \tag{4.65}$$

Clearly, if we are given Q_μ^{-1} and Q_κ^{-1}, we can evaluate 4.65 to give Q_k^{-1}.

Careful consideration of 4.65 shows that $\kappa K'$ is proportional to the compressional energy density of the mode, $\mu M'$ is proportional to the shear energy density of the mode and $\omega_k^2 \rho_0 N$ is proportional to the kinetic energy density of the mode. This is not surprising since Q^{-1} is related to the fractional energy loss per cycle.

Equation 4.65 is also the basis for the inverse problem: given observations of Q_k^{-1} for many modes, determine $Q_\kappa^{-1}(r,\omega)$ and $Q_\mu^{-1}(r,\omega)$. Of course, we need to know the elastic structure to calculate the energy densities in 4.65 but it is believed that the spherically averaged Earth structure is sufficiently well known that $\rho_0 N$, $\kappa K'$ and $\mu M'$ can be regarded as known for each mode. (There are a few exceptions to this, *i.e.*, modes which have turning points close to internal discontinuities can be extremely sensitive to structure in the vicinity of the turning point.) If we assume the energy densities are known, 4.65 is a *linear* inverse problem for Q^{-1}. If Q_μ^{-1} and Q_κ^{-1} are doubled everywhere then Q_k^{-1} is doubled. Linear inverse problems are well-studied and we shall consider this one in some detail. (For a full discussion of the Q inversion problem see Masters and Gilbert, 1983 or Widmer at al, 1991 or Parker, 1994.)

The main problem we have in constraining Q structure is that we have very few strictly independent constraints on the unknown model. A large proportion of the dataset is made up of Q measurements for fundamental spheroidal modes. The energy distributions of these modes are dominated by shear energy in the upper mantle. Such modes are dominantly sensitive to Q_μ with depth sensitivity given by $\mu M' r^2$ in 4.65. We plot this for the modes ${}_0S_{21} \rightarrow {}_0S_{38}$ in figure 4.1. Note the extreme similarity of these functions and it is possible to construct any one of these functions from a linear combination of the seventeen others to about one part in a million. Clearly, if all eighteen of our data are to be independent constraints, the measurements must be extremely precise (to a part in a million!). Given the fact that the observations are good to a few percent, we know that our dataset has redundant data in it. One way of proceeding is to "rank and winnow" the data. To see how this is done we consider the simplest version of 4.65, *i.e.*,

$$\gamma_j \pm \sigma_j = \int_0^a g_j(r)\, m(r)\, dr \tag{4.66}$$

where g_j is a data kernel or "representor" and $m(r)$ is our model.

We look for a recombination of our data, γ_j, which are orthogonal and precise. Our data will have a covariance matrix, E_{ij}, which is typically taken to be diagonal with elements σ_i^2, *i.e.*,

$$E_{ij} = \sigma_i^2 \delta_{ij} \tag{4.67}$$

First we divide 4.66 through by σ_j to make the covariance matrix be the unit matrix, *i.e.*,

$$\frac{\gamma_i}{\sigma_i} \pm 1 = \int \frac{g_i(r)}{\sigma_i} m(r)\, dr = \int g_i'(r) m(r)\, dr = \gamma_i' \quad \text{say}$$
$$\text{and} \quad \mathbf{E}' = \mathbf{I} \tag{4.68}$$

Let the new data have representors which are linear combinations of the old representors with coefficients $\mathbf{B}$, *i.e.*,

$$\begin{aligned} \mathbf{B}\cdot\gamma' &= \int \mathbf{B}\cdot\mathbf{g}'(r)\, m(r)\, dr \\ \text{or} \quad \mathbf{d} &= \int \mathbf{G}(r)\, m(r)\, dr \end{aligned} \tag{4.69}$$

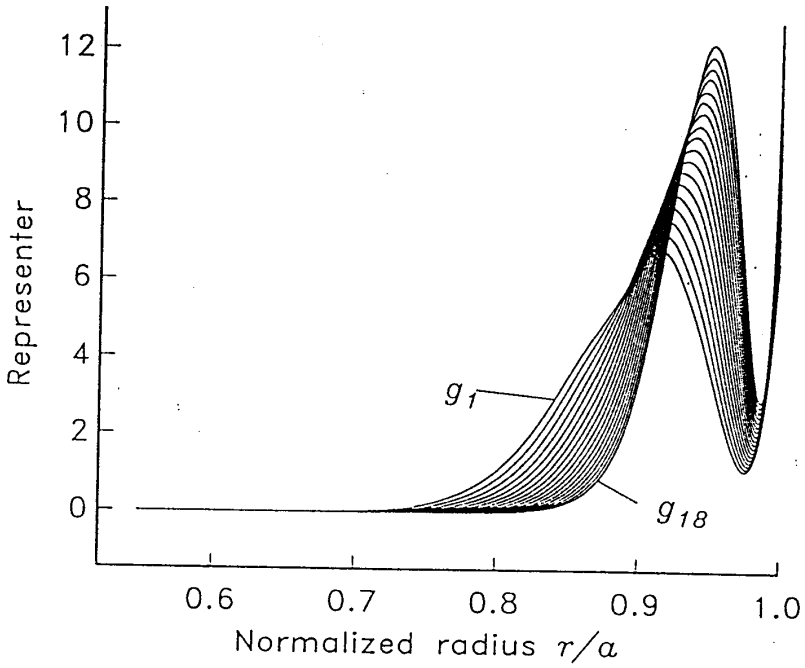

Figure 4.1 $\mu M' r^2$ for ${}_0S_{21}, (g_1)$ to ${}_0S_{38}(g_{18})$. Note the extreme similarity of the kernels (sometimes called representers) to one another.

where $\mathbf{d} = \mathbf{B} \cdot \gamma'$, $\mathbf{G} = \mathbf{B} \cdot \mathbf{g}'$ and $\mathbf{B}$ is chosen so that the new data are orthogonal, *i.e.*,

$$\int G_i(r) G_j(r)\, dr = \delta_{ij}$$

$$\text{or} \quad \int \mathbf{G} \cdot \mathbf{G}^T\, dr = \mathbf{I}$$

$$\text{or} \quad \int \mathbf{B} \cdot \mathbf{g}' \cdot \mathbf{g}'^T \cdot \mathbf{B}^T\, dr = \mathbf{I}$$

$$\text{or} \quad \mathbf{B} \cdot \int \mathbf{g}' \cdot \mathbf{g}'^T\, dr \cdot \mathbf{B}^T = \mathbf{I}$$

or

$$\mathbf{B} \cdot \Gamma \cdot \mathbf{B}^T = \mathbf{I} \tag{4.70}$$

where

$$\Gamma = \int \mathbf{g}' \cdot \mathbf{g}'^T\, dr.$$

To find $\mathbf{B}$, we decompose Γ into its eigenvalues and eigenvectors (it is a real, symmetric matrix so there are plenty of algorithms around for doing this):

$$\Gamma \cdot \mathbf{U} = \mathbf{U} \cdot \Lambda \tag{4.71}$$

where the columns of $\mathbf{U}$ are the eigenvectors and Λ is the diagonal matrix of eigenvalues. Note that $\mathbf{U}^T \cdot \mathbf{U} = \mathbf{U} \cdot \mathbf{U}^T = \mathbf{I}$ so equation 4.70 can be written

$$\mathbf{I} = \mathbf{B}\mathbf{U}\Lambda\mathbf{U}^T\mathbf{B}^T \tag{4.72}$$

By inspection

$$\mathbf{B} = \Lambda^{-\frac{1}{2}}\,\mathbf{U}^T \tag{4.73}$$

and our new data, $\mathbf{B}\cdot\gamma' = \mathbf{d}$, have orthogonal kernels $\mathbf{G} = \mathbf{B}\cdot\mathbf{g}'$. The new data also have a covariance matrix given by

$$\mathbf{B}\cdot\mathbf{E}'\cdot\mathbf{B}^T = \mathbf{B}\cdot\mathbf{I}\cdot\mathbf{B}^T = \Lambda^{-1} \tag{4.74}$$

If we rank the eigenvalues and eigenvections of Γ in order of decreasing magnitude, our first datum, d_1, will be the most precise and will have an error $\sqrt{1/\lambda_1}$. The second datum d_2, has error $1/\sqrt{\lambda_2}$ and so on. At some point, our new datum will be very imprecise so that we might truncate the dataset when $\sqrt{1/\lambda_n}$ exceeds some threshold value (this is called "winnowing").

The current data set of observed degenerate frequencies and attenuations is summarized in table 4.1 at the end of this chapter. There are a total of 204 measurements of $q(=1000/Q)$. Performing the above procedure on this data set results in a set of ranked data with errors as shown in fig 4.2. Even if we are willing to accept errors in $1000/Q$ of 10, there are only 60 useful data.

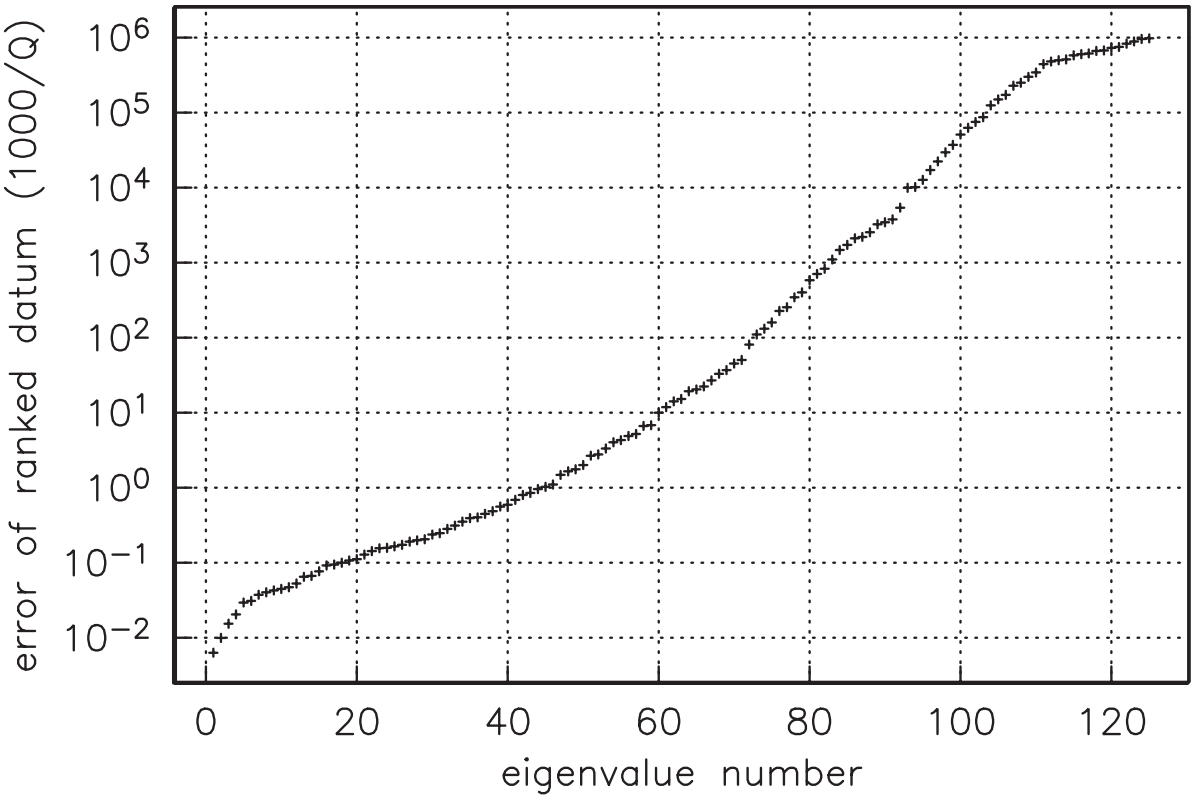

Figure 4.2 Errors of ranked $1000/Q$ data – about 60 data have useful errors

Clearly, any attempt at model construction is going to require additional constraints to be able to say much about Q structure inside the Earth. One solution we might pick (for no very good reason other than it is simple) is the solution with $\int m^2\,dr$ minimized. This is constructed in the following fashion. We have

$$\mathbf{d} = \int \mathbf{G}(r)\,m(r)\,dr$$

Let

$$m(r) = \sum \alpha_i G_i(r)$$

then

$$d_j = \sum \alpha_i \int G_i G_j \, dr = \sum \alpha_i \delta_{ij} = \alpha_j$$

Thus

$$m(r) = \sum d_i G_i(r) \tag{4.75}$$

Note that the coefficients in this expansion are just our new data and so become increasingly imprecise as i increases. It is also almost always true that $G_i(r)$ become increasingly wiggly as i increases, *i.e.*, the smoothest parts of the model are the most precisely determined. Other (more sensible) solutions requiring positivity and/or smoothness of $m(r)$ or that $m(r)$ is a monotonically decreasing or increasing function of depth are described in the papers cited above.

An alternative response to having a poorly contrained inverse problem such as the q problem is to seek parameterized models which are made up of a few homogeneous shells, say. This was the approach taken in making model QL6 (Durek and Ekstrom, 1995) and also in making the q model associated with PREM. We compare these models with a new model designed to fit the q data of table 4.1 in Fig. 4.2. Attenuation is most pronounced in the asthenosphere and in the inner core. This model has some bulk attenuation in the upper mantle but its location is not well constrained – some bulk attenuaton (somewhere) is required to fit the radial mode attenuation measurements.

The fit of QL6 and the new model to some of the mode data is shown in figures 4.3 and 4.4. The red line shows the fit of QL6 while the black line shows the fit of the new model. Note that the q data for fundamental spheroidal modes comes from travelling wave analyses of Rayleigh waves (starting at about $l = 40$) and, for fundamental toroidal modes, from analyses of Love waves (starting at about $l = 30$)

Almost nothing can be said about frequency dependence of Q from the mode dataset. The average Q_μ of the mantle (about 250) is very similar to the Q inferred from the attenuation of ScS body waves with periods of a few seconds. This is taken to be supportive of the assumption that Q is roughly independent of frequency. We find the inner core to be extremely attenuating (in fact, more recent inversions have a Q_μ of about 70 in the inner core which is quite compatible with measurements of differential body-wave attenuation).

Equation 4.56 can also be used to improve the spherically averaged elastic structure of the Earth given estimates of the degenerate frequencies of multiplets. Before we look at this problem we first would like to extend 4.56 to include perturbations in the radii of internal discontinuities.

4.9 Boundary perturbations . The variational principle we have been considering can be written in general as

$$\mathcal{L} = \int_V L \, dV \quad \text{and} \quad \delta\mathcal{L} = 0$$

where L is a Lagrangian density and is a function of "fields", *i.e.*,

$$L = L(\mathbf{q}, \dot{\mathbf{q}}, m_i, \lambda)$$

where $m_i = \rho, \mu, \kappa$, etc, $\lambda = \omega_k^2$, and $\mathbf{q} = \mathbf{s}, \phi_1$, etc. For the variational principle to be satisfied ($\delta\mathcal{L} = 0$) we must satisfy the Euler-Lagrange equations:

$$\left(\frac{\partial \dot{L}}{\partial \dot{\mathbf{q}}}\right) - \frac{\partial L}{\partial \mathbf{q}} = 0$$

with the boundary conditions

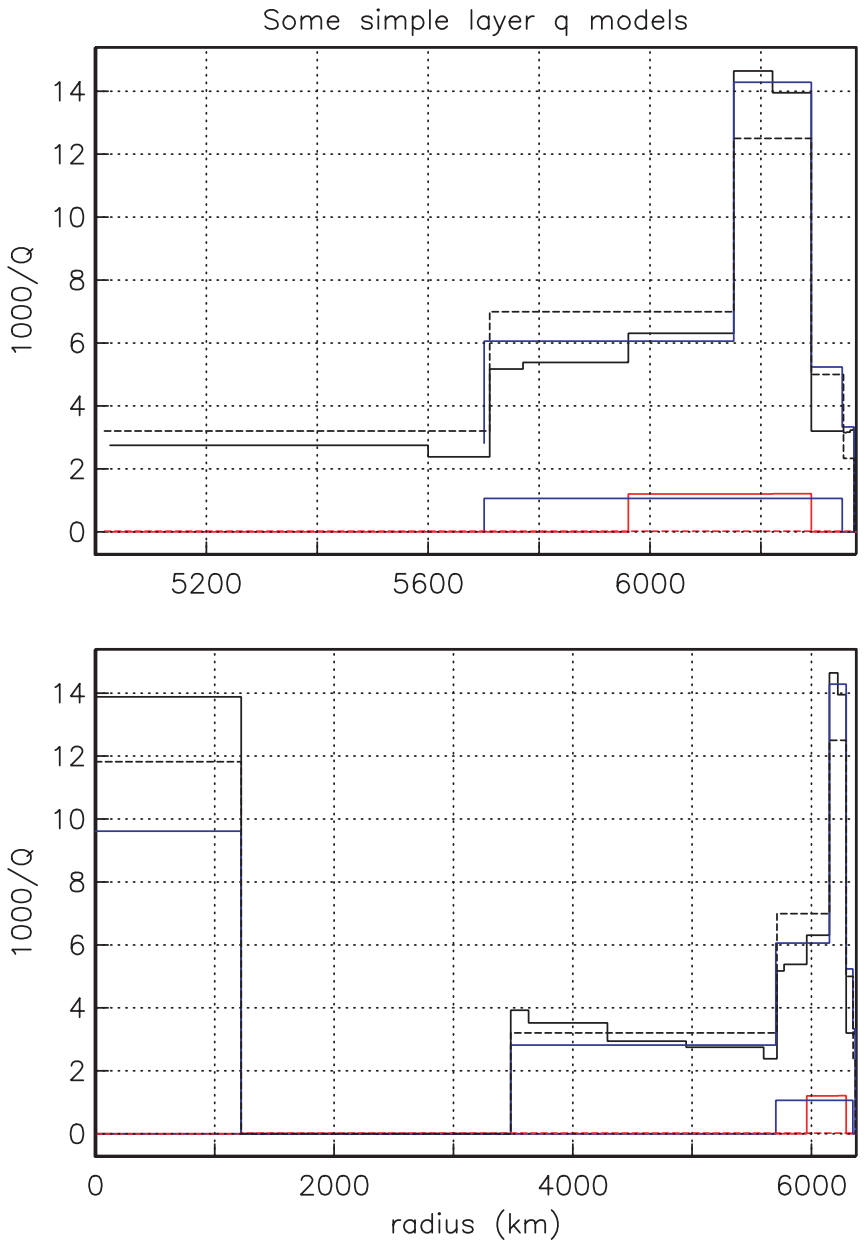

Figure 4.2 Some simple layered q models. The dashed line is the PREM mode, the blue line is QL6, and the black/red line is a new q_μ/q_κ model. Top panel shows detail in the upper mantle

$$\left[\frac{\partial L}{\partial \dot{\mathbf{q}}}\right]_-^+ \cdot \hat{\mathbf{n}} = 0$$

Now suppose $m \to m + \delta m$ and suppose the perturbed problem also has $\delta\mathcal{L} = 0$ then the contribution from the perturbations in the field is zero to first order and we have

$$\int_V \left(\frac{\partial L}{\partial m_i}\delta m_i + \frac{\partial L}{\partial \lambda}\delta\lambda\right) dV = 0$$

or

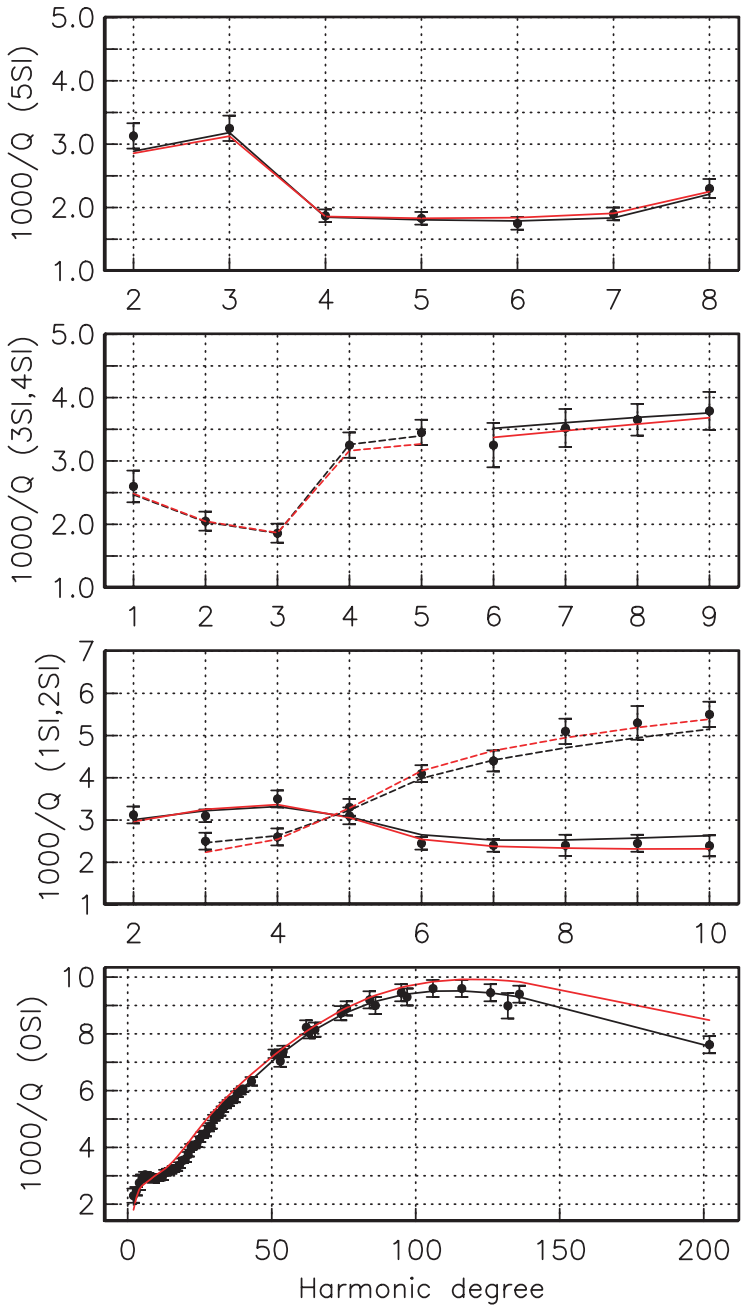

Figure 4.3 Fit of QL6 (red line) and the new model (black line) to spheroidal mode attenuation observations. The dashed lines in the middle two panels are the fits to the ${}_2S$ and ${}_4S$ modes respectively. QL6 systematicall misfits the fundamental modes

$$\delta\lambda \int_V \frac{\partial L}{\partial \lambda}\, dV = -\int_V \frac{\partial L}{\partial m_i} \delta m_i\, dV$$

This is the equation that we have been using all along. Now suppose that this equation applies to the case of a perturbation in a boundary, δh. We would expect the answer to look like

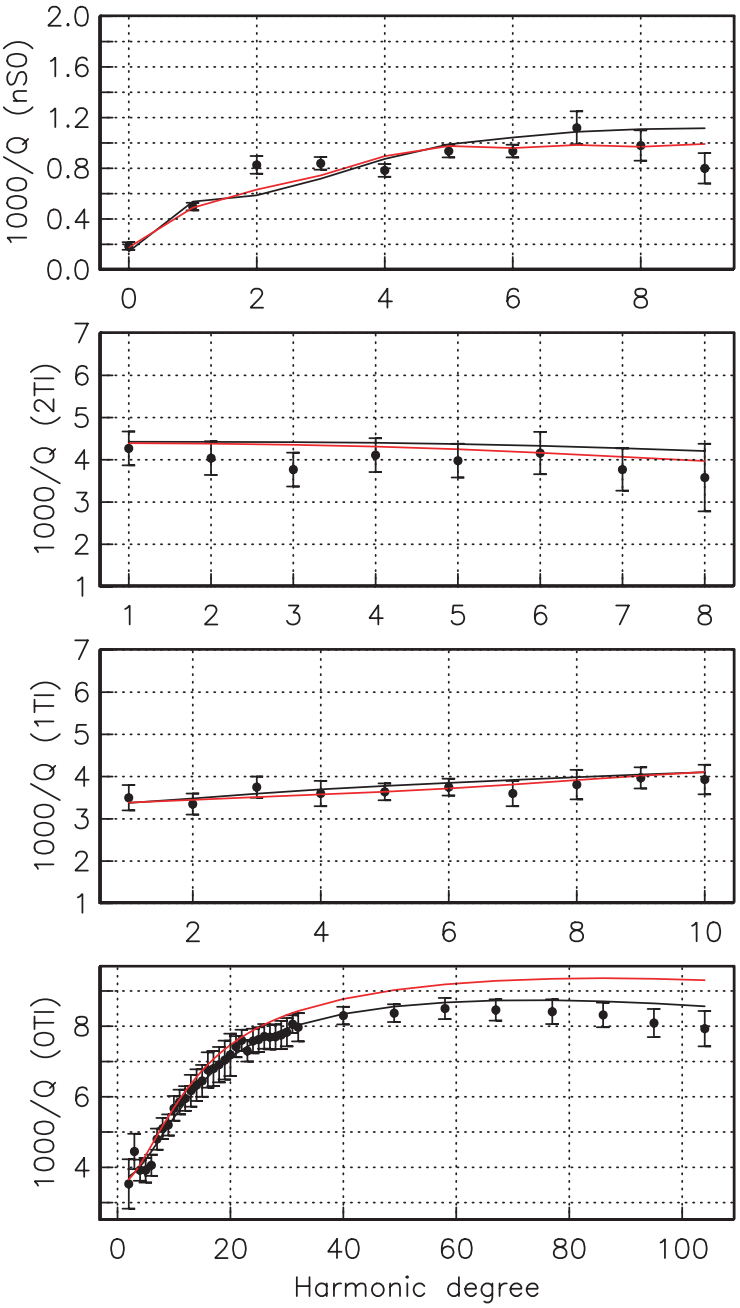

Figure 4.4 Fit of QL6 (red line) and the new model (black line) to toroidal mode and radial mode (top panel) attenuation observations. Again, QL6 systematically misfits the fundamental modes

$$\delta\lambda \int_V \frac{\partial L}{\partial \lambda}\, dV = \int_S [L]^+_- \delta h\, dS$$

where S is the surface, δh is the normal displacement to the boundary and $[L]^+_-$ is the difference in the Lagrangian above and below the interface. This is the form that was originally used and is wrong.

The reason that this equation is wrong is that the perturbed fields do not satisfy the boundary condition and we must add another term to fix this up, *i.e.*,

$$\delta\lambda \int_V \frac{\partial L}{\partial \lambda}\, dV = \int_S \left[L - \frac{\partial L}{\partial \dot{q}_i} \dot{q}_j n_i n_j \right]_-^+ \delta h\, dS \tag{4.76}$$

As an example, consider the use of 4.76 when

$$L = \rho\omega^2 y^2 - \mu (y')^2$$

and there is a discontinuity in ρ and μ at h (this is almost the toroidal mode problem). The Euler-Lagrange equations give

$$(\mu y')' + \rho\omega^2 y = 0$$

and $\mu y'$ vanishes at the end points. Then 4.76 gives

$$\delta\omega^2 \int \rho y^2\, dx = \left[L - \frac{\partial L}{\partial y'} y' \right]_-^+ \delta h \tag{4.77}$$

but

$$\begin{aligned} L - \frac{\partial L}{\partial y'} y' &= \rho\omega^2 y^2 - \mu (y')^2 - (-2\mu y') y' \\ &= \rho\omega^2 y^2 + \mu (y')^2 \end{aligned}$$

Note that the incorrect expression would give $[\rho\omega^2 y^2 - \mu (y')^2]_-^+ \delta h$ for the right hand side of 4.77 which, if ρ is continuous at the interface, has precisely the wrong sign!

To proceed in the general case, we consider the perturbation to the equations of motion when a boundary is perturbed and use the boundary conditions to calculate the perturbations in the fields $\delta\mathbf{s}$, $\delta\phi_1$ and $\delta\mathbf{T}$ which are required to keep the boundary conditions satisfied. For example, consider a welded boundary. Now

$$[\mathbf{s} + \delta\mathbf{s}]_{h+\delta h^-}^{h+\delta h^+} = 0$$

where $h + \delta h$ is the radius of the perturbed discontinuity. Expand $\mathbf{s}$ in a Taylor series so

$$\mathbf{s}(h + \delta h) = \mathbf{s}(h) + \delta h \partial_r \mathbf{s}(h) + \cdots$$

therefore

$$[\mathbf{s} + \delta h \partial_r \mathbf{s} + \delta\mathbf{s}]_{h^-}^{h^+} = 0$$

or

$$\delta\mathbf{s} = -\delta h [\partial_r \mathbf{s}]_-^+ \tag{4.78}$$

Thus we can calculate $\delta\mathbf{s}$ in terms of the perturbation in the boundary and the radial derivative of the unperturbed eigenfunctions. In this way we can eliminate all references to the unknown perturbations in $\mathbf{s}$ and replace them with terms proportional to δh. A complete list of substitutions is:

$$\begin{array}{rcc} [\delta\mathbf{s}] = -\delta h [\partial_r \mathbf{s}]_-^+ & \text{welded} & \\ [\delta s_r] = -\delta h [\partial_r s_r]_-^+ & \text{fluid/solid} & \\ [\delta\mathbf{T} \cdot \hat{\mathbf{r}}] = -\delta h [\delta_r \mathbf{T} \cdot \hat{\mathbf{r}}]_-^+ & \text{all} & \\ [\delta\phi_1] = -\delta h [\partial_r \phi_1]_-^+ & \text{all} & \\ [\partial_r \delta\phi_1 + 4\pi G\rho_0 \delta s_r] = -\delta h [\partial_r (\partial_r \phi_1 + 4\pi G\rho_0 s_r)]_-^+ & \text{all} & \end{array} \tag{4.79}$$

where all terms on the right are evaluated at the unperturbed boundary. One other complication arises because moving a discontinuity causes a perturbation in ρ_0, μ, κ in $h \to h + \delta h$ but ϕ_0 is perturbed everywhere. In effect, a shell of density $[\rho]_-^+$ of thickness δh is added so

$$\left.\begin{aligned}\delta\phi_0 &= \frac{4\pi G h^2}{r}[\rho]^+_-\delta h \quad \text{for} \quad r > b \\ &= \text{constant} \quad \text{for} \quad 0 < r < b\end{aligned}\right\} \tag{4.80}$$

We now go through the perturbation theory using 4.79 and 4.80 to eliminate the field perturbations. The result is

$$\begin{aligned}\delta\omega^2 \int \rho_0 \mathbf{s}^* \cdot \mathbf{s}\, dV = &\int_V \rho_0 \left[\mathbf{s}\cdot\mathbf{s}^*\nabla(\nabla\delta\phi_0) + \nabla\delta\phi_0(\mathbf{s}^*\cdot(\nabla\mathbf{s})^T - \mathbf{s}^*\cdot(\nabla\cdot\mathbf{s})\right] dV \\ &- \delta h \int_S [\nabla\mathbf{s}^* \cdot\cdot \mathbf{C} : \nabla\mathbf{s} + \rho_0(\mathbf{s}^*\cdot\nabla\phi_1 + \mathbf{s}\cdot\nabla\phi_1^* + \mathbf{s}\cdot\mathbf{s}^*\nabla(\nabla\phi_0)) \\ &- \nabla\phi_0((\mathbf{s}^*\cdot(\nabla\mathbf{s})^T - \mathbf{s}^*(\nabla\cdot\mathbf{s})) - \omega^2\mathbf{s}\cdot\mathbf{s}^*) \\ &+ \frac{1}{4\pi G}\nabla\phi_1\cdot\nabla\phi_1^* - \hat{\mathbf{r}}\cdot[\nabla\mathbf{s}^*\cdot\cdot\mathbf{C}:\nabla\mathbf{s} + \nabla\mathbf{s}\cdot\cdot\mathbf{C}:\nabla\mathbf{s}^* \\ &+ \nabla\phi_1\cdot(\frac{1}{4\pi G}\nabla\phi_1^* + \rho_0\mathbf{s}^*) + \nabla\phi_1^*(\frac{1}{4\pi G}\nabla\phi_1 + \rho_0\mathbf{s})]\Big]^+_- \cdot\hat{\mathbf{r}}\, dS\end{aligned} \tag{4.81}$$

This rather complicated equation can be cast in a form suitable for computation using the usual vector spherical harmonics. The result is

$$\delta\omega^2 \int_0^a \rho_0 N r^2\, dr = -\delta h[\kappa K'' + \mu M'' + \rho_0 R]^+_- \tag{4.82}$$

where

$$\begin{aligned}K'' &= F^2 - (\partial_r U)^2 \\ M'' &= \tfrac{1}{3}\left[F^2 - (2\partial_r U)^2\right] + \frac{l(l+1)}{r^2}[(U-V)^2 - (r\partial_r V)^2 + W^2 - (r\partial_r W)^2] \\ &\quad + \frac{1}{r^2}[l(l+1)-2]l(l+1)[V^2+W^2]\end{aligned} \tag{4.83}$$

N, R are defined in equation 4.56. Equation 4.82 allows us to compute the perturbation in a mode frequency when a boundary is moved by δh. We can combine 4.82 and 4.56 to give the starting point for the inverse problem for spherically averaged structure:

$$\frac{\delta\omega}{\omega} = \int \left(K\frac{\delta\kappa}{\kappa} + M\frac{\delta\mu}{\mu} + R\frac{\delta\rho}{\rho}\right) dr + \sum_k A_k \delta h_k \tag{4.84}$$

where K, M, R and A_k can be computed for each mode given a starting model and $\delta\omega$ can be interpreted as $\omega_{observed} - \omega_{model}$. Equation 4.84 is a *linearized* inverse problem and must be solved iteratively, *i.e.*, at each iteration we find new $\delta\kappa$, $\delta\mu$, $\delta\rho$, δh_k which (partially) fit the $\delta\omega$'s then K, M, R and A_k are recomputed for the perturbed model. If we have enough observations of modes of different kinds (e.g., $PKIKP$ equivalent, ScS equivalent etc), K, M, R and A_k will be significantly different functions of depth for each mode and we will be able to learn about the details of Earth structure. In practice, the success of this procedure is entirely dependent upon the quality of the estimates of the degenerate eigenfrequencies and bias in the observations is common.

4.10 Estimating degenerate eigenfrequencies . An important result which we shall prove in chapter 5 is the "diagonal sum rule." Any aspherical perturbation will cause a multiplet to be split but the diagonal sum rule states that, to first order in small quantities, the sum of the singlet frequencies is just the degenerate frequency of the multiplet. This is often taken to mean that, if we measure the center frequency of a split multiplet for a good geographical distribution of source-receiver pairs, the average frequency will be the frequency of

the spherically averaged Earth. There are some hidden assumptions in this statement which we shall look at later. Where do degenerate frequency estimates come from? Measurements of peak frequencies from single recordings can provide good degenerate frequency estimates for highly excited, isolated multiplets. Such frequency measurements form simple geographic patterns when viewed as a function of the pole of the great circle joining the source and receiver and the mean of this pattern can be shown to be a good estimate of the degenerate frequency (see later chapters). Unfortunately, this analysis is confined to a small subset of modes – mainly the fundamental spheroidal modes. These modes do not sample the deep Earth and are incapable of giving us high resolution estimates of Earth structure. For this, we require overtone measurements and to obtain overtone measurements we have to use multiple-record data analysis techniques. We consider two techniques – "stacking" and "stripping." Reconsider 4.35:

$$\mathbf{s}(\mathbf{r},\mathbf{r}_0,t)=\sum_{n,l}\sum_{i=1}^{6}{}_n\mathbf{G}_l^i(\mathbf{r},\mathbf{r}_0)\psi_i(t)\star\frac{1}{{}_n\omega_l^2}{}_nC_l(t)$$

$$\text{where}\quad {}_nC_l(t)=[1-\cos({}_n\omega_l t)e^{-{}_n\alpha_l t}]H(t)$$

This equation tells us that, as $t\to\infty$, we get a nonzero static offset. In practice, we remove the mean from the recording so the static offset is removed. Suppose we have made an estimate of $\psi(t)$ and let the n,l'th mode be denoted by k and let a single component of recording for the $\mathbf{r},\mathbf{r}_0$ source-receiver pair be denoted by j. Define

$$B_{jk}=-\frac{1}{\omega_k^2}\sum_{i=1}^{6}{}_kG_j^i\psi_i(t)$$

$$C_k(t)=\cos(\omega_k t)e^{-\alpha_k t}H(t)$$

then 4.35 becomes

$$s_j(t)=\sum_k B_{jk}(t)\star C_k(t) \tag{4.85}$$

Note that $\psi(t)$ is usually close to being a δ function in time so that B_{jk} will be a slowly varying function of frequency. In fact, we may take B_{jk} to be independent of frequency in a small frequency band which encompasses several modes of interest. Equation (4.85) becomes

$$s_j(\omega)=\sum_k B_{jk}(\omega)C_k(\omega)\simeq\sum_k B_{jk}C_k(\omega) \tag{4.86}$$

Remember that we taper the data when we take the FFT so 4.86 can be regarded as an inverse problem to recover tapered resonance function, $C_k(\omega)$, if B_{jk} can be computed. We assume that we have a good enough Earth model and source mechanism so that a reasonable estimate of B_{jk} can be made. Equation 4.86 can be rewritten:

$$\mathbf{s}(\omega)=\mathbf{B}\cdot\mathbf{C}(\omega)$$

Stacking is

$$\mathbf{s}'(\omega)=\mathbf{B}^T\cdot\mathbf{s}(\omega)=\mathbf{B}^T\cdot\mathbf{B}\cdot\mathbf{C}(\omega) \tag{4.87}$$

Stripping is

$$\mathbf{s}''(\omega)=\mathbf{B}^{-1}\cdot\mathbf{s}(\omega)=\mathbf{B}^{-1}\cdot\mathbf{B}\cdot\mathbf{C}(\omega) \tag{4.88}$$

Consider stacking first. A multiplet consists of singlets of the form

$$\mathbf{s}=U\mathbf{A}_l^m+V\mathbf{B}_l^m+W\mathbf{C}_l^m$$

where

$$\mathbf{A}_l^m = \hat{\mathbf{r}} Y_l^m, \quad \mathbf{B}_l^m = \nabla_1 Y_l^m \quad \text{and} \quad \mathbf{C}_l^m = -\hat{\mathbf{r}} \times \nabla_1 Y_l^m$$

Inspection of 4.33 shows that $\mathbf{B}$ has a similar form. Now

$$\int \mathbf{A}_l^{m*} \cdot \mathbf{A}_{l'}^{m'} \, d\Omega = \int \mathbf{B}_l^{m*} \cdot \mathbf{B}_{l'}^{m'} \, d\Omega = \int \mathbf{C}_l^{m*} \cdot \mathbf{C}_{l'}^{m'} \, d\Omega = 0$$

unless $l = l'$ and $m = m'$. Similarly all cross products of $\mathbf{A}$'s, $\mathbf{B}$'s and $\mathbf{C}$'s are zero. Now suppose that we have a dense set of source-receiver pairs which are globally distributed. The matrix product $\mathbf{B}^T \cdot \mathbf{B}$ then tends to a surface integral and becomes diagonally dominant. Thus $\mathbf{s}'$ becomes proportional to $\mathbf{C}$ and, performing the operation 4.87 at each frequency, gives us an estimate of the spectrum of each multiplet resonance function.

Stripping is a little more straightforward. We simply form a generalized inverse of $\mathbf{B}$ so that $\mathbf{s}''$ should give a direct estimate of $\mathbf{C}$. Since $\mathbf{B}$ is independent of frequency, we need only form its inverse once and and then apply it to each frequency in turn. The advantage of stripping is that it only requires as many records as modes in the band (in principle) and so usually works better than stacking. On the other hand, stacking is usually less sensitive to errors in source mechanisms, etc. An example of stripping is given in Figure 1.14. The center frequency and attenuation rate of each multiplet can now be estimated from their stacks and strips and can be used as data in the inverse problem for spherically averaged structure. Care should be taken to avoid bias from the signal due to aspherical structure. In particular, both stacking and stripping assume that there is an even distribution of singlets within a multiplet. Clearly, if the singlets are clumped to one end of a multiplet, adding up many records will tend to give a peak at that end of the multiplet and will not give a peak at the degenerate frequency. Usually, when this happens the strips have multiple peaks (see example of ${}_1S_4$ in figure 4.5) and so the problem can be diagnosed. Occasionally one obtains a clear single-peak strip at the extreme end of a multiplet which, if interpreted as the degenerate frequency, introduces bias into the dataset.

For most high l ($l \geq 10$) multiplets, the distribution of singlets within a multiplet is sufficiently uniform that stacking or stripping with a good geographical distribution of source-receiver pairs gives strips with peaks close to the degenerate frequencies. Figures 4.6 and 4.7 show strips for ${}_0S_l$ and ${}_0T_l$ modes and the center frequencies of the ${}_0S_l$ modes measured from the strips can be compared with those obtained from the analysis of individual recordings (Fig. 4.8). The agreement is good but both datasets show unusual jumps in the ω/l curve (Figure 4.8). As we shall see later, such jumps are caused by coupling to toroidal modes and the frequencies again should not be interpreted as belonging to isolated spheroidal modes. The cause of this coupling is dominantly the Coriolis force and so can be modeled. We can estimate the mean shift of a hybrid multiplet's frequency from the uncoupled degenerate value and correct the data so that it can be used to constrain the spherically averaged structure.

For modes which cannot be analyzed by multiplet stacking and stripping or by a single record analysis, we must model the split spectra directly or try and isolate each singlet within the multiplet. The degenerate frequency can then be estimated by invoking the diagonal sum rule. Modes which must be analyzed in this fashion are the low l, high Q multiplets which sample into the core (see Ritzwoller *et al.*, 1986, 1988). The occurrence of the deep 1994 Bolivian event has resulted in many new accurate degenerate frequencies for such modes.

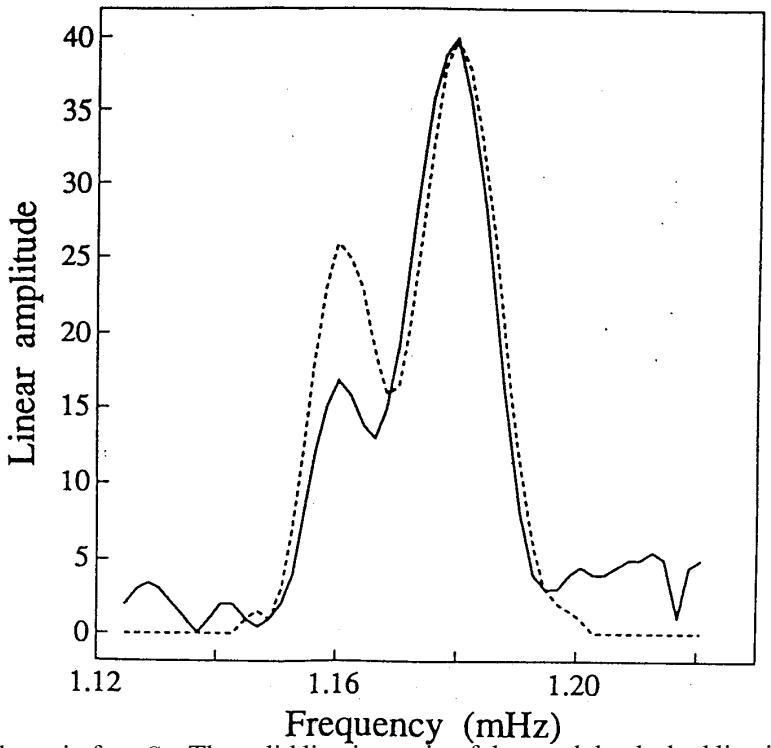

Figure 4.5 A multiplet strip for ${}_1S_4$. The solid line is a strip of data and the dashed line is a strip of synthetic data. This demonstrates that multiplet stripping is incapable of giving good degenerate frequencies for broadly split multiplets with a non-uniform distribution of singlets.

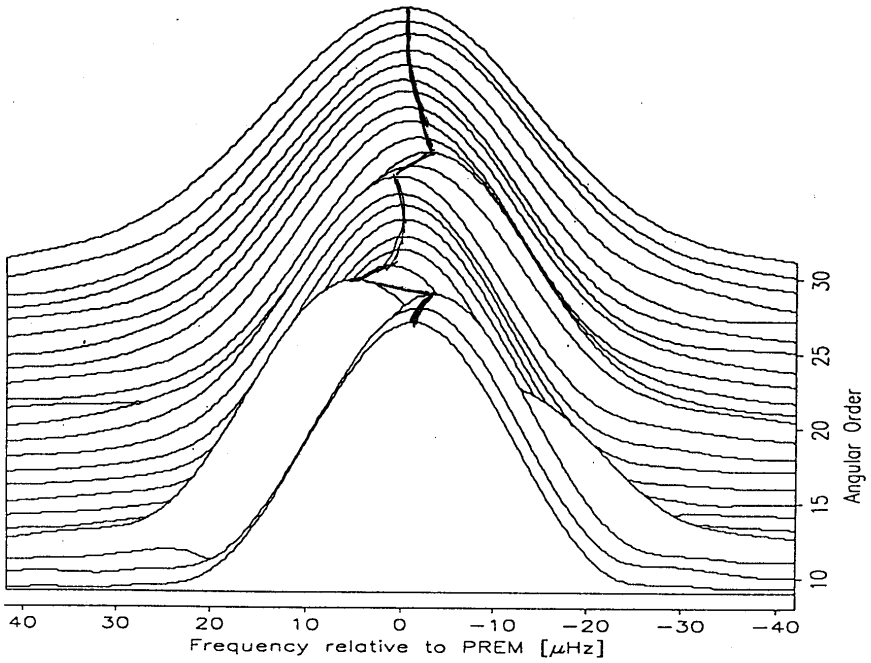

Figure 4.6 The results of stripping fundamental spheroidal modes ${}_0S_8$ to ${}_0S_{30}$. the strips are centered at the frequency predicted by each mode for PREM. Note the "tears" in the peak shifts caused by Coriolis coupling to nearby toroidal modes.

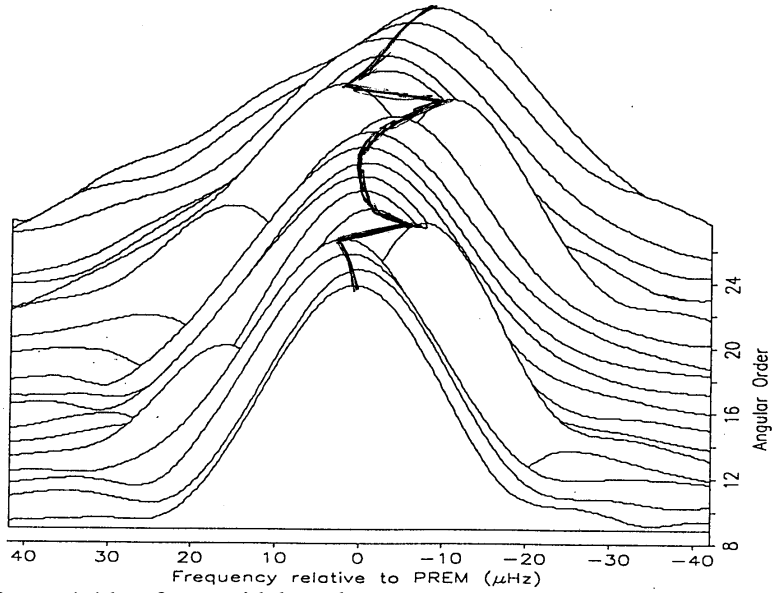

Figure 4.7 As for figure 4.4 but for toroidal modes ${}_0T_8$ to ${}_0T_{26}$.

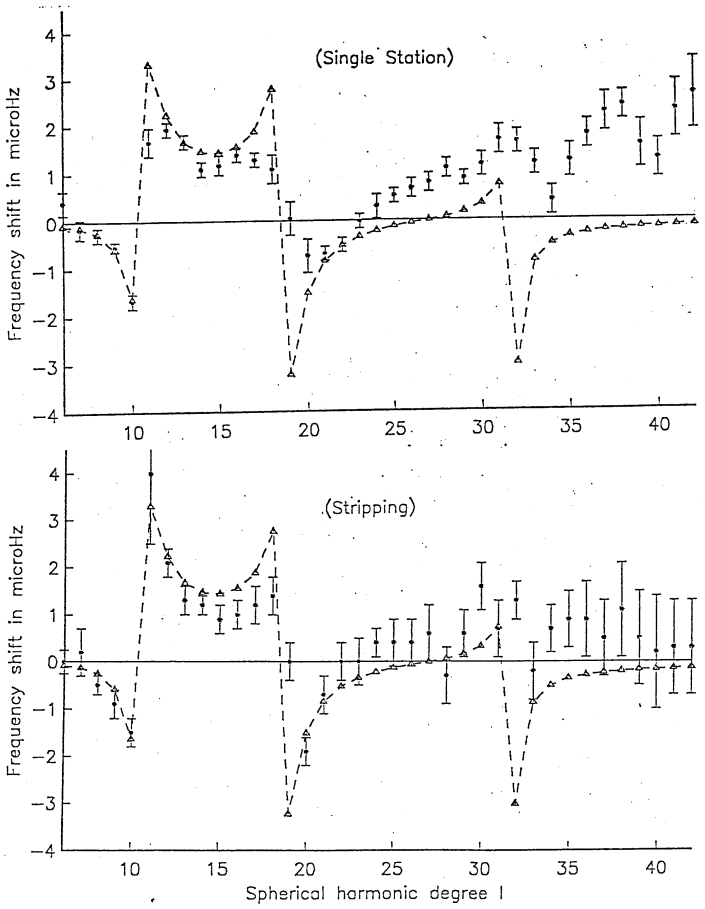

Figure 4.8 Fundamental spheroidal mode peak frequencies plotted relative to those of model 1066A obtained by (top) looking at peak shifting patterns from single record analyses and (bottom) by using the multiplet stripping technique. The triangels are estimates of the theoretical peak shift due to Coriolis coupling (see chapter 5).

Currently we have about 900 reliable degenerate frequency estimates which are being analyzed for spherically averaged structure (table 4.1). The ability of this mode dataset to constrain structure are discussed in the reprint on "resolution".

Some general conclusions:

1) If allowed, small amounts of transverse isotropy ($\approx 0.2\%$) throughout the solid regions of the Earth. This is in contrast to PREM which has about 2% in the top 200 km. In fact, there is a strong trade-off between the depth at which anisotropy is allowed to extend and the size of discontinuities in the upper mantle (e.g. Montagner and Anderson, 1989). The jump in shear velocity at the 410 km discontinuity tends to disappear if significant anisotropy is allowed to extend below about 200 km.
2) Models with sharp upper-mantle discontinuities fit the data better than smooth upper-mantle models. Sharp discontinuities cause a measurable "solotone effect" in some overtone sequences – particularly the ${}_nS_0$ radial modes.
3) Modes which sample strongly near the core-mantle boundary tend to be poorly fit suggesting that we might not have a correct parameterization of structure here. Allowing sharp discontinuities just above or below the core-mantle boundary gives a modest improvement in fit to these data.

Continued improvement of spherically averaged models will require careful attention to biases in the degenerate frequency data set since quality, rather than quantity, is what is required to give good resolution of Earth structure.

TABLE 4.1 Mode frequencies and attenuations

Mode	f_{obs} μHz	f_{PREM} μHz	q^a_{obs}	q_{PREM}	ref.[b]	Mode	f_{obs} μHz	f_{PREM} μHz	q_{obs}	q_{PREM}	ref.
${}_0S_2$	309.25 ± 0.25	309.28	2.30 ± .25	1.962	A	${}_0T_{15}$	2211.16 ± 0.40	2210.34	6.45 ± .45	6.572	RR
${}_0T_2$	378.70 ± 0.50	379.17	3.53 ± .65	3.994	A	${}_7S_1$		2224.25		4.018	
${}_2S_1$		403.96		2.520		${}_2S_9$	2229.30 ± 0.45	2228.75	5.30 ± .40	5.312	ss
${}_0S_3$	468.46 ± 0.15	468.56	2.46 ± .15	2.395	A	${}_2T_2$	2232.00 ± 1.00	2230.84	4.04 ± .40	4.878	ss,RR
${}_0T_3$	585.45 ± 0.50	586.16	4.45 ± .50	4.167	A	${}_0S_{14}$	2229.80 ± 0.25	2231.40	3.15 ± .10	3.352	32[c],RR
${}_0S_4$	646.82 ± 0.10	647.07	2.75 ± .25	2.680	A	${}_3S_5$		2234.54		11.122	I
${}_1S_2$	680.13 ± 0.20	679.85	3.12 ± .20	3.222	26[c],A	${}_4S_4$	2278.50 ± 0.30	2279.60	3.25 ± .20	3.446	26,ss
${}_0T_4$	765.64 ± 0.30	765.66	3.92 ± .30	4.382	A	${}_1T_8$	2280.00 ± 0.70	2280.23	3.81 ± .35	4.308	ss,RR
${}_0S_0$	814.38 ± 0.01	814.31	0.19 ± .03	0.188	21[c],A	${}_2T_3$	2294.90 ± 1.50	2294.97	3.77 ± .40	4.836	ss
${}_0S_5$	840.01 ± 0.10	840.42	2.92 ± .15	2.812	A	${}_0T_{16}$	2326.40 ± 0.30	2325.19	6.76 ± .50	6.690	RR
${}_0T_5$	928.30 ± 0.25	928.24	3.92 ± .35	4.621	RR,A	${}_0S_{15}$	2344.95 ± 0.15	2346.38	3.18 ± .10	3.463	32[c],RR
${}_2S_2$		937.85		10.432	I	${}_1S_{11}$	2346.20 ± 0.50	2347.54		2.674	W
${}_1S_3$	939.90 ± 0.20	939.83	3.01 ± .15	3.537	27	${}_5S_4$	2379.25 ± 0.15	2379.52	1.87 ± .10	2.044	27,ss
${}_3S_1$	944.35 ± 0.15	943.95	1.17 ± .05	1.209	34[c]	${}_2T_4$	2379.50 ± 0.80	2379.86	4.11 ± .40	4.775	ss,RR
${}_0S_6$	1037.53 ± 0.10	1038.21	3.04 ± .10	2.879	A	${}_2S_{10}$	2403.60 ± 0.50	2402.93	5.50 ± .30	5.518	32,ss
${}_0T_6$	1079.20 ± 0.20	1078.83	4.06 ± .30	4.868	RR,A	${}_6S_2$		2410.68		10.788	I
${}_3S_2$	1106.30 ± 0.30	1106.21	3.30 ± .30	2.728	27[c]	${}_4S_5$	2411.20 ± 0.30	2411.43	3.45 ± .20	3.541	ss
${}_1S_4$	1172.78 ± 0.20	1172.85	3.50 ± .20	3.689	27	${}_0T_{17}$	2440.32 ± 0.40	2439.09	6.80 ± .50	6.795	RR
${}_0T_7$	1221.15 ± 0.20	1220.70	4.80 ± .30	5.112	37,RR	${}_1T_9$	2452.20 ± 0.50	2452.49	3.97 ± .25	4.399	RR
${}_0S_7$	1231.05 ± 0.10	1231.79	2.95 ± .15	2.923	27	${}_0S_{16}$	2456.90 ± 0.15	2458.22	3.25 ± .10	3.586	32[c],RR
${}_1T_1$	1235.30 ± 0.50	1236.11	3.50 ± .30	3.847	A,RR	${}_2T_5$	2484.90 ± 2.00	2485.09	3.98 ± .40	4.693	ss
${}_2S_3$	1242.95 ± 0.15	1242.19	2.50 ± .20	2.407	A	${}_2S_0$	2509.00 ± 0.35	2510.48	0.83 ± .05	.805	21,A
${}_1T_2$	1319.15 ± 0.20	1320.13	3.35 ± .25	3.901	A,RR	${}_7S_2$	2519.00 ± 1.50	2517.29	3.55 ± .50	2.929	ss
${}_0T_8$	1356.60 ± 0.35	1356.11	5.10 ± .30	5.346	34,RR	${}_3S_6$	2548.90 ± 0.35	2549.64	3.25 ± .35	3.629	RR
${}_1S_5$	1370.00 ± 0.20	1370.27	3.10 ± .20	3.426	27	${}_0T_{18}$	2553.35 ± 0.40	2552.22	6.91 ± .50	6.890	32[c],RR
${}_2S_4$	1379.70 ± 0.20	1379.20	2.60 ± .20	2.630	27	${}_1S_{12}$		2555.06		2.738	M
${}_4S_1$	1411.70 ± 0.20	1412.64	2.60 ± .25	2.817	ss	${}_0S_{17}$	2565.80 ± 0.30	2567.12	3.28 ± .11	3.719	32[c],RR
${}_0S_8$	1412.85 ± 0.10	1413.51	2.92 ± .10	2.964	27[c],RR	${}_2S_{11}$	2572.30 ± 0.35	2572.16		5.676	40/RR
${}_3S_3$		1417.19		11.000	I	${}_2T_6$	2609.65 ± 2.00	2610.08	4.16 ± .50	4.591	ss
${}_1T_3$	1438.50 ± 0.30	1439.13	3.75 ± .25	3.955	A,RR	${}_1T_{10}$	2620.20 ± 0.80	2620.02	3.93 ± .35	4.479	ss
${}_0T_9$	1487.07 ± 0.20	1486.61	5.20 ± .30	5.566	RR	${}_4S_6$		2626.93		11.136	I
${}_2S_5$	1515.60 ± 0.30	1514.93	3.30 ± .20	3.309	27	${}_0T_{19}$	2665.76 ± 0.20	2664.71	7.04 ± .55	6.974	RR
${}_1S_6$	1521.50 ± 0.20	1522.04	2.45 ± .15	2.893	27	${}_0S_{18}$	2672.50 ± 0.30	2673.30	3.38 ± .10	3.860	RR
${}_0S_9$	1577.55 ± 0.15	1578.28	2.90 ± .15	3.005	27[c],RR	${}_3S_7$	2687.20 ± 1.20	2686.33	3.52 ± .30	3.713	ss
${}_1T_4$	1585.50 ± 0.40	1585.50	3.60 ± .30	4.006	A,RR	${}_5S_5$	2703.50 ± 0.20	2703.36	1.83 ± .10	1.990	27,ss
${}_0T_{10}$	1613.67 ± 0.40	1613.26	5.67 ± .35	5.773	RR	${}_2S_{12}$	2737.50 ± 0.60	2737.31	4.58 ± .50	5.769	32
${}_1S_0$	1631.57 ± 0.05	1631.34	0.50 ± .03	0.667	21[c],A	${}_2T_7$	2751.50 ± 2.50	2753.73	3.77 ± .50	4.476	ss
${}_1S_7$	1654.55 ± 0.15	1655.51	2.40 ± .15	2.687	27	${}_1S_{13}$		2766.24		2.895	M
${}_2S_6$	1681.30 ± 0.30	1680.84	4.10 ± .20	4.203	27	${}_0T_{20}$	2777.59 ± 0.40	2776.67	7.19 ± .60	7.050	RR
${}_5S_1$		1713.79		11.019	I	${}_0S_{19}$	2776.10 ± 0.40	2776.98	3.53 ± .10	4.006	RR
${}_4S_2$	1721.65 ± 0.20	1722.30	2.05 ± .15	2.303	ss	${}_1T_{11}$	2783.00 ± 1.00	2783.31		4.546	WT
${}_0S_{10}$	1725.60 ± 0.20	1726.47	2.92 ± .10	3.050	32[c],RR	${}_3S_8$	2820.50 ± 0.60	2819.64	3.65 ± .25	3.794	27
${}_0T_{11}$	1737.42 ± 0.20	1736.85	5.85 ± .35	5.963	RR	${}_6S_3$	2821.85 ± 0.15	2821.72	2.20 ± .20	2.345	27
${}_1T_5$	1750.15 ± 0.30	1750.49	3.64 ± .20	4.061	A,RR	${}_8S_1$	2872.65 ± 0.20	2873.36	0.95 ± .10	1.075	26,ss
${}_1S_8$	1797.80 ± 0.25	1799.30	2.40 ± .25	2.635	27	${}_0S_{20}$	2877.95 ± 0.40	2878.37	3.57 ± .10	4.154	33[c],RR
${}_3S_4$		1833.30		11.113	I	${}_0T_{21}$	2888.67 ± 0.50	2888.20	7.42 ± .30	7.118	RR,tvf
${}_0T_{12}$	1858.82 ± 0.20	1857.94	5.95 ± .35	6.138	RR	${}_2S_{13}$	2897.00 ± 0.70	2899.90		5.738	W
${}_0S_{11}$	1861.30 ± 0.40	1862.42	2.94 ± .10	3.105	RR	${}_2T_8$	2912.70 ± 1.50	2913.97	3.58 ± .80	4.363	RR
${}_2S_7$	1865.20 ± 0.40	1864.96	4.40 ± .25	4.726	ss	${}_1T_{12}$		2943.21		4.601	
${}_1T_6$	1925.30 ± 0.30	1925.61	3.75 ± .20	4.129	ss,RR	${}_3S_9$	2951.00 ± 0.60	2951.58	3.79 ± .30	3.865	34,RR
${}_1S_9$	1962.00 ± 0.40	1963.74	2.45 ± .25	2.629	27	${}_1S_{14}$		2975.79		3.408	M
${}_0T_{13}$	1977.88 ± 0.20	1976.99	6.17 ± .45	6.297	RR	${}_0S_{21}$	2977.30 ± 0.20	2977.73	3.76 ± .10	4.303	33[c],RR
${}_6S_1$	1983.20 ± 1.00	1980.38	1.77 ± .60	1.538	ss	${}_0T_{22}$	3000.96 ± 0.50	2999.37	7.60 ± .30	7.178	32[c],G
${}_0S_{12}$	1989.00 ± 0.30	1990.37	2.95 ± .10	3.173	32[c],RR	${}_5S_6$	3011.55 ± 0.15	3010.69	1.75 ± .10	1.975	27
${}_4S_3$	2048.35 ± 0.15	2048.97	1.86 ± .15	2.083	27,ss	${}_4S_7$		3013.63		11.151	I
${}_2S_8$	2050.00 ± 0.35	2049.21	5.10 ± .30	5.057	27	${}_2S_{14}$	3063.00 ± 2.00	3063.60		5.322	40/34
${}_5S_2$	2090.60 ± 0.30	2091.28	3.13 ± .20	3.146	ss	${}_0S_{22}$	3074.70 ± 0.20	3075.27	4.02 ± .10	4.450	33[c],tvf
${}_0T_{14}$	2095.43 ± 0.20	2094.36	6.33 ± .45	6.442	RR	${}_7S_3$		3082.21		11.190	I
${}_1T_7$	2103.20 ± 0.30	2103.79	3.60 ± .30	4.214	ss,RR	${}_3S_{10}$	3082.12 ± 0.50	3084.79		3.933	W
${}_0S_{13}$	2111.58 ± 0.10	2112.94	3.11 ± .10	3.255	32[c],RR	${}_2T_9$		3087.52		4.265	
${}_1S_{10}$	2146.50 ± 0.50	2148.42	2.39 ± .25	2.643	WT	${}_6S_4$		3092.11		2.894	
${}_5S_3$	2168.80 ± 0.20	2169.66	3.25 ± .20	3.420	27,ss	${}_1T_{13}$		3100.46		4.648	
${}_2T_1$	2187.00 ± 2.00	2187.83	4.27 ± .40	4.904	ss	${}_0T_{23}$	3111.28 ± 0.50	3110.25	7.30 ± .40	7.232	33[c],tvf

TABLE 4.1 continued

Mode	f_{obs} μHz	f_{PREM} μHz	q^a_{obs}	q_{PREM}	ref.[b]	Mode	f_{obs} μHz	f_{PREM} μHz	q_{obs}	q_{PREM}	ref.
${}_1S_{15}$	3171.50 ± 1.50	3170.55		4.922	40/34	${}_3T_9$	3843.00 ± 5.00	3853.78		4.276	WT
${}_0S_{23}$	3170.70 ± 0.15	3171.26	4.07 ± .10	4.594	33[c],tvf	${}_1T_{18}$		3859.82		4.874	
${}_9S_1$		3197.91		4.486		${}_4S_{10}$	3864.07 ± 0.70	3864.58		3.307	W
${}_3T_1$		3203.50		4.636		${}_2S_{18}$		3874.44		2.489	M
${}_8S_2$		3214.23		2.954		${}_9S_4$	3878.40 ± 1.50	3877.95	1.71 ± .20	1.940	ss
${}_0T_{24}$	3222.50 ± 0.40	3220.90	7.28 ± .35	7.281	32[c],tvf	${}_0T_{30}$	3882.90 ± 0.70	3881.75	7.55 ± .40	7.479	38,tvf
${}_3S_{11}$	3219.52 ± 0.55	3221.27		4.002	W	${}_0S_{31}$	3904.70 ± 0.25	3905.40	5.14 ± .10	5.571	33,tvf
${}_9S_2$	3230.50 ± 0.50	3231.75	2.46 ± .30	2.456	ss	${}_1S_{20}$	3939.97 ± 0.80	3941.56		6.434	W
${}_3T_2$		3234.09		4.615		${}_7S_6$	3956.00 ± 0.50	3958.72	1.85 ± .20	1.983	ss
${}_2S_{15}$		3240.89		3.878	M	${}_6S_9$	3964.50 ± 3.00	3965.35		3.119	WT
${}_1T_{14}$	3255.00 ± 1.50	3255.59		4.691	WT	${}_3S_{16}$	3966.85 ± 0.70	3966.87		4.408	W
${}_0S_{24}$	3265.50 ± 0.20	3265.89	4.11 ± .10	4.734	33[c],tvf	${}_0T_{31}$	3992.60 ± 0.80	3991.62	8.06 ± .25	7.501	G
${}_6S_5$		3266.82		3.683		${}_0S_{32}$	3994.00 ± 0.25	3995.04	5.22 ± .10	5.671	33,H,tvf
${}_2T_{10}$	3267.50 ± 3.50	3270.21		4.193	WT	${}_3T_{10}$	3990.00 ± 5.00	3996.61		4.218	WT
${}_3S_0$	3272.52 ± 0.20	3271.18	0.84 ± .03	.923	21,A	${}_1T_{19}$	4006.00 ± 2.00	4007.17		4.930	WT
${}_3T_3$		3279.74		4.585		${}_4S_{11}$	4007.10 ± 0.70	4010.47		3.513	W
${}_8S_3$		3283.64		3.916		${}_2T_{14}$	4011.00 ± 4.50	4016.39		4.155	WT
${}_5S_7$	3292.00 ± 0.30	3290.76	1.90 ± .10	2.029	27	${}_{10}S_2$	4040.50 ± 1.00	4032.33	1.17 ± .15	5.217	27
${}_0T_{25}$	3333.00 ± 0.60	3331.35	7.32 ± .30	7.324	32[c],tvf	${}_{11}S_2$		4058.47		7.638	I
${}_1S_{16}$	3340.84 ± 1.50	3338.62		6.024	W	${}_0S_{33}$	4083.50 ± 0.30	4084.52	5.35 ± .10	5.766	S,tvf
${}_3T_4$		3340.20		4.546		${}_1S_{21}$	4085.64 ± 0.65	4088.34		6.429	W
${}_0S_{25}$	3358.85 ± 0.15	3359.38	4.29 ± .10	4.869	33[c],tvf	${}_2S_{19}$		4092.40		2.457	M
${}_3S_{12}$	3361.36 ± 0.45	3362.07		4.074	W	${}_0T_{32}$	4102.50 ± 0.80	4101.44	7.65 ± .40	7.520	T,tvf
${}_{10}S_1$		3394.09		11.213	I	${}_4S_0$	4106.43 ± 0.25	4105.76	0.79 ± .03	1.032	21,A
${}_4S_8$		3396.91		11.160	I	${}_3S_{17}$	4124.01 ± 0.60	4125.58		4.497	W
${}_6S_6$		3403.86		3.905		${}_3T_{11}$		4151.80		4.164	
${}_1T_{15}$	3407.00 ± 1.50	3408.95		4.733	WT	${}_4S_{12}$	4153.50 ± 1.00	4152.98		3.643	W
${}_7S_4$	3411.10 ± 0.60	3413.23		2.996		${}_1T_{20}$	4152.00 ± 2.50	4153.05		4.990	40/34
${}_3T_5$		3415.15		4.500		${}_5S_{10}$		4157.00		11.175	I
${}_0T_{26}$	3443.00 ± 0.60	3441.64	7.41 ± .30	7.362	32[c],tvf	${}_8S_5$	4165.30 ± 0.25	4166.20	1.60 ± .15	1.636	27
${}_2S_{16}$		3443.46		2.821	M	${}_0S_{34}$	4172.50 ± 0.30	4173.90	5.48 ± .10	5.857	S,tvf
${}_0S_{26}$	3451.35 ± 0.15	3451.91	4.44 ± .10	5.000	33[c],tvf	${}_2T_{15}$	4190.00 ± 2.00	4196.12		4.180	WT
${}_2T_{11}$	3456.00 ± 2.50	3457.67		4.150	WT	${}_6S_{10}$	4211.20 ± 0.30	4210.76		2.822	WT
${}_1S_{17}$	3493.39 ± 0.85	3493.94		6.309	W	${}_0T_{33}$	4212.20 ± 1.00	4211.23		7.537	T
${}_3T_6$		3504.29		4.449		${}_1S_{22}$	4231.47 ± 0.80	4234.40		6.418	W
${}_3S_{13}$	3507.55 ± 0.55	3507.44		4.152	W	${}_7S_7$	4234.10 ± 0.30	4237.85	2.20 ± .30	2.409	ss
${}_5S_8$	3526.00 ± 0.60	3525.65	2.30 ± .15	2.391	27	${}_0S_{35}$	4261.70 ± 0.30	4263.23	5.57 ± .10	5.945	S,tvf
${}_0S_{27}$	3543.10 ± 0.15	3543.65	4.49 ± .10	5.125	33,tvf	${}_3S_{18}$	4283.80 ± 0.70	4285.98		4.586	W
${}_0T_{27}$	3553.30 ± 0.50	3551.80	7.35 ± .30	7.397	tvf	${}_4S_{13}$	4292.05 ± 1.10	4295.21		3.728	W
${}_6S_7$		3552.60		3.919		${}_1T_{21}$	4295.00 ± 1.00	4297.42		5.055	WT
${}_9S_3$	3556.50 ± 0.40	3554.98	1.45 ± .15	1.286	27	${}_{12}S_1$		4300.34		4.466	
${}_1T_{16}$	3560.50 ± 1.00	3560.73		4.777	WT	${}_{10}S_3$		4300.92		3.451	
${}_3T_7$		3607.30		4.393		${}_4T_1$		4304.57		4.528	
${}_0S_{28}$	3634.20 ± 0.15	3634.76	4.67 ± .08	5.244	33,tvf	${}_2S_{20}$		4310.64		2.440	M
${}_1S_{18}$	3643.75 ± 0.60	3644.94		6.395	W	${}_3T_{12}$	4317.00 ± 6.00	4318.29		4.120	WT
${}_2T_{12}$	3640.50 ± 2.50	3646.13		4.134	WT	${}_0T_{34}$	4322.20 ± 1.00	4321.00		7.553	T
${}_3S_{14}$	3656.20 ± 0.55	3657.11		4.234	W	${}_9S_5$		4324.87		11.117	I
${}_2S_{17}$		3657.42		2.564	M	${}_4T_2$		4326.83		4.527	
${}_7S_5$	3657.78 ± 0.35	3659.75	2.05 ± .20	2.095	ss	${}_{12}S_2$		4330.16		4.357	
${}_0T_{28}$	3663.50 ± 0.50	3661.86	7.35 ± .30	7.427	32,tvf	${}_0S_{36}$	4351.10 ± 0.30	4352.53	5.66 ± .10	6.030	S,tvf
${}_{11}S_1$		3685.48		1.507		${}_4T_3$		4360.07		4.527	
${}_8S_4$		3702.73		10.692	I	${}_2T_{16}$	4367.00 ± 3.50	4372.15		4.211	WT
${}_4S_9$	3707.50 ± 1.50	3708.76		2.950	WT	${}_1S_{23}$	4376.25 ± 1.20	4379.84		6.405	W
${}_1T_{17}$	3710.00 ± 1.00	3711.01		4.824	WT	${}_{10}S_4$		4381.16		4.217	
${}_3T_8$		3723.89		4.335		${}_4T_4$		4404.14		4.527	
${}_0S_{29}$	3724.70 ± 0.20	3725.34	4.76 ± .10	5.358	33,tvf	${}_0T_{35}$	4432.00 ± 1.00	4430.75		7.566	T
${}_6S_8$	3737.50 ± 2.00	3737.62		3.615	WT	${}_8S_6$		4435.24		2.268	
${}_0T_{29}$	3773.20 ± 0.70	3771.84	7.45 ± .40	7.455	32,tvf	${}_4S_{14}$	4435.30 ± 0.85	4439.08		3.784	W
${}_5S_9$		3777.80		11.168	I	${}_1T_{22}$	4440.00 ± 2.00	4440.27		5.124	WT
${}_1S_{19}$	3792.23 ± 0.90	3793.89		6.426	W	${}_0S_{37}$	4440.20 ± 0.35	4441.84	5.69 ± .10	6.111	S,H
${}_3S_{15}$	3810.98 ± 0.60	3810.48		4.319	W	${}_3S_{19}$	4446.13 ± 0.70	4447.56		4.675	W
${}_0S_{30}$	3814.80 ± 0.20	3815.52	5.05 ± .10	5.467	33,tvf	${}_7S_8$	4448.00 ± 1.00	4452.59		3.111	WT
${}_2T_{13}$	3830.50 ± 3.50	3832.88		4.138	WT	${}_5S_{11}$	4458.00 ± 2.00	4456.55		2.669	

TABLE 4.1 continued

Mode	f_{obs} μHz	f_{PREM} μHz	q^a_{obs}	q_{PREM}	ref.[b]	Mode	f_{obs} μHz	f_{PREM} μHz	q_{obs}	q_{PREM}	ref.
${}_4T_5$		4458.81		4.526		${}_3T_{16}$	5040.00 ± 4.50	5054.35		4.121	WT
${}_{11}S_3$		4462.42		2.235		${}_0S_{44}$	5067.60 ± 0.60	5069.01		6.615	S
${}_{10}S_5$		4469.75		4.129		${}_7S_{12}$	5069.25 ± 1.60	5071.02		3.936	W
${}_3T_{13}$	4482.00 ± 7.00	4494.38		4.090	WT	${}_{11}S_5$	5072.60 ± 0.25	5074.41	1.56 ± .12	1.503	27
${}_{13}S_1$	4494.60 ± 0.35	4495.73	1.30 ± .40	1.360	WT	${}_0T_{41}$	5090.60 ± 1.50	5089.15		7.617	T
${}_4T_6$		4523.86		4.526		${}_1S_{28}$	5088.65 ± 2.60	5097.80		6.360	W
${}_1S_{24}$	4521.03 ± 1.20	4524.68		6.391	W	${}_3S_{23}$	5098.42 ± 0.80	5098.49		4.999	W
${}_2S_{21}$		4528.88		2.430	M	${}_4T_{12}$	5116.00 ± 6.00	5119.49		4.517	WT
${}_0S_{38}$	4529.50 ± 0.35	4531.20	5.88 ± .10	6.190	S,tvf	${}_1T_{27}$	5129.00 ± 2.00	5131.50		5.525	WT
${}_6S_{11}$		4534.94		11.182	I	${}_5S_{14}$	5136.40 ± 0.80	5136.81		2.691	W
${}_0T_{36}$	4541.80 ± 1.00	4540.49		7.578	T	${}_9S_8$	5138.50 ± 3.50	5144.45		2.117	WT
${}_2T_{17}$	4543.00 ± 2.00	4544.86		4.245	WT	${}_0S_{45}$	5157.90 ± 0.60	5159.01		6.680	S
${}_1T_{23}$	4580.00 ± 2.00	4581.59		5.198	WT	${}_2S_{24}$		5182.42		2.447	M
${}_4S_{15}$	4584.00 ± 1.50	4585.74		3.820	W/WT	${}_{13}S_3$	5193.90 ± 0.25	5193.82	1.15 ± .10	1.101	27
${}_4T_7$		4599.04		4.527		${}_0T_{42}$	5200.50 ± 1.50	5198.89		7.621	T
${}_3S_{20}$	4608.98 ± 0.90	4609.89		4.761	W	${}_4S_{19}$	5200.63 ± 1.55	5206.51		3.862	W
${}_7S_9$	4612.00 ± 2.50	4617.95		3.548	WT	${}_2T_{21}$	5202.00 ± 2.50	5210.67		4.399	WT
${}_0S_{39}$	4618.90 ± 0.35	4620.61	5.97 ± .10	6.266	33,tvf	${}_8S_9$	5207.00 ± 2.00	5211.87		1.994	WT
${}_9S_6$		4620.88		3.020		${}_6S_{13}$	5233.50 ± 2.50	5233.88		3.944	WT
${}_0T_{37}$	4651.40 ± 1.00	4650.23		7.588	T	${}_1S_{29}$	5233.02 ± 1.50	5239.29		6.363	W
${}_8S_7$	4645.15 ± 0.60	4650.46		2.844		${}_3T_{17}$	5234.00 ± 8.00	5242.20		4.171	WT
${}_1S_{25}$	4662.65 ± 2.10	4668.93		6.378	W	${}_0S_{46}$	5248.20 ± 0.60	5249.12		6.743	S
${}_3T_{14}$		4677.69		4.078		${}_4T_{13}$	5243.00 ± 7.00	5251.78		4.505	WT
${}_{12}S_3$		4683.62		11.585	I	${}_3S_{24}$	5262.94 ± 0.85	5261.42		5.050	W
${}_4T_8$		4684.10		4.527		${}_1T_{28}$	5264.50 ± 2.00	5265.22		5.611	WT
${}_5S_{12}$	4696.80 ± 0.60	4695.98		2.593	W	${}_7S_{13}$		5288.15		11.194	I
${}_0S_{40}$	4708.40 ± 0.40	4710.10	6.06 ± .10	6.339	S,tvf	${}_{12}S_4$		5293.80		11.333	I
${}_2T_{18}$	4710.00 ± 2.50	4714.71		4.281	WT	${}_{15}S_1$		5295.75		1.471	
${}_1T_{24}$	4721.00 ± 2.00	4721.36		5.276	WT	${}_0T_{43}$	5310.30 ± 1.50	5308.63		7.625	T
${}_4S_{16}$	4729.85 ± 1.50	4735.78		3.842	W	${}_5S_{15}$	5327.26 ± 1.20	5330.11		2.894	W
${}_2S_{22}$		4746.99		2.424	M	${}_0S_{47}$	5338.50 ± 0.60	5339.35		6.804	S
${}_0T_{38}$	4761.20 ± 1.30	4759.96		7.597	T	${}_{11}S_6$	5348.28 ± 0.50	5351.70	2.31 ± .25	2.158	
${}_{11}S_4$	4766.05 ± 0.25	4766.86	1.37 ± .07	1.425	27	${}_5T_1$		5353.50		5.012	
${}_7S_{10}$	4763.50 ± 4.50	4767.76		3.756	WT	${}_{16}S_1$		5355.04		4.984	
${}_3S_{21}$	4771.58 ± 0.80	4772.64		4.845	W	${}_4S_{20}$	5362.19 ± 1.30	5369.24		3.862	W
${}_4T_9$		4778.82		4.527		${}_5T_2$		5370.60		5.010	
${}_0S_{41}$	4798.10 ± 0.40	4799.67		6.411	S	${}_2T_{22}$	5366.00 ± 2.50	5372.32		4.440	WT
${}_1S_{26}$	4809.11 ± 1.40	4812.57		6.368	W	${}_{14}S_2$		5374.58		4.938	
${}_{13}S_2$	4844.70 ± 0.35	4845.26	1.02 ± .05	1.138	27	${}_1S_{30}$	5373.06 ± 1.80	5379.96		6.371	W
${}_1T_{25}$	4859.50 ± 2.00	4859.60		5.357	WT	${}_9S_9$	5381.55 ± 3.00	5389.25		2.696	WT
${}_3T_{15}$		4865.33		4.089		${}_4T_{14}$	5384.50 ± 4.50	5393.54		4.488	WT
${}_0T_{39}$	4871.00 ± 1.30	4869.69		7.605	T	${}_5T_3$		5396.19		5.007	
${}_9S_7$		4872.64		2.041		${}_1T_{29}$	5399.50 ± 2.50	5397.51		5.697	WT
${}_2T_{19}$	4874.00 ± 3.00	4882.09		4.319	–	${}_2S_{25}$		5398.22		2.734	M
${}_4T_{10}$	4885.00 ± 5.00	4883.02		4.526	WT	${}_{14}S_3$		5407.52		4.866	
${}_5S_0$	4885.50 ± 0.30	4884.17	0.94 ± .03	1.086	21,A	${}_6S_{14}$	5411.00 ± 2.00	5410.08		3.857	W/34
${}_0S_{42}$	4887.90 ± 0.50	4889.34		6.481	S	${}_0T_{44}$	5419.90 ± 1.50	5418.38		7.627	T
${}_4S_{17}$	4885.32 ± 1.20	4889.38		3.854	W	${}_3S_{25}$	5424.50 ± 2.50	5425.56		4.835	WT
${}_8S_8$	4902.34 ± 2.00	4908.07		2.384	WT	${}_3T_{18}$	5414.00 ± 7.00	5427.08		4.232	WT
${}_6S_{12}$		4911.92		11.188	I	${}_0S_{48}$	5429.00 ± 0.60	5429.70		6.865	S
${}_{10}S_6$		4914.11		11.470	I	${}_5T_4$		5430.22		5.002	
${}_7S_{11}$	4915.50 ± 3.00	4916.94		3.870	WT	${}_{13}S_4$		5455.12		4.811	
${}_5S_{13}$	4925.46 ± 1.10	4924.40		2.590	W	${}_5T_5$		5472.60		4.996	
${}_{14}S_1$		4925.38		11.350	I	${}_{10}S_7$		5489.22		11.287	I
${}_3S_{22}$	4932.87 ± 0.90	4935.56		4.926	W	${}_5S_{16}$	5505.95 ± 1.10	5506.96		3.117	W
${}_1S_{27}$	4952.77 ± 1.60	4955.54		6.361	W	${}_8S_{10}$	5506.78 ± 1.00	5508.75		2.031	W
${}_2S_{23}$		4964.89		2.425	M	${}_1S_{31}$	5513.54 ± 2.10	5519.76		6.385	W
${}_0S_{43}$	4977.70 ± 0.50	4979.12	6.33 ± .15	6.549	S,H/G	${}_0S_{49}$	5519.50 ± 0.70	5520.16		6.924	S
${}_0T_{40}$	4980.70 ± 1.30	4979.42	8.30 ± .25	7.611	T,G	${}_5T_6$		5523.25		4.987	
${}_1T_{26}$		4996.30		5.440		${}_{12}S_5$		5527.66		4.539	
${}_4T_{11}$	4993.50 ± 4.50	4996.59		4.523	WT	${}_0T_{45}$	5529.80 ± 1.50	5528.13		7.630	T
${}_4S_{18}$	5043.66 ± 1.10	5046.41		3.860	W	${}_1T_{30}$	5527.50 ± 1.50	5528.40		5.783	WT
${}_2T_{20}$	5044.50 ± 4.00	5047.32		4.359	WT	${}_2T_{23}$	5525.50 ± 2.50	5532.41		4.481	WT

TABLE 4.1 continued

Mode	f_{obs} μHz	f_{PREM} μHz	q^a_{obs}	q_{PREM}	ref.[b]	Mode	f_{obs} μHz	f_{PREM} μHz	q_{obs}	q_{PREM}	ref.
${}_4S_{21}$	5526.07 ± 1.30	5534.06		3.861	W	${}_7S_{15}$		6038.97		11.205	I
${}_{14}S_4$	5543.30 ± 0.60	5541.84	1.30 ± .15	1.346	WT	${}_1T_{34}$	6039.50 ± 3.50	6039.22		6.113	WT
${}_4T_{15}$	5538.00 ± 7.00	5544.83		4.462	WT	${}_4T_{18}$		6051.83		4.362	
${}_{15}S_2$		5557.32		9.752	I	${}_3S_{28}$		6053.73		2.377	M
${}_{11}S_7$		5563.67		3.563		${}_{11}S_8$		6055.80		11.532	I
${}_5T_7$		5582.08		4.976		${}_0S_{55}$	6066.50 ± 1.50	6065.26		7.255	S
${}_2S_{26}$	5579.00 ± 3.00	5582.65		5.148	WT	${}_2S_{29}$	6068.14 ± 1.30	6066.18		5.460	W
${}_6S_{15}$	5600.20 ± 1.30	5602.51		3.673	W	${}_1S_{35}$	6061.83 ± 2.40	6069.14		6.494	W
${}_3T_{19}$	5607.00 ± 4.50	5608.11		4.296	WT	${}_0T_{50}$	6079.00 ± 3.00	6076.99		7.630	T
${}_0S_{50}$	5610.30 ± 0.70	5610.73		6.982	S	${}_5T_{13}$		6102.68		4.816	
${}_9S_{10}$	5605.54 ± 1.60	5610.93		3.127	W	${}_{17}S_1$	6122.60 ± 1.50	6129.05		1.396	
${}_3S_{26}$		5620.49		2.489	M	${}_3T_{22}$	6125.00 ± 6.00	6129.31		4.456	50
${}_0T_{46}$	5639.50 ± 2.00	5637.89		7.631	T	${}_{12}S_8$	6133.30 ± 0.40	6137.17	1.85 ± .10	1.763	WT,ss
${}_{12}S_6$		5646.58		3.743		${}_5S_{20}$	6152.22 ± 1.90	6155.98		3.579	W
${}_5T_8$		5649.00		4.961		${}_0S_{56}$	6158.30 ± 1.50	6156.48		7.306	S
${}_1T_{31}$	5656.00 ± 3.00	5657.96		5.868	WT	${}_2T_{27}$	6151.00 ± 6.00	6159.71		4.633	WT
${}_1S_{32}$	5652.36 ± 2.40	5658.62		6.404	WT	${}_{13}S_6$		6161.19		1.541	
${}_7S_{14}$		5663.80		11.200	I	${}_1T_{35}$	6166.00 ± 3.50	6164.06		6.189	WT
${}_5S_{17}$	5669.85 ± 1.30	5673.69		3.295	W	${}_8S_{14}$	6165.07 ± 4.60	6170.65		3.904	WT
${}_2T_{24}$	5684.50 ± 4.00	5691.09		4.522	WT	${}_0T_{51}$	6188.80 ± 3.00	6186.78		7.628	T
${}_{16}S_2$		5697.12		3.042		${}_9S_{12}$	6185.07 ± 0.90	6187.26		2.150	W
${}_4S_{22}$	5695.00 ± 1.50	5700.49		3.861	W/WT	${}_{10}S_{10}$	6185.10 ± 1.40	6190.88		2.658	W
${}_0S_{51}$	5701.60 ± 0.80	5701.42	7.30 ± .15	7.039	S,H	${}_1S_{36}$	6195.00 ± 3.00	6203.83		6.534	W/WT
${}_4T_{16}$	5709.00 ± 7.00	5705.48		4.431	WT	${}_4S_{25}$	6197.23 ± 1.60	6204.82		3.868	W
${}_8S_{11}$	5709.54 ± 1.50	5717.48		3.095	W	${}_5T_{14}$		6217.17		4.768	
${}_5T_9$		5723.92		4.943		${}_{16}S_3$		6222.36		11.598	I
${}_{10}S_8$	5735.00 ± 7.00	5737.09		3.550	WT	${}_2S_{30}$	6228.56 ± 1.20	6225.58		5.524	W
${}_6S_0$	5742.43 ± 0.30	5740.25	0.94 ± .03	1.095	WT,A	${}_4T_{19}$		6234.50		4.334	
${}_2S_{27}$	5746.13 ± 0.90	5745.07		5.316	W	${}_6S_{18}$	6238.10 ± 1.40	6235.56		3.236	W
${}_0T_{47}$	5749.30 ± 2.00	5747.66		7.631	T	${}_0S_{57}$	6250.00 ± 1.30	6247.80		7.357	S
${}_3T_{20}$	5785.00 ± 8.00	5785.19		4.357	WT	${}_3S_{29}$		6270.74		2.372	M
${}_1T_{32}$	5786.50 ± 3.00	5786.24		5.952	WT	${}_1T_{36}$	6287.50 ± 3.00	6287.87		6.263	WT
${}_0S_{52}$	5792.50 ± 1.20	5792.22		7.095	S	${}_0T_{52}$	6298.50 ± 3.00	6296.58		7.626	T
${}_1S_{33}$	5788.81 ± 2.10	5796.49		6.429	W	${}_3T_{23}$	6299.00 ± 6.00	6297.60		4.491	WT
${}_5T_{10}$		5806.78		4.919		${}_2T_{28}$	6306.50 ± 5.50	6313.75		4.667	50
${}_6S_{16}$	5806.74 ± 1.40	5808.40		3.474	W	${}_5S_{21}$	6310.38 ± 2.20	6316.82		3.632	W
${}_{13}S_5$		5834.28		4.079		${}_8S_{15}$	6314.11 ± 6.50	6317.11		3.990	WT
${}_5S_{18}$	5829.20 ± 2.00	5835.59		3.422	W	${}_{15}S_4$	6323.30 ± 1.00	6332.35	2.60 ± .20	2.507	
${}_3S_{27}$		5836.74		2.389	M	${}_1S_{37}$	6331.98 ± 3.30	6337.41		6.578	W
${}_2T_{25}$	5843.00 ± 3.50	5848.47		4.561	WT	${}_0S_{58}$	6341.80 ± 1.50	6339.21		7.406	S
${}_{12}S_7$		5855.88		2.360		${}_5T_{15}$		6339.76		4.713	
${}_0T_{48}$	5859.20 ± 2.00	5857.43		7.631	T	${}_4S_{26}$	6365.49 ± 1.30	6373.42		3.876	W
${}_4S_{23}$	5861.48 ± 1.40	5868.03		3.861	W	${}_2S_{31}$	6385.16 ± 1.20	6384.20		5.585	W
${}_4T_{17}$	5870.00 ± 9.00	5874.88		4.396	WT	${}_{17}S_2$		6395.21		4.327	
${}_8S_{12}$	5869.04 ± 2.50	5876.05		3.565	–	${}_6T_1$		6397.86		4.955	
${}_0S_{53}$	5883.80 ± 1.50	5883.13	7.04 ± .20	7.149	S,O	${}_{13}S_7$	6393.00 ± 3.50	6398.97		2.613	
${}_9S_{11}$	5880.83 ± 0.90	5885.77		2.416	W	${}_{18}S_1$		6402.12		5.271	
${}_5T_{11}$		5897.53		4.891		${}_0T_{53}$	6408.50 ± 3.00	6406.38		7.623	T
${}_2S_{28}$	5903.81 ± 1.10	5906.03		5.393	W	${}_1T_{37}$	6412.50 ± 2.50	6410.74		6.333	WT
${}_1T_{33}$	5915.00 ± 3.50	5913.31		6.034	WT	${}_6T_2$		6412.65		4.948	
${}_{14}S_5$		5929.81		8.644	I	${}_7S_{16}$		6413.76		11.211	I
${}_1S_{34}$	5929.20 ± 2.90	5933.35		6.459	W	${}_4T_{20}$	6410.40 ± 5.00	6420.67		4.316	50
${}_{10}S_9$	5939.00 ± 4.50	5941.76		3.125	WT	${}_{19}S_1$		6427.44		11.165	I
${}_3T_{21}$	5955.00 ± 6.00	5958.71		4.411	WT	${}_0S_{59}$	6434.60 ± 1.70	6430.72		7.454	W
${}_0T_{49}$	5969.00 ± 2.00	5967.21	8.37 ± .25	7.631	T,G	${}_6T_3$		6434.81		4.938	
${}_0S_{54}$	5975.10 ± 1.40	5974.14	7.38 ± .20	7.203	S,G	${}_{11}S_9$	6435.50 ± 2.50	6437.12		1.594	WT
${}_5S_{19}$	5988.49 ± 2.20	5995.82		3.513	W	${}_6S_{19}$	6446.15 ± 1.80	6447.44		3.197	W
${}_5T_{12}$		5996.15		4.856		${}_{17}S_3$		6452.27		4.679	
${}_2T_{26}$	6001.00 ± 4.50	6004.65		4.598	WT	${}_{10}S_{11}$	6446.66 ± 2.50	6454.44		2.637	W
${}_6S_{17}$	6020.71 ± 1.20	6021.31		3.325	W	${}_3T_{24}$	6461.00 ± 7.00	6464.14		4.517	
${}_8S_{13}$	6018.93 ± 3.50	6024.43		3.778	WT	${}_6T_4$		6464.29		4.924	
${}_{15}S_3$	6030.90 ± 0.35	6035.22	1.20 ± .10	1.241	WT	${}_8S_{16}$	6468.00 ± 6.50	6464.75		4.057	WT
${}_4S_{24}$	6028.67 ± 1.50	6036.26		3.864	W	${}_2T_{29}$	6459.50 ± 5.00	6466.83		4.698	50

TABLE 4.1 continued

Mode	f_{obs} μHz	f_{PREM} μHz	q^a_{obs}	q_{PREM}	ref.[b]	Mode	f_{obs} μHz	f_{PREM} μHz	q_{obs}	q_{PREM}	ref.
${}_1S_{38}$	6465.34 ± 2.70	6469.86		6.627	W	${}_{10}S_{13}$	6863.79 ± 2.90	6874.43		3.601	W
${}_5T_{16}$	6470.00 ± 5.00	6470.62		4.651		${}_4S_{29}$	6872.95 ± 1.30	6877.18		3.917	W
${}_{15}S_5$		6475.31		4.113		${}_0S_{64}$	6896.00 ± 5.00	6889.58		7.678	S
${}_5S_{22}$	6473.56 ± 1.90	6478.57		3.678	W	${}_{18}S_3$	6886.50 ± 0.80	6891.93	1.23 ± .08	1.174	WT
${}_9S_{13}$	6479.69 ± 0.90	6483.50		2.063	W	${}_1T_{41}$	6893.00 ± 5.00	6894.00		6.580	50
${}_3S_{30}$		6487.70		2.368	M	${}_5T_{19}$	6901.00 ± 5.00	6914.69		4.433	
${}_{14}S_6$		6493.51		11.069	I	${}_2T_{32}$	6911.00 ± 4.50	6920.90		4.784	WT
${}_6T_5$		6501.07		4.907		${}_3S_{32}$		6921.36		2.363	M
${}_0T_{54}$	6518.50 ± 3.00	6516.18		7.620	T	${}_7S_{19}$	6919.81 ± 4.50	6921.84		4.175	W
${}_0S_{60}$	6526.90 ± 1.50	6522.32		7.501	W	${}_{11}S_{11}$	6915.00 ± 9.00	6922.23		3.088	WT
${}_1T_{38}$	6533.80 ± 4.00	6532.73		6.400	50	${}_{20}S_1$	6954.50 ± 1.50	6954.04	1.45 ± .25	1.141	WT
${}_4S_{27}$	6535.54 ± 1.70	6541.80		3.886	W	${}_0T_{58}$	6959.20 ± 3.00	6955.42	8.50 ± .30	7.604	T,G
${}_2S_{32}$	6541.09 ± 1.50	6542.03		5.643	W	${}_6T_{12}$		6956.77		4.714	
${}_6T_6$		6545.07		4.887		${}_3T_{27}$	6949.50 ± 5.00	6956.93		4.557	50
${}_{18}S_2$	6537.00 ± 2.00	6545.69	1.79 ± 0.30	1.876	ss	${}_5S_{25}$	6965.94 ± 2.00	6967.92		3.803	W
${}_{13}S_8$	6552.00 ± 3.50	6553.59		3.591		${}_4T_{23}$	6978.00 ± 7.00	6980.21		4.309	50
${}_{16}S_4$		6568.64		3.389		${}_0S_{65}$	6989.00 ± 5.00	6981.61	8.15 ± .25	7.720	S,G
${}_7S_0$	6584.80 ± 0.70	6580.71	1.12 ± 0.13	1.135		${}_1S_{42}$		6988.22		6.852	
${}_{15}S_6$		6595.93		4.489		${}_2S_{35}$	7011.91 ± 2.30	7010.52		5.800	W
${}_6T_7$		6596.24		4.864		${}_1T_{42}$	7013.50 ± 3.50	7013.05		6.633	WT
${}_1S_{39}$	6594.33 ± 3.40	6601.16		6.679	W	${}_9S_{15}$	7026.49 ± 1.20	7029.82		2.325	WT
${}_4T_{21}$	6600.00 ± 6.00	6608.12		4.307	50	${}_{10}S_{14}$	7031.00 ± 4.00	7038.76		3.859	WT
${}_5T_{17}$	6596.00 ± 7.00	6609.94		4.583		${}_4S_{30}$	7038.11 ± 1.30	7043.91		3.938	W
${}_{12}S_9$		6610.23		11.602	I	${}_{14}S_8$	7039.00 ± 1.50	7047.89		2.070	WT
${}_0S_{61}$	6619.00 ± 3.00	6614.00		7.547	S	${}_6S_{22}$	7050.31 ± 1.70	7048.18		3.324	W
${}_7S_{17}$	6610.15 ± 3.80	6614.22		4.110	W	${}_6T_{13}$		7049.19		4.680	T
${}_2T_{30}$	6609.00 ± 3.50	6619.02		4.728	WT	${}_0T_{59}$	7069.30 ± 3.00	7065.24		7.599	
${}_0T_{55}$	6628.50 ± 3.00	6625.98		7.617	T	${}_2T_{33}$	7064.00 ± 4.00	7070.65		4.811	50
${}_3T_{25}$	6622.50 ± 3.50	6629.35		4.536	WT	${}_0S_{66}$	7081.00 ± 5.00	7073.71		7.760	S
${}_5S_{23}$	6635.43 ± 1.80	6641.17		3.720	W	${}_{19}S_2$		7078.81		11.007	I
${}_1T_{39}$	6655.00 ± 4.00	6653.89		6.464	WT	${}_5T_{20}$	7074.00 ± 5.00	7080.11		4.356	
${}_6S_{20}$	6653.89 ± 1.40	6654.48		3.202	W	${}_7S_{20}$	7077.02 ± 3.60	7081.96		4.182	W
${}_6T_8$		6654.50		4.838		${}_{15}S_7$		7085.82		11.488	I
${}_{13}S_9$		6686.16		3.861		${}_1S_{43}$		7115.01		6.914	
${}_{10}S_{12}$	6687.00 ± 3.00	6687.11		3.104	W	${}_3T_{28}$	7110.00 ± 5.00	7119.64		4.562	50
${}_2S_{33}$	6697.19 ± 1.40	6699.04		5.698	W	${}_5S_{26}$	7132.66 ± 1.80	7131.42		3.846	W
${}_3S_{31}$		6704.57		2.365	M	${}_1T_{43}$	7131.00 ± 5.00	7131.51		6.683	50
${}_0S_{62}$	6711.00 ± 3.00	6705.78	8.23 ± .25	7.592	S,H	${}_3S_{33}$		7138.07		2.360	M
${}_4S_{28}$	6702.65 ± 1.90	6709.77		3.900	W	${}_{12}S_{11}$	7135.66 ± 0.90	7138.82		1.956	W
${}_{11}S_{10}$	6706.02 ± 1.30	6712.42		2.345	W	${}_6T_{14}$		7148.14		4.644	
${}_6T_9$		6719.78		4.810		${}_{11}S_{12}$	7144.00 ± 5.00	7149.61		2.725	WT
${}_1S_{40}$	6728.29 ± 3.90	6731.31		6.734	W	${}_{16}S_6$	7149.30 ± 0.40	7153.68	1.75 ± .15	1.352	WT
${}_0T_{56}$	6738.80 ± 3.00	6735.79		7.613	T	${}_{13}S_{10}$		7155.54		11.652	I
${}_5T_{18}$	6759.00 ± 5.00	6757.93		4.509		${}_8S_{18}$		7162.43		11.222	I
${}_7S_{18}$	6762.70 ± 6.00	6766.28		4.150	WT	${}_4T_{24}$	7156.00 ± 8.00	7163.04		4.313	50
${}_9S_{14}$	6766.50 ± 1.50	6768.24		2.063	W	${}_2S_{36}$	7164.41 ± 2.50	7164.96		5.847	W
${}_2T_{31}$	6764.00 ± 4.50	6770.36		4.756	50	${}_0S_{67}$	7175.00 ± 6.00	7165.89		7.799	S
${}_{14}S_7$	6773.00 ± 2.50	6772.89		3.026		${}_0T_{60}$	7179.20 ± 3.00	7175.06		7.594	T
${}_1T_{40}$	6773.50 ± 4.00	6774.29		6.524	WT	${}_{10}S_{15}$	7196.00 ± 3.00	7209.25		3.746	W
${}_8S_{17}$		6788.22		11.217	I	${}_4S_{31}$	7204.41 ± 2.20	7209.87		3.963	W
${}_6T_{10}$		6791.98		4.780		${}_2T_{34}$	7213.00 ± 4.00	7219.63		4.838	50
${}_3T_{26}$	6792.00 ± 5.00	6793.54		4.548	50	${}_6S_{23}$	7234.75 ± 1.50	7233.92		3.425	W
${}_4T_{22}$	6787.00 ± 5.00	6795.04		4.306	50	${}_9S_{16}$	7232.73 ± 2.60	7239.58		3.133	W
${}_0S_{63}$	6803.00 ± 5.00	6797.64	8.04 ± .20	7.635	S,O	${}_1S_{44}$		7240.71		6.977	
${}_5S_{24}$	6800.78 ± 2.40	6804.39		3.761	W	${}_{18}S_4$	7238.30 ± 0.30	7241.00	1.09 ± .05	1.060	WT
${}_{16}S_5$	6830.00 ± 0.50	6836.41	1.85 ± .10	1.720	WT	${}_7S_{21}$	7248.37 ± 2.90	7247.61		4.166	W
${}_0T_{57}$	6849.00 ± 3.00	6845.61		7.609	T	${}_1T_{44}$	7248.50 ± 3.00	7249.42		6.730	50
${}_{17}S_4$		6854.04		11.690	I	${}_6T_{15}$		7253.56		4.609	
${}_6S_{21}$	6855.20 ± 1.80	6855.03		3.246	W	${}_5T_{21}$		7253.69		4.286	
${}_2S_{34}$	6852.39 ± 1.50	6855.21		5.750	W	${}_0S_{68}$	7268.00 ± 6.00	7258.14		7.838	S
${}_1S_{41}$		6860.33		6.792		${}_3T_{29}$	7271.00 ± 4.50	7281.77		4.565	50
${}_{12}S_{10}$	6860.00 ± 5.00	6861.33		3.022	WT	${}_0T_{61}$	7290.00 ± 3.00	7284.88		7.588	T
${}_6T_{11}$		6871.01		4.748		${}_5S_{27}$	7291.93 ± 2.30	7294.59		3.892	W

TABLE 4.1 continued

Mode	f_{obs} μHz	f_{PREM} μHz	q^a_{obs}	q_{PREM}	ref.[b]	Mode	f_{obs} μHz	f_{PREM} μHz	q_{obs}	q_{PREM}	ref.
${}_2S_{37}$	7318.55 ± 2.10	7318.53		5.890	W	${}_2T_{37}$	7653.00 ± 3.00	7661.93		4.924	WT
${}_4T_{25}$	7336.00 ± 9.00	7343.40		4.318	50	${}_{15}S_8$		7664.98		11.231	I
${}_0S_{69}$	7361.00 ± 7.00	7350.47		7.875	S	${}_7T_7$		7667.63		4.741	
${}_{14}S_9$	7345.00 ± 0.80	7354.08	2.13 ± .15	1.892	WT	${}_{10}S_{17}$	7673.49 ± 1.40	7675.89		2.580	W
${}_3S_{34}$		7354.71		2.358	M	${}_{20}S_3$		7685.74		7.229	I
${}_{20}S_2$	7360.00 ± 3.50	7357.09	1.73 ± .35	1.940	ss	${}_{11}S_{14}$	7679.00 ± 3.50	7686.80		2.504	WT
${}_1S_{45}$		7365.35		7.041		${}_{16}S_8$		7689.68		4.011	
${}_6T_{16}$		7365.37		4.574		${}_{13}S_{11}$		7693.02		11.669	I
${}_1T_{45}$	7362.50 ± 4.50	7366.83		6.773	WT	${}_4T_{27}$	7694.00 ± 7.00	7697.46		4.326	WT
${}_2T_{35}$	7362.00 ± 4.00	7367.85		4.865	WT	${}_9S_{19}$	7689.69 ± 4.50	7698.29		4.030	WT
${}_4S_{32}$	7369.39 ± 1.60	7374.98		3.992	W	${}_4S_{34}$	7700.08 ± 1.90	7702.48		4.062	W
${}_0T_{62}$	7290.00 ± 3.00	7394.70		7.582	T	${}_1T_{48}$	7715.50 ± 5.50	7716.44		6.886	50
${}_9S_{17}$	7398.33 ± 3.00	7403.56		3.675	WT	${}_7T_8$		7717.14		4.735	
${}_6S_{24}$	7412.49 ± 2.10	7413.13		3.534	W	${}_0S_{73}$	7736.00 ± 7.00	7720.47		8.012	S
${}_{11}S_{13}$	7411.50 ± 4.00	7417.49		2.379	WT	${}_0T_{65}$	7731.00 ± 3.00	7724.15		7.563	T
${}_7S_{22}$	7418.73 ± 2.00	7419.40		4.127	W	${}_1S_{48}$		7733.33		7.236	
${}_{10}S_{16}$	7420.12 ± 1.60	7422.64		3.038	W	${}_6T_{19}$		7738.59		4.474	
${}_8S_0$	7429.00 ± 1.00	7424.13	0.98 ± .12	1.174	WT	${}_6S_{26}$	7756.13 ± 2.10	7757.89		3.733	W
${}_5T_{22}$		7434.43		4.226		${}_3T_{32}$	7757.50 ± 4.50	7764.94		4.572	WT
${}_0S_{70}$	7455.00 ± 7.00	7442.86		7.911	S	${}_{15}S_9$	7768.00 ± 3.50	7771.75		4.008	
${}_3T_{30}$	7439.00 ± 4.50	7443.36		4.567	WT	${}_7T_9$		7772.53		4.730	
${}_{12}S_{12}$	7449.50 ± 1.00	7455.08		1.754	W	${}_2S_{40}$	7774.94 ± 2.50	7773.95		6.005	W
${}_5S_{28}$	7455.36 ± 2.10	7457.18		3.939	W	${}_{12}S_{13}$	7767.92 ± 0.70	7777.00		1.758	W
${}_{17}S_5$		7461.22		10.212	I	${}_5S_{30}$	7778.52 ± 2.60	7780.00		4.034	W
${}_2S_{38}$	7473.00 ± 1.80	7471.21		5.931	W	${}_7S_{24}$	7778.87 ± 2.30	7780.08		4.013	W
${}_{16}S_7$	7471.50 ± 1.00	7474.14	1.45 ± .12	1.250	WT	${}_3S_{36}$		7787.76		2.355	M
${}_6T_{17}$		7483.49		4.540		${}_{21}S_3$		7801.59		5.862	
${}_1T_{46}$	7483.50 ± 4.00	7483.78		6.813	WT	${}_{17}S_8$		7805.05		1.838	
${}_1S_{46}$		7488.98		7.106		${}_2T_{38}$	7798.00 ± 4.00	7807.76		4.956	50
${}_{21}S_1$		7495.27		4.718		${}_5T_{24}$		7810.82		4.155	
${}_7T_1$		7498.57		4.762		${}_0S_{74}$	7830.00 ± 7.00	7813.15	8.73 ± .25	8.043	S,O
${}_0T_{63}$	7511.00 ± 3.00	7504.52		7.576	T	${}_{22}S_1$	7822.40 ± 0.50	7819.54	0.95 ± .05	1.304	WT
${}_{19}S_3$		7504.81		4.384		${}_{14}S_{11}$	7813.16 ± 7.00	7823.54		3.769	WT
${}_7T_2$		7511.20		4.760		${}_1T_{49}$	7830.00 ± 6.00	7832.22		6.918	WT
${}_{21}S_2$		7514.86		4.577		${}_7T_{10}$		7833.70		4.725	
${}_2T_{36}$	7505.00 ± 5.00	7515.28		4.894	WT	${}_0T_{66}$	7842.00 ± 3.00	7833.97		7.555	T
${}_{18}S_5$		7517.39		4.365		${}_8S_{20}$	7846.85 ± 6.50	7843.35		4.106	WT
${}_4T_{26}$	7512.00 ± 5.00	7521.46		4.322	WT	${}_1S_{49}$		7854.14		7.300	
${}_7T_3$		7530.11		4.758		${}_4S_{35}$	7859.58 ± 1.80	7864.82		4.102	W
${}_0S_{71}$	7548.00 ± 7.00	7535.33		7.946	S	${}_4T_{28}$	7863.00 ± 8.00	7871.66		4.331	WT
${}_8S_{19}$		7536.41		11.229	I	${}_6T_{20}$		7875.57		4.443	
${}_4S_{33}$	7536.51 ± 1.90	7539.19		4.025	W	${}_{15}S_{10}$	7896.00 ± 6.00	7897.49		3.224	WT
${}_{19}S_4$		7540.90		4.538		${}_{23}S_1$		7899.09		11.631	I
${}_9S_{18}$	7541.47 ± 4.00	7552.78		3.907	W	${}_7T_{11}$		7900.55		4.720	
${}_7T_4$		7555.27		4.754		${}_0S_{75}$	7925.00 ± 7.00	7905.88		8.074	S
${}_3S_{35}$		7571.27		2.357	M	${}_9S_{20}$		7910.21		11.235	I
${}_{17}S_6$		7580.67		4.230		${}_{11}S_{15}$		7919.06		3.012	
${}_7T_5$		7586.61		4.750		${}_2S_{41}$	7921.24 ± 3.90	7924.01		6.038	W
${}_6S_{25}$	7588.13 ± 2.10	7587.27		3.640	W	${}_3T_{33}$	7914.50 ± 4.50	7924.89		4.576	WT
${}_7S_{23}$	7593.92 ± 1.70	7597.20		4.073	W	${}_6S_{27}$	7921.94 ± 1.70	7926.36		3.810	W
${}_1T_{47}$	7597.00 ± 5.00	7600.31		6.851	50	${}_{10}S_{18}$	7936.46 ± 1.10	7938.48		2.434	W
${}_3T_{31}$	7600.00 ± 5.00	7604.42		4.569	50	${}_5S_{31}$	7941.78 ± 2.40	7940.16		4.080	W
${}_6T_{18}$		7607.90		4.506		${}_0T_{67}$	7952.00 ± 4.00	7943.78	8.46 ± .30	7.548	T,G
${}_1S_{47}$		7611.63		7.171		${}_1T_{50}$	7948.50 ± 3.50	7947.68		6.947	WT
${}_0T_{64}$	7621.00 ± 3.00	7614.33		7.569	T	${}_2T_{39}$	7943.50 ± 3.00	7952.75		4.990	WT
${}_5S_{29}$	7616.88 ± 2.50	7619.01		3.987	W	${}_{13}S_{12}$	7950.00 ± 5.50	7955.03		4.043	WT
${}_5T_{23}$		7620.80		4.181		${}_{18}S_6$		7957.04		2.530	
${}_2S_{39}$	7623.39 ± 2.70	7623.02		5.970	W	${}_7S_{25}$	7964.31 ± 2.80	7966.58		3.960	W
${}_7T_6$		7624.09		4.746		${}_7T_{12}$		7972.96		4.715	
${}_0S_{72}$	7642.00 ± 7.00	7627.87		7.979	S	${}_1S_{50}$		7974.10		7.363	
${}_{17}S_7$		7635.12		4.372		${}_8S_{21}$	7976.33 ± 4.25	7989.31		4.156	
${}_{14}S_{10}$	7624.00 ± 4.00	7635.75		2.574	WT	${}_0S_{76}$	8019.00 ± 7.00	7998.68	8.90 ± .25	8.103	S,G/H
${}_{19}S_5$		7661.84		2.726		${}_5T_{25}$		8002.38		4.148	

TABLE 4.1 continued

Mode	f_{obs} μHz	f_{PREM} μHz	q^a_{obs}	q_{PREM}	ref.[b]	Mode	f_{obs} μHz	f_{PREM} μHz	q_{obs}	q_{PREM}	ref.
${}_3S_{37}$		8004.19		2.353	M	${}_4T_{31}$		8385.31		4.361	
${}_6T_{21}$		8018.91		4.413		${}_3T_{36}$	8395.00 ± 10.0	8401.09		4.598	WT
${}_4S_{36}$	8019.95 ± 1.50	8026.22		4.146	W	${}_1T_{54}$	8402.00 ± 6.00	8406.75		7.044	50
${}_4T_{29}$		8044.29		4.339		${}_{12}S_{15}$	8402.99 ± 1.00	8411.28		1.840	W
${}_7T_{13}$		8050.83		4.711		${}_7T_{17}$		8414.71		4.696	
${}_0T_{68}$	8062.00 ± 4.00	8053.59		7.540	T	${}_5S_{34}$	8409.00 ± 4.00	8416.62		4.191	W/WT
${}_1T_{51}$	8058.00 ± 6.00	8062.83		6.975	50	${}_{11}S_{18}$	8420.49 ± 9.00	8418.49		3.976	WT
${}_2S_{42}$	8072.00 ± 4.80	8073.21		6.069	W	${}_6S_{30}$	8417.21 ± 3.10	8427.41		3.952	W
${}_3T_{34}$	8080.00 ± 5.00	8084.26		4.581	WT	${}_{15}S_{12}$	8426.74 ± 2.00	8432.73		1.747	W
${}_{13}S_{13}$	8084.46 ± 9.00	8091.46		3.907		${}_3S_{39}$		8436.86		2.350	M
${}_0S_{77}$	8112.00 ± 7.00	8091.55		8.131	S	${}_{16}S_{10}$	8433.00 ± 3.00	8437.72		1.291	WT
${}_{19}S_6$		8093.14		10.515	I	${}_8S_{24}$	8434.49 ± 7.00	8440.00		4.211	–
${}_1S_{51}$		8093.25		7.425		${}_1S_{54}$		8446.31		7.603	
${}_6S_{28}$	8088.18 ± 2.10	8093.69		3.871	W	${}_{10}S_{20}$	8444.79 ± 1.40	8446.66		2.560	W
${}_2T_{40}$	8089.00 ± 5.00	8096.87		5.027	WT	${}_0S_{81}$	8490.00 ± 8.00	8463.61		8.232	S
${}_{12}S_{14}$	8088.30 ± 0.90	8097.37		1.809	W	${}_{20}S_5$	8465.50 ± 2.00	8471.58	1.76 ± .25	1.571	WT
${}_5S_{32}$	8099.06 ± 2.10	8099.56		4.122	W	${}_{13}S_{15}$	8469.42 ± 9.00	8474.42		2.968	WT
${}_{11}S_{16}$	8101.00 ± 5.00	8107.03		3.514	WT	${}_6T_{24}$		8487.69		4.332	
${}_{20}S_4$	8118.00 ± 2.00	8116.77	1.38 ± .25	1.278	ss	${}_0T_{72}$	8503.00 ± 4.00	8492.80		7.507	T
${}_{16}S_9$	8116.00 ± 2.00	8117.59		1.392	WT	${}_4S_{39}$	8499.51 ± 2.40	8504.92		4.293	W
${}_{15}S_{11}$	8122.42 ± 2.00	8130.95		1.999	W	${}_2S_{45}$	8508.96 ± 4.50	8515.75		6.150	W
${}_7T_{14}$		8134.04		4.707		${}_7T_{18}$		8518.35		4.691	
${}_8S_{22}$	8127.86 ± 4.40	8136.99		4.188	WT	${}_1T_{55}$	8514.40 ± 7.00	8520.94		7.063	50
${}_7S_{26}$	8154.33 ± 2.30	8155.16		3.919	W	${}_2T_{43}$	8507.00 ± 8.00	8523.66		5.153	WT
${}_0T_{69}$	8173.00 ± 4.00	8163.40		7.533	T	${}_7S_{28}$	8522.63 ± 3.00	8533.66		3.876	W
${}_6T_{22}$		8168.68		4.385		${}_{24}S_1$		8550.62		4.963	
${}_1T_{52}$	8171.00 ± 7.00	8177.72		7.000	50	${}_8T_1$		8551.15		4.975	
${}_0S_{78}$	8207.00 ± 8.00	8184.47		8.158	S	${}_4T_{32}$	8548.00 ± 7.00	8553.86		4.377	WT
${}_4S_{37}$	8184.38 ± 1.50	8186.69		4.192	W	${}_0S_{82}$	8585.00 ± 8.00	8556.77		8.254	S
${}_5T_{26}$		8193.48		4.159		${}_3T_{37}$	8548.00 ± 5.00	8558.49		4.609	WT
${}_{10}S_{19}$	8195.52 ± 1.10	8197.96		2.428	W	${}_{22}S_3$		8559.91		3.686	
${}_{22}S_2$	8200.00 ± 2.00	8207.04	1.67 ± .25	1.397	41	${}_{23}S_2$		8561.36		5.004	
${}_1S_{52}$		8211.63		7.486		${}_8T_2$		8561.68		4.974	
${}_4T_{30}$	8196.00 ± 10.0	8215.47		4.348	50	${}_1S_{55}$		8562.68		7.659	
${}_3S_{38}$		8220.55		2.352	M	${}_{11}S_{19}$		8568.59		4.020	
${}_2S_{43}$	8219.54 ± 4.10	8221.56		6.098	W	${}_5T_{28}$		8568.60		4.218	
${}_7T_{15}$		8222.48		4.703		${}_5S_{35}$	8570.59 ± 2.90	8574.62		4.218	W
${}_{14}S_{12}$		8224.06		11.684	I	${}_8T_3$		8577.46		4.973	
${}_2T_{41}$	8230.00 ± 8.00	8240.08		5.066	WT	${}_{24}S_2$		8585.28		11.454	I
${}_3T_{35}$	8234.00 ± 10.0	8243.00		4.589	50	${}_6S_{31}$	8588.30 ± 2.70	8594.46		3.975	W
${}_{17}S_9$		8248.53		11.488	I	${}_8S_{25}$	8590.61 ± 7.50	8596.24		4.205	–
${}_5S_{33}$	8253.59 ± 2.60	8258.32		4.159	W	${}_{22}S_4$		8598.40		4.877	
${}_{13}S_{14}$	8254.84 ± 6.50	8258.94		3.502	WT	${}_8T_4$		8598.47		4.970	
${}_6S_{29}$	8255.78 ± 2.10	8260.57		3.918	W	${}_{18}S_8$		8599.27		2.423	
${}_9S_0$	8268.00 ± 2.00	8262.64	0.80 ± .15	1.190	WT	${}_0T_{73}$	8613.00 ± 5.00	8602.59		7.499	T
${}_{11}S_{17}$	8265.00 ± 8.00	8268.00		3.821	WT	${}_{23}S_3$		8602.59		2.605	
${}_0T_{70}$	8282.00 ± 4.00	8273.20		7.524	T	${}_8T_5$		8624.69		4.967	
${}_0S_{79}$	8302.00 ± 8.00	8277.46		8.184	S	${}_7T_{19}$		8626.95		4.685	
${}_9S_{21}$		8283.85		11.241	I	${}_1T_{56}$	8631.00 ± 8.00	8634.93		7.081	50
${}_8S_{23}$	8282.21 ± 8.00	8287.05		4.205	–	${}_{21}S_5$		8639.18		4.429	
${}_1T_{53}$	8290.00 ± 7.00	8292.35		7.023	50	${}_{20}S_6$		8642.79		4.644	
${}_{18}S_7$		8301.04		1.444		${}_0S_{83}$	8679.00 ± 8.00	8649.99		8.275	S
${}_7T_{16}$		8316.07		4.700		${}_3S_{40}$		8653.08		2.360	M
${}_6T_{23}$		8324.95		4.358		${}_{25}S_1$	8658.00 ± 2.00	8655.17	1.35 ± .25	1.185	ss
${}_1S_{53}$		8329.31		7.545		${}_8T_6$		8656.08		4.964	
${}_7S_{27}$	8342.30 ± 1.70	8344.50		3.892	W	${}_6T_{25}$		8656.69		4.309	
${}_4S_{38}$	8342.15 ± 2.20	8346.24		4.242	W	${}_9S_{22}$		8657.36		11.248	I
${}_2S_{44}$	8360.54 ± 4.30	8369.08		6.124	W	${}_2S_{46}$	8656.02 ± 4.80	8661.61		6.173	W
${}_0S_{80}$	8395.00 ± 8.00	8370.50		8.208	S	${}_4S_{40}$	8663.48 ± 2.80	8662.79		4.335	W
${}_{21}S_4$		8373.62		11.544	I	${}_2T_{44}$	8654.00 ± 8.00	8663.95		5.200	50
${}_2T_{42}$	8370.00 ± 8.00	8382.36		5.108	WT	${}_{19}S_7$		8671.41		10.411	I
${}_5T_{27}$		8382.56		4.183		${}_{10}S_{21}$	8675.90 ± 2.50	8673.48		2.922	W
${}_0T_{71}$	8392.00 ± 4.00	8383.00		7.516	T	${}_1S_{56}$		8678.47		7.713	

TABLE 4.1 continued

Mode	f_{obs} μHz	f_{PREM} μHz	q^a_{obs}	q_{PREM}	ref.[b]	Mode	f_{obs} μHz	f_{PREM} μHz	q_{obs}	q_{PREM}	ref.
${}_{12}S_{16}$	8689.38 ± 1.80	8691.79		2.225	W	${}_{8}T_{13}$		9017.75		4.900	
${}_{8}T_{7}$		8692.62		4.959		${}_{1}S_{59}$		9022.73		7.864	
${}_{20}S_{7}$		8706.24		5.731		${}_{25}S_{2}$	9026.00 ± 2.00	9022.91	1.21 ± .10	1.269	WT
${}_{0}T_{74}$	8723.00 ± 5.00	8712.37		7.489	T	${}_{0}S_{87}$	9057.00 ± 9.00	9023.43		8.350	S
${}_{3}T_{38}$	8702.00 ± 8.00	8715.17		4.622	50	${}_{3}T_{40}$	9020.00 ± 10.0	9026.32		4.653	WT
${}_{4}T_{33}$	8711.00 ± 8.00	8721.15		4.395	50	${}_{9}S_{23}$		9030.75		11.255	I
${}_{7}S_{29}$	8712.29 ± 3.00	8722.02		3.870	W	${}_{10}S_{23}$	9025.00 ± 10.0	9038.42		3.756	WT
${}_{11}S_{20}$	8724.19 ± 5.00	8726.69		3.927	W	${}_{0}T_{77}$	9054.00 ± 5.0	9041.69	8.41 ± .35	7.461	T,G
${}_{5}S_{36}$	8726.95 ± 3.50	8732.50		4.237	W	${}_{19}S_{9}$	9044.00 ± 8.00	9047.16		1.632	WT
${}_{8}T_{8}$		8734.26		4.953		${}_{5}S_{38}$	9043.67 ± 2.70	9048.53		4.258	W
${}_{14}S_{13}$	8731.00 ± 3.50	8734.78		2.097	WT	${}_{4}T_{35}$	9050.00 ± 7.00	9052.02		4.438	WT
${}_{16}S_{11}$	8729.00 ± 5.00	8736.47		1.816	WT	${}_{10}S_{0}$	9059.00 ± 2.00	9056.12		1.206	
${}_{7}T_{20}$		8740.51		4.677		${}_{13}S_{17}$	9053.82 ± 3.00	9063.12		2.083	W
${}_{0}S_{84}$	8774.00 ± 8.00	8743.27	9.20 ± .30	8.296	S,O	${}_{2}T_{47}$	9071.00 ± 8.00	9078.56		5.359	50
${}_{18}S_{9}$	8735.00 ± 7.00	8747.40		4.299	WT	${}_{4}S_{42}$		9085.50		2.346	M
${}_{1}T_{57}$	8748.00 ± 10.0	8748.74		7.097	50	${}_{8}S_{28}$	9074.00 ± 7.00	9086.85		4.143	–
${}_{15}S_{13}$		8749.54		11.679	I	${}_{1}T_{60}$	9087.00 ± 9.00	9089.22		7.137	50
${}_{5}T_{29}$		8751.14		4.257		${}_{8}T_{14}$		9089.28		4.882	
${}_{13}S_{16}$	8741.38 ± 1.60	8752.25		2.313	W	${}_{2}S_{49}$		9094.25		6.239	WT
${}_{8}S_{26}$	8753.56 ± 7.00	8756.06		4.191	–	${}_{7}S_{31}$	9089.29 ± 2.80	9095.12		3.875	W
${}_{6}S_{32}$	8759.31 ± 3.20	8761.80		3.991	W	${}_{16}S_{13}$	9088.37 ± 5.50	9095.71		3.627	
${}_{8}T_{9}$		8780.96		4.946		${}_{6}S_{34}$	9092.08 ± 3.00	9097.31		4.004	W
${}_{1}S_{57}$		8793.72		7.765		${}_{5}T_{31}$	9096.00 ± 7.00	9105.98		4.337	
${}_{19}S_{8}$	8792.95 ± 8.00	8797.85		3.536		${}_{11}S_{22}$	9103.06 ± 2.40	9111.59		3.153	W
${}_{2}T_{45}$	8785.00 ± 6.00	8803.22		5.250	WT	${}_{7}T_{23}$		9111.72		4.629	
${}_{2}S_{47}$	8807.27 ± 5.10	8806.64		6.196	W	${}_{0}S_{88}$	9151.00 ± 9.00	9116.92		8.365	S
${}_{17}S_{10}$		8817.00		11.146	I	${}_{3}S_{43}$	9138.26 ± 2.30	9131.62		4.510	W
${}_{3}S_{41}$	8823.12 ± 2.60	8819.77		4.400	W	${}_{1}S_{60}$		9136.57		7.911	
${}_{0}T_{75}$	8834.00 ± 5.00	8822.15		7.480	T	${}_{12}S_{18}$	9138.54 ± 5.00	9145.99		3.073	
${}_{6}T_{26}$		8831.46		4.290		${}_{17}S_{12}$	9145.50 ± 3.00	9151.28		2.163	WT
${}_{8}T_{10}$		8832.70		4.937		${}_{0}T_{78}$	9164.00 ± 6.00	9151.46		7.451	T
${}_{18}S_{10}$		8836.23		4.985		${}_{8}T_{15}$		9165.71		4.862	
${}_{0}S_{85}$	8867.00 ± 8.00	8836.60		8.315	S	${}_{14}S_{15}$	9163.00 ± 4.00	9168.47		3.598	
${}_{21}S_{6}$	8849.50 ± 0.80	8850.77	1.58 ± .10	1.351	WT	${}_{21}S_{7}$	9170.05 ± 1.50	9173.79	1.58 ± .10	1.250	WT
${}_{7}T_{21}$		8859.08		4.665		${}_{3}T_{41}$	9166.00 ± 8.00	9180.76		4.670	WT
${}_{1}T_{58}$	8857.00 ± 9.00	8862.38		7.112	50	${}_{6}T_{28}$		9194.29		4.271	
${}_{10}S_{22}$	8864.67 ± 2.50	8868.46		3.417	W	${}_{9}S_{24}$	9190.00 ± 5.00	9196.93		3.929	WT
${}_{4}S_{41}$		8869.34		2.348	M	${}_{1}T_{61}$	9196.00 ± 8.00	9202.44		7.148	50
${}_{3}T_{39}$	8858.00 ± 8.00	8871.12		4.637	WT	${}_{5}S_{39}$	9200.63 ± 3.20	9206.92		4.259	W
${}_{4}T_{34}$	8873.00 ± 6.00	8887.20		4.416	WT	${}_{0}S_{89}$	9246.00 ± 9.00	9210.47		8.380	S
${}_{8}T_{11}$		8889.44		4.927		${}_{2}T_{48}$	9205.00 ± 8.00	9214.61		5.416	50
${}_{5}S_{37}$	8884.50 ± 2.90	8890.43		4.250	W	${}_{4}T_{36}$	9208.00 ± 8.00	9215.65		4.462	50
${}_{11}S_{21}$	8896.96 ± 3.35	8904.37		3.606	W	${}_{24}S_{3}$		9218.64		10.287	I
${}_{1}S_{58}$		8908.46		7.816		${}_{2}S_{50}$		9236.83		6.261	
${}_{7}S_{30}$	8902.52 ± 2.40	8909.23		3.870	W	${}_{7}T_{24}$		9246.21		4.601	
${}_{8}S_{27}$	8912.00 ± 7.50	8919.60		4.170	WT	${}_{8}T_{16}$		9247.01		4.839	
${}_{6}S_{33}$	8926.92 ± 2.70	8929.44		4.000	W	${}_{1}S_{61}$		9250.01		7.955	
${}_{0}S_{86}$	8962.00 ± 8.00	8929.99	8.90 ± .30	8.333	S,G	${}_{8}S_{29}$	9242.65 ± 8.00	9257.65		4.114	–
${}_{5}T_{30}$		8930.17		4.298		${}_{0}T_{79}$	9274.00 ± 6.00	9261.21		7.441	T
${}_{0}T_{76}$	8943.00 ± 5.00	8931.93		7.471	T	${}_{20}S_{8}$		9262.17		11.298	I
${}_{12}S_{17}$	8930.60 ± 5.00	8933.91		2.612	WT	${}_{6}S_{35}$	9257.99 ± 3.70	9265.32		4.006	W
${}_{2}T_{46}$	8932.00 ± 7.00	8941.43		5.303	WT	${}_{15}S_{14}$		9270.16		11.706	I
${}_{23}S_{4}$	8937.00 ± 2.00	8941.57	1.35 ± .10	1.235	WT	${}_{5}T_{32}$		9279.00		4.372	
${}_{17}S_{11}$		8942.70		3.946		${}_{7}S_{32}$	9279.15 ± 2.30	9279.63		3.882	W
${}_{16}S_{12}$		8944.33		3.522		${}_{3}S_{44}$	9290.13 ± 2.50	9286.52		4.564	W
${}_{2}S_{48}$		8950.86		6.218	WT	${}_{23}S_{5}$	9290.00 ± 0.80	9289.58	1.15 ± .10	1.112	WT
${}_{8}T_{12}$		8951.13		4.914		${}_{4}S_{43}$		9301.61		2.345	M
${}_{1}T_{59}$	8970.00 ± 8.00	8975.87		7.125	50	${}_{0}S_{90}$	9339.00 ± 9.00	9304.07		8.394	S
${}_{3}S_{42}$	8976.89 ± 2.45	8976.05		4.455	W	${}_{16}S_{14}$		9304.36		2.698	
${}_{7}T_{22}$		8982.76		4.650		${}_{1}T_{62}$	9306.00 ± 7.00	9315.53		7.157	50
${}_{14}S_{14}$	8982.00 ± 4.00	8985.12		3.019	WT	${}_{12}S_{19}$	9320.02 ± 7.00	9329.10		3.469	WT
${}_{22}S_{5}$		9005.25		11.708	I	${}_{8}T_{17}$		9333.20		4.813	
${}_{6}T_{27}$		9011.09		4.277		${}_{3}T_{42}$	9323.00 ± 8.00	9334.44		4.688	WT

TABLE 4.1 continued

Mode	f_{obs} μHz	f_{PREM} μHz	q^a_{obs}	q_{PREM}	ref.[b]	Mode	f_{obs} μHz	f_{PREM} μHz	q_{obs}	q_{PREM}	ref.
${}_{14}S_{16}$	9334.00 ± 4.00	9337.18		3.543		${}_{9}T_{4}$		9621.48		4.773	
${}_{11}S_{23}$	9327.00 ± 2.00	9341.10		2.863	W	${}_{3}T_{44}$	9615.00 ± 7.00	9639.58		4.723	WT
${}_{2}T_{49}$	9338.00 ± 8.00	9349.55		5.475	50	${}_{7}S_{34}$	9636.83 ± 2.70	9644.54		3.899	W
${}_{9}S_{25}$	9343.00 ± 6.00	9351.55		4.017		${}_{9}T_{5}$		9645.80		4.762	
${}_{19}S_{10}$	9353.00 ± 2.00	9357.39	1.98 ± .25	1.479	WT	${}_{23}S_{6}$		9646.41		7.094	I
${}_{1}S_{62}$		9363.08		7.997		${}_{12}S_{21}$	9642.81 ± 8.00	9647.81		3.867	WT
${}_{26}S_{1}$		9364.82		11.554	I	${}_{24}S_{5}$		9647.92		4.675	
${}_{5}S_{40}$	9360.49 ± 3.90	9365.67		4.256	W	${}_{19}S_{11}$	9644.00 ± 4.00	9653.75		1.872	
${}_{0}T_{80}$	9384.00 ± 6.00	9370.95		7.430	T	${}_{1}T_{65}$	9647.00 ± 7.00	9654.15		7.180	50
${}_{13}S_{18}$	9365.05 ± 1.40	9371.79		2.038	W	${}_{2}S_{53}$		9659.62		6.326	
${}_{4}T_{37}$	9390.00 ± 7.00	9378.12		4.485	WT	${}_{9}S_{27}$	9657.00 ± 7.00	9660.38		4.088	
${}_{2}S_{51}$		9378.59		6.282		${}_{13}S_{19}$	9663.55 ± 1.20	9671.80		2.054	W
${}_{6}T_{29}$		9379.50		4.272		${}_{9}T_{6}$		9674.96		4.750	
${}_{18}S_{11}$		9384.31		11.660	I	${}_{0}S_{94}$	9718.00 ± 9.00	9678.99		8.438	S
${}_{7}T_{25}$		9386.54		4.564		${}_{5}S_{42}$	9679.32 ± 3.10	9684.42		4.239	W
${}_{0}S_{91}$	9435.00 ± 9.00	9397.73		8.407	S	${}_{7}T_{27}$		9686.26		4.465	
${}_{10}S_{24}$		9404.05		11.263	I	${}_{4}T_{39}$	9679.00 ± 9.00	9699.82		4.530	WT
${}_{8}T_{18}$		9424.29		4.783		${}_{0}T_{83}$	9715.00 ± 7.00	9700.14		7.398	T
${}_{25}S_{3}$		9424.61		2.646		${}_{24}S_{6}$		9700.17		4.089	
${}_{1}T_{63}$	9422.00 ± 7.00	9428.51		7.166	50	${}_{1}S_{65}$		9700.36		8.113	
${}_{8}S_{30}$	9421.74 ± 8.00	9431.74		4.083	–	${}_{9}T_{7}$		9708.96		4.735	
${}_{6}S_{36}$	9423.84 ± 3.10	9433.35		4.005	W	${}_{17}S_{14}$	9705.00 ± 5.00	9709.08		2.165	WT
${}_{17}S_{13}$	9429.00 ± 3.00	9435.93		1.804	WT	${}_{22}S_{7}$		9716.00		4.489	
${}_{3}S_{45}$	9441.41 ± 3.00	9440.80		4.618	W	${}_{8}T_{21}$		9727.24		4.671	
${}_{5}T_{33}$	9440.00 ± 7.00	9449.69		4.402		${}_{4}S_{45}$		9733.71		2.343	M
${}_{7}S_{33}$	9457.46 ± 2.10	9462.76		3.890	W	${}_{3}S_{47}$	9750.64 ± 2.50	9747.60		4.724	W
${}_{1}S_{63}$		9475.81		8.038		${}_{9}T_{8}$		9747.78		4.719	
${}_{0}T_{81}$	9495.00 ± 6.00	9480.69		7.420	T	${}_{2}T_{52}$	9740.00 ± 10.0	9747.83		5.661	50
${}_{2}T_{50}$	9479.00 ± 10.0	9483.40		5.536	50	${}_{14}S_{18}$	9741.70 ± 5.50	9748.85		2.707	WT
${}_{27}S_{1}$	9494.00 ± 3.00	9485.84	1.35 ± .24	1.542	WT	${}_{25}S_{4}$		9749.46		3.347	
${}_{3}T_{43}$	9472.00 ± 7.00	9487.38		4.706	WT	${}_{6}T_{31}$		9750.03		4.287	
${}_{0}S_{92}$	9529.00 ± 9.00	9491.43		8.418	S	${}_{1}T_{66}$	9753.70 ± 9.00	9766.83		7.187	50
${}_{12}S_{20}$	9487.18 ± 7.00	9493.18		3.724	WT	${}_{22}S_{8}$		9766.99		4.488	
${}_{21}S_{8}$	9492.00 ± 3.00	9496.96	1.45 ± .10	1.497	WT	${}_{6}S_{38}$	9760.55 ± 3.00	9768.94		4.004	W
${}_{9}S_{26}$	9503.00 ± 5.00	9505.55		4.063	WT	${}_{0}S_{95}$	9813.00 ± 9.00	9772.85	9.45 ± .30	8.447	S,O
${}_{4}S_{44}$		9517.68		2.344	M	${}_{10}S_{25}$		9777.27		11.271	I
${}_{2}S_{52}$		9519.52		6.304	WT	${}_{5}T_{35}$		9785.86		4.443	
${}_{8}T_{19}$		9520.30		4.749		${}_{16}S_{15}$		9786.62		11.714	I
${}_{5}S_{41}$	9511.00 ± 4.00	9524.84		4.249	W	${}_{8}S_{32}$	9767.23 ± 7.00	9788.23		4.023	–
${}_{14}S_{17}$	9514.00 ± 4.50	9526.65		3.162		${}_{20}S_{9}$	9810.00 ± 10.0	9790.64		3.485	WT
${}_{7}T_{26}$		9533.08		4.519		${}_{3}T_{45}$	9776.00 ± 9.00	9791.08		4.741	50
${}_{4}T_{38}$	9523.00 ± 7.00	9539.49		4.509	50	${}_{9}T_{9}$		9791.40		4.700	
${}_{1}T_{64}$	9533.00 ± 8.00	9541.38		7.174	50	${}_{2}S_{54}$		9798.87		6.348	WT
${}_{6}T_{30}$		9565.17		4.279		${}_{12}S_{22}$		9799.02		3.939	
${}_{9}T_{1}$		9577.68		4.792		${}_{0}T_{84}$	9825.00 ± 7.00	9809.85		7.387	T
${}_{11}S_{24}$	9572.88 ± 2.00	9578.38		2.757	W	${}_{1}S_{66}$		9812.22		8.148	
${}_{28}S_{1}$		9579.07		4.744		${}_{11}S_{25}$	9811.00 ± 5.00	9814.25		2.769	WT
${}_{0}S_{93}$	9624.00 ± 9.00	9585.19		8.429	S	${}_{9}S_{28}$	9814.28 ± 8.50	9816.78		4.100	
${}_{26}S_{2}$		9586.48		4.754		${}_{7}S_{35}$	9820.29 ± 2.70	9824.99		3.908	W
${}_{9}T_{2}$		9587.42		4.788		${}_{21}S_{9}$		9828.72		4.309	
${}_{1}S_{64}$		9588.23		8.077		${}_{8}T_{22}$		9838.26		4.626	
${}_{0}T_{82}$	9605.00 ± 6.00	9590.42		7.409	T	${}_{9}T_{10}$		9839.82		4.680	
${}_{3}S_{46}$	9603.01 ± 2.70	9594.48		4.672	W	${}_{5}S_{43}$	9835.77 ± 5.00	9844.43		4.227	W
${}_{15}S_{15}$	9595.53 ± 2.00	9597.78		2.004	W	${}_{7}T_{28}$		9846.40		4.402	
${}_{6}S_{37}$	9599.00 ± 3.50	9601.27		4.005	W	${}_{4}T_{40}$	9844.20 ± 8.00	9859.20		4.550	50
${}_{9}T_{3}$		9602.02		4.781		${}_{27}S_{2}$	9871.00 ± 3.00	9865.33	1.10 ± .12	1.266	WT
${}_{22}S_{6}$		9603.76		6.315		${}_{0}S_{96}$	9908.00 ± 9.00	9866.75		8.455	S
${}_{26}S_{3}$		9604.98		4.727		${}_{22}S_{9}$		9871.01		9.425	I
${}_{8}S_{31}$	9593.74 ± 8.00	9608.74		4.052	–	${}_{2}T_{53}$	9870.00 ± 12.0	9878.43		5.725	50
${}_{24}S_{4}$		9615.50		4.537		${}_{1}T_{67}$	9869.20 ± 7.00	9879.42		7.192	50
${}_{2}T_{51}$	9610.00 ± 10.0	9616.16		5.598	50	${}_{11}S_{0}$	9892.00 ± 5.00	9887.92		1.202	
${}_{5}T_{34}$		9618.51		4.426		${}_{9}T_{11}$		9893.01		4.658	
${}_{8}T_{20}$		9621.27		4.712		${}_{18}S_{12}$		9894.79		2.975	

TABLE 4.1 continued

Mode	f_{obs} μHz	f_{PREM} μHz	q^a_{obs}	q_{PREM}	ref.[b]	Mode	f_{obs} μHz	f_{PREM} μHz	q_{obs}	q_{PREM}	ref.
${}_{20}S_{10}$		9900.15		4.259		${}_{4}S_{46}$		9949.71		2.343	M
${}_{3}S_{48}$	9908.12 ± 4.00	9900.17		4.775	W	${}_{12}S_{23}$		9950.43		3.965	
${}_{26}S_{4}$		9910.84		9.693	I	${}_{9}T_{12}$		9950.95		4.634	
${}_{0}T_{85}$	9935.00 ± 8.00	9919.55		7.376	T	${}_{5}T_{36}$	9943.00 ± 7.00	9952.11		4.453	
${}_{1}S_{67}$		9923.84		8.182		${}_{8}T_{23}$		9954.41		4.579	
${}_{15}S_{16}$	9921.25 ± 1.50	9926.89		1.857	W	${}_{0}S_{97}$	10003.0 ± 9.00	9960.70		8.461	S
${}_{6}T_{32}$		9933.27		4.293		${}_{13}S_{20}$	9953.63 ± 1.50	9961.02		2.114	W
${}_{6}S_{39}$	9928.85 ± 2.30	9936.22		4.004	W	${}_{8}S_{33}$		9969.78		3.997	
${}_{2}S_{55}$		9937.26		6.372		${}_{9}S_{29}$		9975.13		4.106	
${}_{17}S_{15}$	9931.93 ± 5.50	9938.07		2.835	W	${}_{23}S_{7}$		9983.94		1.497	
${}_{3}T_{46}$	9926.00 ± 7.00	9941.90		4.758	WT	${}_{1}T_{68}$		9991.93		7.197	
${}_{19}S_{12}$		9945.85		11.627	I	${}_{14}S_{19}$	9979.63 ± 5.00	9994.61		2.461	

a) $q \equiv 1000/Q$; b) Reference number or mode type; c) Coriolis or second order rotation correction applied.
G Gabi Laske – personal communication (surface wave analysis)
H Dalton et al,2006 (surface wave analysis)
O Selby and Woodhouse 2000 (surface wave analysis)
RR Resovsky and Ritzwoller (web page)
ss singlet stripping
A improved results from Andaman earthquake (singlet stripping)
W regional multiplet stripping (Widmer-Schnidrig, 2002)
WT multiplet stripping (Widmer Thesis)
tvf q estimated using time variable filtering
T see tab.t.fundamentals on the rem webpage (combination of several studies)
S see tab.t.fundamentals on the rem webpage (combination of several studies)
I denotes a mode a mode whose energy is trapped within the inner core or on the inner-core boundary (unlikely to be observed).
M denotes a Stoneley mode trapped on the core-mantle boundary (unlikely to be observed).